LOSS OF MITOCHONDRIAL QUALITY CONTROL PROTEIN YME1 IS DELETERIOUS TO THE VIABILITY OF YEAST LACKING TAFAZZIN

by

Gerard J. Gaspard

Submitted in partial fulfillment of the requirements
for the degree of Doctor of Philosophy

at

Dalhousie University
Halifax, Nova Scotia
June 2014

For

Rosalie

Vishwam & Madeleine

TABLE OF CONTENTS

LIST OF TABLES

LIST OF FIGURES

ABSTRACT

The *Saccharomyces cerevisiae TAZ1* gene is an orthologue of human *TAZ*; both encode the protein tafazzin. Tafazzin is a transacylase that transfers acyl chains with unsaturated fatty acids from other phospholipids to monolysocardiolipin (MLCL) to generate cardiolipin (CL) with a prevalence of unsaturated fatty acids. Transacylase activity is evolutionarily conserved between yeast and humans, as *TAZ1* deficiency in yeast can be compensated for by the expression of human *TAZ*. Mutations in human *TAZ* cause Barth Syndrome (BTHS), a fatal infant disease biochemically characterized by reduced CL mass, increased MLCL levels and mitochondrial dysfunction. Although a plethora of symptoms are manifested, children with BTHS primarily suffer from cardiomyopathy and neutropenia. How an inability of tafazzin to function results in Barth syndrome pathology is not clear. To uncover cellular processes that require tafazzin to maintain cell health, I performed a Synthetic Genetic Array (SGA) analysis using *taz1*Δ yeast cells to identify genes whose deletion aggravated their fitness. The genome-wide screen identified that the mitochondrial quality-control protein Yme1 was crucial for yeast cell growth in the absence of tafazzin function. I then explored mechanisms that lead to the decrease in cell fitness in yeast lacking both tafazzin and Yme1, and found severe mitochondrial ultrastructural defects, defective mitophagy and ineffective superoxide scavenging. Mitophagy is a quality-control process cells use to rid themselves of damaged mitochondria. I show that these are not caused by gross changes in mitochondrial phospholipid levels, increased superoxide generation, or abnormal vacuolar function. I was able to identify an important role for tafazzin in mitochondrial dynamics. The SGA screen also uncovered several other cellular processes that require tafazzin that can be explored by future researchers interested in CL metabolism, mitochondrial function, or Barth syndrome.

LIST OF ABBREVIATIONS AND SYMBOLS USED

AAA	ATPases associated with diverse cellular activities
AAC	Adenosine diphosphate - Adenosine triphosphate Carrier
ADP	Adenosine diphosphate
ADP:O	Amount of oxygen atom reduced per ADP converted to ATP
AGE-BSA	Bovine serum albumin with glycolaldehyde
AIF	Apoptosis inducing factor
ALCAT1	Acyl-CoA:lysocardiolipin acyltransferase-1
Atg11	Autophagy related gene 11
Atg32	Autophagy related gene 32
ATP	Adenosine triphosphate
BN-PAGE	Blue native-poly acrylamide gel electrophoresis
bp	Base pairs of nucleotides
BSA	Bovine serum albumin
BTHS	Barth Syndrome
CCCP	2-[2-(3-Chlorophenyl) hydrazinylyidene]propanedinitrile
CDP	Cytidine diphosphate
CDP-DAG	CDP-diacylglycerol
Cds1	Cytidine diphosphate diacylglycerol synthase 1
Cds2	cytidine diphosphate diacylglycerol synthase 2
CL	Cardiolipin
Cld1	CL deacylase 1
CLm	Mature CL
ClonNAT	Nourseothricin
CLp	Premature or *de novo* CL
CLS	CL synthase in fruit fly
Cls1	CL Synthase 1
CoA	Co-enzyme A
CTP	Cytidine triphosphate
D	Aspartate
Da	Dalton
DNP	2,4-Dinitrophenylhydrazone
DNPH	2,4-Dinitrophenylhydrazine
DTT	Dithiothreitol
E 10.5	Embryonic day 10.5
EDTA	Eythylene-diamine tetra-acetic acid (disodium salt used)
ER	Endoplasmic reticulum
ETC	Electron transport chain
EUROSCARF	European *Saccharomyces cerevisiae* archive for functional analysis
FITC	Fluorescein isothiocyanate
FL	Full-length mRNA
G-3-P	Glycerol-3-phosphate
Gep4	Genetic interactors of prohibitins 4
GFP	Green fluorescent protein
GTE	Glucose Tris EDTA buffer for yeast fractionation

GTP	Guanosine triphosphate
H	Histidine
HeLa	Henrietta Lacks
HEPES	4-(2-hydroxyethyl)-1-piperazineethanesulfonic acid
HIS3	Histidine 3 structural gene of histidine biosynthetic pathway
IMS	Inter membrane space of mitochondria
iPLA2γ	Calcium-independent phospholipase A2 γ
KAN	Kanamycin
Kbp	Kilo base pairs
KDa	Kilo dalton
L4-CL	Tetralinoleoyl CL
LB	Luria Bertani
LC3	Microtubule-associated protein 1 light chain 3
LDB3	LIM domain binding 3
LPC	Lyso-phosphatidylcholine
MAP1LC3	Microtubule-associated protein 1 light chain 3
MAT **a**	Mating type **a**
MAT α	Mating type α
Mdm35	Mitochondrial distribution and morphology 35
MFApr	*MAT***a** activated promoter
Mg	Milli gram
Mgm1	Mitochondrial genome maintenance 1
MICOS	Mitochondrial contact site
MIM	Mitochondrial inner membrane
min	Minutes
MINOS	Mitochondrial inner membrane organizing system
Mito PLD	Mitochondrial phopholipase D
MitOS	Mitochondrial organizing structure
ml	Milliliter
MLCL	Monolyso-CL
MLCLAT1	MLCL acyltransferase 1
mM	Milli molar
MOM	Mitochondrial outer membrane
NAT	Nourseothricin
nmol	Nano moles
O4-CL	Tetraoleoyl-CL
Om45	Outer membrane protein 45 of mitochondria
ORF	Open reading frame
OXPHOS	Oxidative phosphorylation
PA	Phosphatidic acid
PBS	Phosphate buffered saline
PC	Phosphatidylcholine
PE	Phosphatidylethanolamine
PG	Phosphatidylglycerol
Pgk1	Phospho-glycerate kinase1
PGP	Phosphatidylglycerol phosphate

Pgs1	PGP synthase 1
PMSF	Phenylmethylsulfonyl fluoride
PTPMT1	Phospho-tyrosine phosphatase localized to the mitochondrion 1
PVDF	Polyvinylidene difluoride
RCR	Respiration control ratio
ROS	Reactive oxygen species
rpm	Rotations per minute
SC	Synthetic complete
SD	Synthetic defined or minimal medium
SD-N	SD without nitrogen source
SD-trp	SD without tryptophan
SD-ura	SD without uracil
SDS	Sodium dodecyl sulphate
SDS-PAGE	Sodium dodecyl sulphate-poly acrylamide gel electrophoresis
SGA	Synthetic genetic array
shRNA	Small hairpin ribonucleic acid
SOD	Super oxide dismutase
Tam41	Translocator assembly and maintenance 41
TEMED	Tetramethylethylenediamine
TLC	Thin layer chromatography
TRIAP 1	TP53 regulated inhibitor of apoptosis 1
Ups1	Unprocessed 1
v/v	Volume by volume
W	Wild-type yeast
Yme1	Yeast mitochondrial escape 1
YP	Yeast extract and peptone
YPD	Yeast peptone with 2% dextrose
YPL	Yeast peptone with 2% lactate
µCi	Micro curie
µg	Micro gram
µL	Micro liter
µM	Micro molar
˚C	Degree centigrade
α	Alpha
γ	Gamma
Δ	Delta
µ	Micro

ACKNOWLEDGEMENTS

This work would not have been possible without the constant support and encouragement of my supervisor Dr. Christopher McMaster; I would like to thank him for being a great mentor and for providing a great atmosphere to work. I appreciate his quiet and calming influence especially during the last two years when life intervened with work. The support and constructive criticism of my research & presentation skills I received from all my advisory committee members and from the aficionados / connoisseurs of yeast at Dal were very helpful.

I would like to thank Dr. Kanki at Kyushu University School of Medical Sciences, Japan for kindly providing the Om45-GFP strains, Mary Ann Trevors at the Centralized Operations of Research Equipment and Supports for her assistance with Electron Microscopy, Steve Whitefield at the Cellular Microscopy and Digital Imaging for helping me to fix our Zeiss microscope.

Pedro, I want to thank you for being a great support and for always having the time to talk about research and life. I want to thank Noelia, Marissa, Melissa, Amy and past members of the McMaster lab for their friendship. I want to thank all the past and present members of ARC; you are the most friendly and supportive group of guys and gals I have worked with. Especially Bob and Debbie for all their efforts to ensure smooth sailing of the lab. Two facts I learned from the great big ARC renovation were never to stick tape on lab benches, it was the toughest thing to get rid off and straight up pine sol is not good on your hands however tough you think you are. Byong and Giban, I want to thank you guys for being great friends, fond memories of lunch time talks mostly about food (of the spicy kind), Giban's busy weekend schedule and crazy Indian train rides, which are packed 5-10 times over the limit and could end badly if you are too possessive of your sleeper.

Finally, *Purnima* can't thank you enough for supporting me all these years without you this would not have been possible. *Vishwam,* love you! for bringing so much joy and an exponential amount of work to my life. Nicky, thanks, for all the encouragement and support during really tough times. To Robyn Spencer thank you for keeping me in working condition. To amma and appa back home thank you for all the support, encouragement and patience. To Rosalie, thank you for all the things you have done for me, I am sad that you are no more but happy that you are done suffering.

CHAPTER 1. INTRODUCTION

Barth Syndrome (BTHS) is a fatal X-linked infant disease linked to mutations in the *TAZ* gene. The protein, tafazzin, is encoded by *TAZ* and is a transacylase that transfers acyl chains with unsaturated fatty acids from phosphatidylcholine (PC) or phosphatidylethanolamine (PE) to monolysocardiolipin (MLCL) to generate mature cardiolipin (CL) containing unsaturated fatty acids [1]. In BTHS, mutations in *TAZ* block its transacylase activity causing loss of mature CL, reduced CL mass and an accumulation of MLCL [2]. A myriad of mitochondrial functions including mitochondrial protein import, maintenance of mitochondrial morphology, mitochondrial bioenergetics, apoptosis, mitophagy, and mitochondrial biogenesis are regulated by CL. Hence, the severe mitochondrial dysfunction and abnormal mitochondrial morphology seen in BTHS is believed to be due to loss of mature CL and / or CL mass. However, the details of cellular processes that cause mitochondrial dysfunction downstream to reduced CL level and loss of mature CL are not known. BTHS patients clinically manifest a plethora of symptoms but the majority of children suffer from cardiomyopathy and neutropenia. How loss of tafazzin function causes a multisystem disorder such as BTHS is not clear. The yeast (*Saccharomyces cerevisiae*) *TAZ1* gene is an orthologue of human *TAZ* and its loss of function can be compensated for by expression of human *TAZ*. Since tafazzin function is conserved between yeast and humans, yeast lacking *TAZ1* serve as valuable model to study BTHS. Therefore, to uncover cellular processes that require tafazzin to maintain cell health, I generated an *S. cerevisiae* strain lacking *TAZ1* and used it to perform a genome-wide survey for genes whose deletions aggravate its growth fitness. This genome-wide survey identified that loss of *YME1* (encodes mitochondrial quality-control

protein Yme1) is deleterious to the viability of *taz1*Δ yeast cells when grown in non-fermentable medium that requires mitochondrial respiration to provide energy. Further, characterization of *taz1*Δ *yme1*Δ cells revealed that mechanisms regulating mitophagy and superoxide detoxification are inefficient in this double mutant. Hence, tafazzin and Yme1 together are required for the maintenance of efficient mitophagy and protection from superoxide induced cellular damage in yeast cells.

1.1 CARDIOLIPIN

Phospholipids are the most abundant lipids in eukaryotic cell membranes. Their general structure consists of two long-chain fatty acids attached to the *sn*-1 and *sn*-2 position of a glycerol backbone. A variety of phospho- head groups are attached to the *sn*-3 position to make different types of phospholipids, with the most abundant being PC, PE, phosphatidylserine (PS), phosphatidylinositol (PI), and phosphatidylglycerol (PG). CL is unique among phospholipids in that it is comprised of four fatty acyl chains, contributed by two PG molecules attached to each other by a central glycerol backbone [3] **(Figure 1.1)**. At 2%, CL is one of the less abundant cellular phospholipids; however, it is found exclusively in the mitochondria where its abundance is enriched to 15% of mitochondrial membrane lipid. The majority of CL is localized to the inner mitochondrial membrane [4-6].

1.2 CL SYNTHESIS IN *Saccharomyces cerevisiae*

CL biosynthesis occurs in the mitochondrial inner membrane (MIM) [3]. The CL biosynthetic pathway is conserved throughout *Eukaryote* **(Figures 1.2 and 1.3)**. The

eukaryotic yeast *S. cerevisiae* gene and protein nomenclature is primarily used here, as this was the organism utilized in this work.

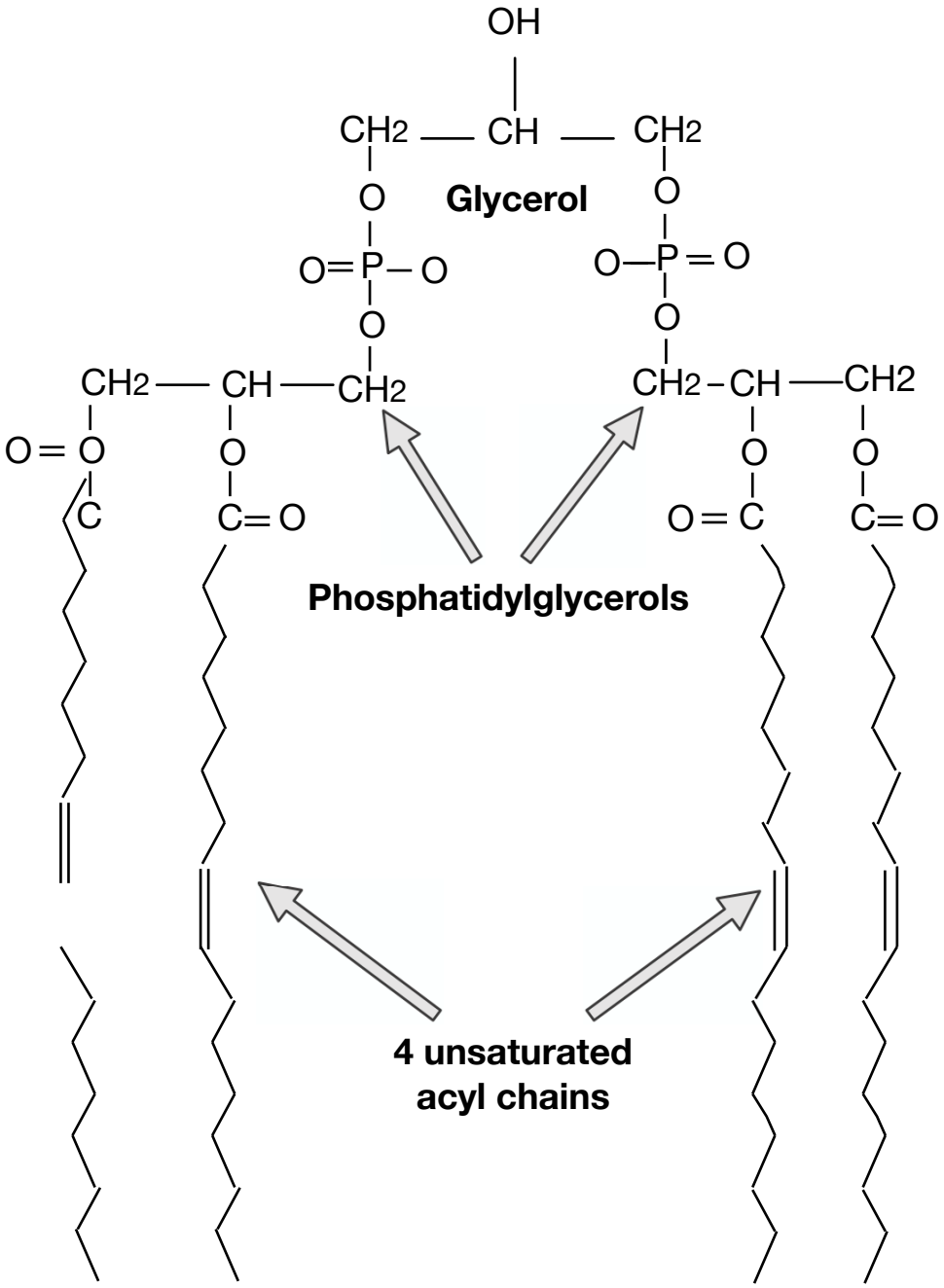

Figure 1.1. CL structure. The schematic shows the unique make up of CL comprising four unsaturated fatty acyl chains from two phosphatidylglycerols attached to each other by a central glycerol moiety.

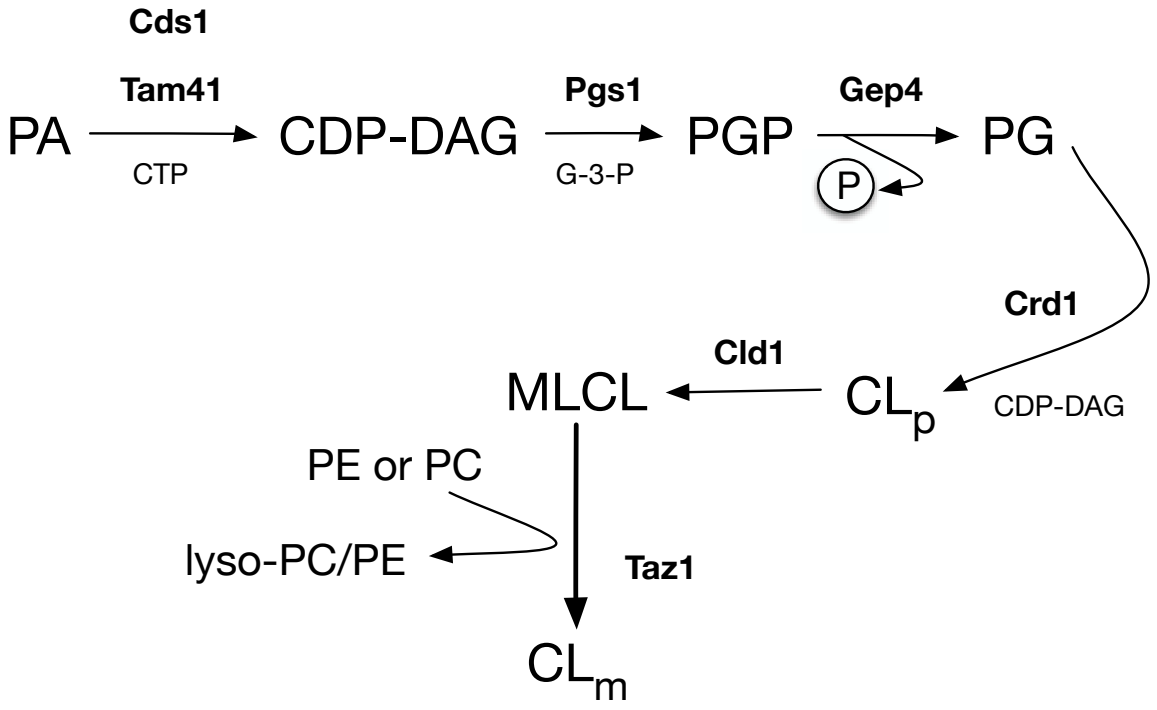

Figure 1.2. CL biosynthesis and acyl chain remodeling in *Saccharomyces cerevisiae*. The enzymes for CL biosynthesis are predominantly located in MIM except for cytidine diphosphate diacylglycerol synthase (Cds1) and possibly Taz1. The former is found in ER and ER-associated MOM and the location of Taz1 is not clear; however, it has been shown to locate to IMS leaflet of both the MIM and MOM. CL synthesis is initiated by the formation of cytidine diphosphate diacylglycerol (CDP-DAG) from phosphatidic acid (PA) by the transfer CDP to PA from cytidine triphosphate (CTP). Both Cds1 and Tam41 can catalyze this reaction, but in yeast the majority of CL is made from CDP-DAG supplied by Tam41. The rate-limiting production of phosphatidylglycerol phosphate (PGP) by the addition of glycerol-3- phosphate (G-3-P) to CDP-DAG is catalyzed by PGP synthase (Pgs1). After the removal of phosphate from PGP by Gep4, phosphatidylglycerol (PG) is then condensed with CDP-DAG by CL synthase (Crd1) to form premature CLp. The *de novo* CLp lacks the abundance of unsaturated fatty acyl species in mature CLm and it undergoes fatty acyl remodeling by the actions of CL deacylase 1 (Cld1) and Taz1. First CLp is deacylated by Cld1 to generate MLCL (has only 3 acyl chains) that is then reacylated by Taz1 by the transfer of acyl chains from PC or PE to produce CLm.

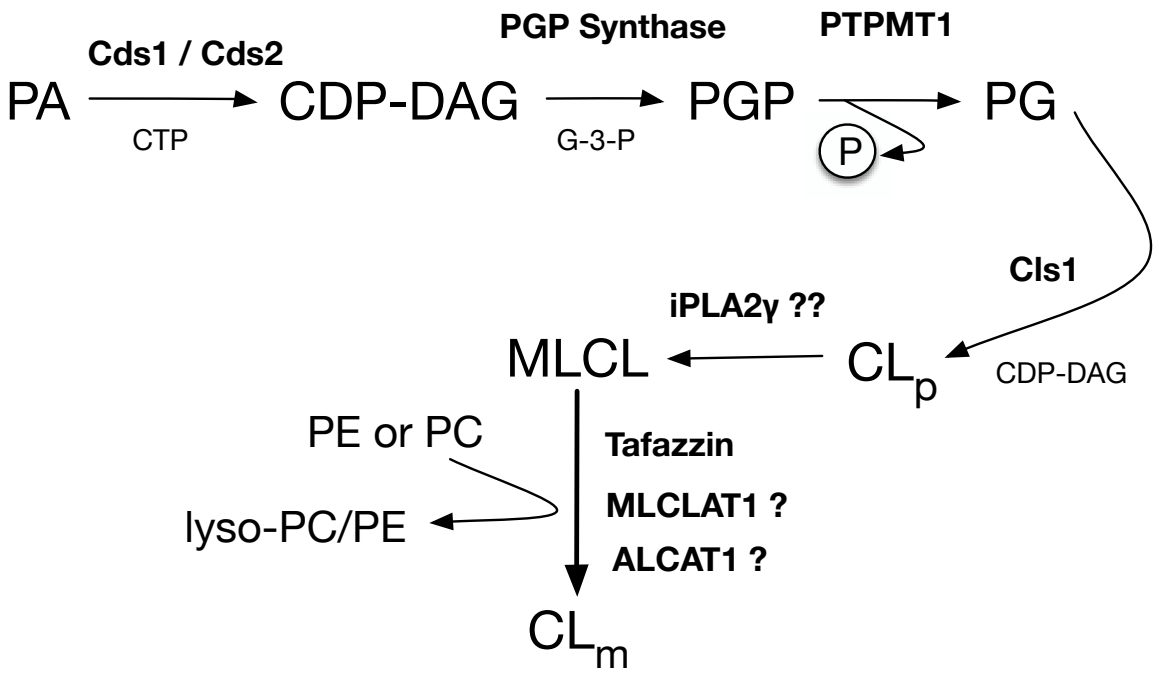

Figure 1.3. CL biosynthesis and acyl chain remodeling in mammals. CL biosynthetic machinery is conserved between yeast and mammals albeit with some minor differences. In mammals, the activities of either cytidine diphosphate diacylglycerol synthase 1 (Cds1) or cytidine diphosphate diacylglycerol synthase 2 (Cds2) supply all the CDP-DAG required for CL synthesis. Phosphotyrosine phosphatase localized to the mitochondrion 1 (PTPMT1), which is unrelated to yeast Gep4, dephosphorylates PGP to PG. In yeast, Cld1 is the only CL deacylase involved in CL remodeling but in mammals, calcium-independent phospholipase A2 gamma (iPLA2γ) and multiple other phospholipases deacylate CLp to MLCL [7]. MLCL acyltransferase (MLCLAT1) located in the matrix leaflet of MIM and ER-mitochondrial associated membrane localized acyl-CoA:lysocardiolipin acyltransferase-1 (ALCAT1) can remodel the acyl chains of CL; however, their relative contributions to CLm pool are not known.

Phosphatidic acid (PA) is delivered from endoplasmic reticulum (ER) associated-mitochondrial outer membrane (MOM) contact sites to the MIM by a PA-specific mitochondrial inner membrane space (IMS) lipid transfer protein, unprocessed 1 (Ups1) [8]. Translocator assembly and maintenance 41 (Tam41), a cytidyltransferase, then transfers CDP from CTP to PA to make CDP-diacylglycerol (CDP-DAG) (Tamura et al. 2013). Alternatively, CDP-DAG synthesized by a CDP-DAG synthase (Cds1) in the ER can be transported to MIM for CL synthesis. However, this transport is inefficient and is a minor contributor to the CDP-DAG used for CL synthesis in yeast as evidenced by low CL levels in *tam41*Δ yeast cells, even after *CDS1* overexpression [9]. CDP-DAG is converted to PG phosphate (PGP) by the addition of glycerol-3-phosphate (G-3-P), catalyzed by PGP synthase (Pgs1), the committed step in the synthesis of CL. Gep4 (genetic interactors of prohibitins 4), a PGP phosphatase, dephosphorylates PGP to PG [10], and PG is then condensed with CDP-DAG by CL synthase 1 (Cls1 or Crd1) to form premature CL.

De novo synthesized CL primarily contains saturated fatty acyl chains and they are specifically replaced with unsaturated fatty acyl species to produce mature CL. Premature CL is deacylated to monolyso-CL (MLCL) by a phospholipase A-like enzyme, CL deacylase 1 (Cld1) [11]. Cld1 specifically removes saturated fatty acyl groups, as evidenced by a significant increase in CL comprised of palmitic (C16:0) and stearic (C18:0) fatty acyl chains in *cld1*Δ strains [11]. Taz1, referred to as tafazzin, then transfers unsaturated fatty acyl chains from PC or PE to MLCL to form mature CL and a lysophospholipid [1,12]. In wild-type yeast, 90% of CL fatty acyl chains are unsaturated, indicating the robustness of this reacylation process [13].

1.3 CL SYNTHESIS IN MAMMALS

CL synthesis is evolutionarily conserved from yeast to mammals, with some minor differences **(Figures 1.2 and 1.3)**. In mammals, as in yeast, CL synthesis takes place predominantly in the MIM. PERLI, the mammalian homologue of Ups1, associates with TP53 regulated inhibitor of apoptosis 1 (TRIAP1) (mammalian homologue of yeast Mdm35) and this dimer transports PA from the MOM to the MIM [14] for the initiation of CL synthesis. Unlike in yeast, where Tam41 is the significant provider of CDP-DAG [9], in humans, two homologs, cytidine diphosphate diacylglycerol synthase 1 (Cds1) and cytidine diphosphate diacylglycerol synthase 2 (Cds2) with different tissue specificities predominantly supply CDP-DAG to PGP synthase to produce PGP [6]. Also, PGP is dephosphorylated by phosphotyrosine phosphatase localized to the mitochondrion 1 (PTPMT1) [15]. Interestingly, PTPMT1 is not related to yeast Gep4 at the amino acid sequence level, with PTPMT1 conserved only among higher eukaryotes. PTPMT1 expression can restore PGP synthesis in *gep4*Δ yeast, resulting in reconstitution of the CL biosynthetic pathway and indicating conservation of their biochemical function [15,16]. Like in yeast, PG is then converted to premature CL in the matrix leaflet of the MIM by CL synthase 1 to synthesize premature CL [17,18].

Several routes have been proposed for the remodeling of premature CL to mature CL in mammals. Mammalian tafazzin, like yeast Taz1, transfers acyl chains from PC or PE to MLCL to produce mature CL [1,19,20]. In addition, it was observed that deletion of calcium-independent phospholipase A2 gamma (iPLA2γ) in mice results in low

myocardial CL levels and reduction in mature CL comprised primarily of L4-CL (tetra-C18:2 acyl species), implicating iPLA2γ in mature CL production [21]. However, it has not been experimentally shown that iPLA2γ directly deacylates CL to MLCL. Moreover, iPLA2γ deletion did not completely deplete mature CL in the mouse heart [16,21]. In mammals, a MLCL acyltransferase (MLCLAT1) located in the matrix leaflet of MIM has also been described [22]. MLCLAT1 produces mature CL by specifically transferring linoleate (18:2) acyl chains to MLCL in an acyl-CoA dependent fashion; however, its relative contribution to the overall mature CL pool is not clear [22]. Moreover, in mammals an acyl-CoA:lysocardiolipin acyltransferase-1 (ALCAT1) located in the ER can also reacylate MLCL to CL, but its contribution to the production of mature CL is also not known [16,23]. However, under oxidative stress or diet-induced obesity, ALCAT1 has been shown to produce CL containing long-chain poly-unsaturated fatty acyl species that are susceptible to oxidative damage resulting in mitochondrial dysfunction [23].

1.4 CL AS A NON-BILAYER FORMING LIPID

Phospholipids, based on their shape and structure, can be classified as bilayer forming (PC) and non-bilayer forming (PE, CL). PC, because of its proportionally sized head group and acyl chains, has a cylindrical structure that has a propensity to form bilayers in an aqueous environment [24]. On the other hand, PE and CL, because of their smaller head groups relative to their acyl chains, are conical and assume hexagonal phase structures in aqueous environments (**Figure 1.4**) [24].

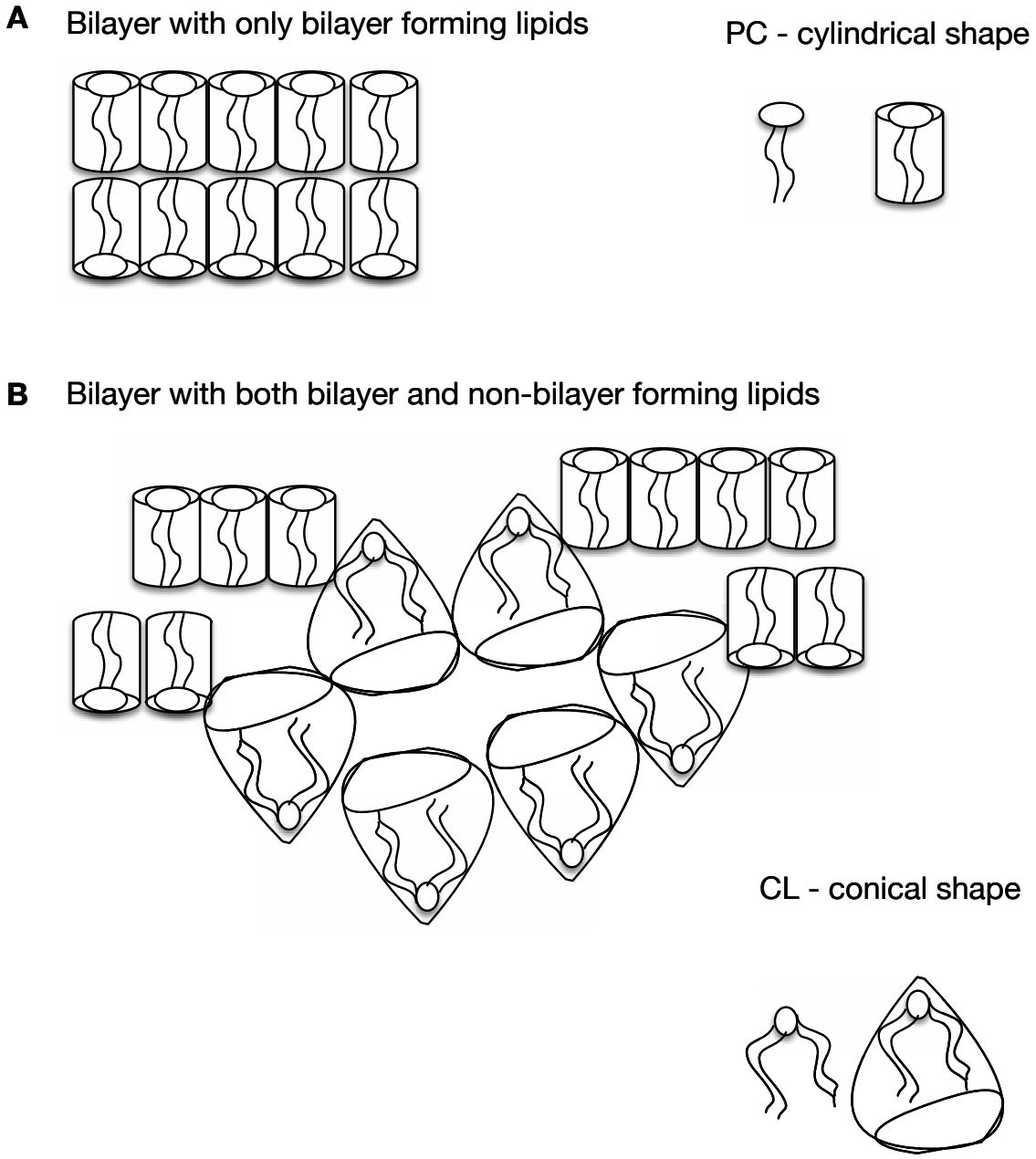

Figure 1.4. Cartoon of bilayer and non-bilayer forming lipids. A. PC, because of its proportionally sized head group and acyl chains, has a cylindrical shape, which enables it to pack tightly to form water tight bilayers in an aqueous environment. **B.** CL, on the other hand, with its smaller head group relative to its acyl chains, is conical and does not pack tightly, and thus forms non-bilayer structures. Biological membranes (mixture of bilayer and non-bilayer) exist as bilayers but the presence of non-bilayer lipids in membranes, especially when they are enriched in microdomains, could disrupt the bilayer structure to facilitate membrane bending and membrane mixing.

The presence of non-bilayer lipids in membranes is believed to enable transient changes in membrane structure that are essential for the transport of some solutes and lipids across membranes, and to facilitate membrane fusion events [5,25-28].

In certain regions of the mitochondria the MOM and MIM are in close apposition. These areas are called contact sites and are important for transport of solutes and lipids across mitochondrial membranes [29-31]. CL is enriched at these contact sites in yeast, and it is believed formation of CL clusters in contact sites is ideal to induce a non-bilayer membrane confirmation to bring the membranes together [6,31,32]. In yeast, several CL-rich contact sites have been defined, including the molecular complexes MICOS (mitochondrial contact site), MINOS (mitochondrial inner membrane organizing system), and MitOS (mitochondrial organizing structure) [33-35]. Loss of proteins forming these complexes results in altered mitochondrial cristae morphology, and these mutants do not tolerate a concomitant deletion of structural genes within the CL biosynthetic pathway, underlining the importance of CL to these membrane appositions [35].

1.5 REGULATION OF MITOCHONDRIAL DYNAMICS BY CL

CL plays a vital role in the maintenance of mitochondrial morphology by regulating mitochondrial fission and fusion [25]. A dynamin-like mitochondrial GTPase, Mgm1 (mitochondrial genome maintenance 1) in yeast and optic atrophy 1 (OPA1) in humans, exist in the MIM as both a long form and a proteolytically cleaved short form. This proteolytic conversion of Mgm1/OPA1 is necessary for mitochondrial fusion and cristae

morphogenesis [36,37]. Decreased CL mass affects mitochondrial morphology by interfering with the proteolytic processing of Mgm1/OPA1 [36,38].

It is now suspected that mitochondrial phospholipase D (Mito PLD), localized to CL-enriched contact sites, can effectively convert CL on the MOM of an adjacent mitochondrion to PA to initiate fusion between the two outer membranes of mitochondria [39]. This idea was confirmed by the lack of fusion and by the accumulation of fragmented mitochondria when Mito PLD activity was blocked in yeast. The role of PA in membrane fusion is not clear; it is thought to recruit additional proteins like soluble N-ethylmaleimide-sensitive factor attachment protein receptors, which in concert with mitofusin might cause MOM fusion [39]. Additionally, PA is also a non-bilayer forming lipid that might facilitate fusion by altering the physical properties of the membrane such as curvature and packing. At present the absolute requirement of CL for mitochondrial fusion is not clear, since yeast lacking CL can maintain mitochondrial morphology. Other anionic phospholipids such as PE and PG might substitute for the lack of CL. In agreement to this notion, mitochondrial fusion is blocked in yeast lacking both CL and PE [40].

1.6 REGULATION OF THE ELECTRON TRANSPORT CHAIN BY CL

CL is not essential for yeast viability: a *crd1*Δ mutant (cannot make CL from PG) can grow on both fermentable (energy from glycolysis) and non-fermentable media (ATP from respiration that requires mitochondrial function) under normal growth conditions

(16˚ - 30˚C); however, such mutant cells grow poorly under heat stress (37˚C) even in fermentable media [41]. Although the *crd1*Δ mutant is viable, its electron transport chain (ETC) complex components, specifically complex IV and V (ATP synthase) activity, maximal respiratory rate, and MIM potential are defective. These defects are more pronounced in fermentable growth media [41]. This phenotype was attributed to increased accumulation of PG (CL precursor) in non-fermentable media, and this lipid could partially substitute for CL. However, ADP-ATP carrier (AAC) activity and oxidative phosphorylation (OXPHOS), that are dependent on CL, were equally defective in both media [41] indicating an absolute requirement of CL for AAC activity. X-ray crystallography of bovine AAC showed that six molecules of CL bound per dimer of AAC and CL was required for proper AAC folding, dimerization and activity [42]. These properties could not be supported by other phospholipids, consistent with a specific requirement for CL in AAC function [42,43]. CL has also been shown to bind and regulate proper folding, oligomerization and activity of other MIM proteins including phosphate carrier, pyruvate carrier, carnitine carrier, complex I, complex III, cytochrome oxidase (complex IV), ATP synthase (complex V), and CL synthase [27,44]. Unlike the absolute requirement of CL for AAC activity, *in vitro* studies showed that other phospholipids, such as CL containing short chain fatty acyl species and MLCL, could partially substitute for CL and maintain the activity of complex I, complex III, complex IV and complex V of the ETC [27]. Although mature CL containing unsaturated fatty acyl chains are not absolutely required for the activities of these mitochondrial proteins, in its absence they are only partially functional and this may impact mitochondrial energy production under stress.

In yeast, CL aids the physical association of ETC complex III with ETC complex IV and this association between these two complexes enables them to exist as two different supercomplexes [45]. One supercomplex comprises a dimer of complex III with a monomer of complex IV (III2IV), and the other supercomplex consists of a dimer of complex III associated to a dimer of complex IV (III2IV2) [46] (**Figure 1.5**). These super complexes are suspected to exist in a higher-order complex with AAC and ATP Synthase, which by nature of proximity of all components of ETC is thought to maximize the efficiency of electron transfer between complexes and prevent electron leakage from the ETC [45,47,48]. The formation of III2IV and III2IV2 supercomplexes was completely abolished in *crd1*Δ cells, and there was an increase in free IV monomer in *taz1*Δ yeast [48,49]. This absence of higher-order ETC complexes in *crd1*Δ yeast may not be essential for mitochondrial respiration under normal circumstances, but might be crucial under stress, as evidenced by significant uncoupling of respiration from phosphorylation at 40˚C, or when the ETC is functioning at a maximal rate of OXPHOS to meet the energy demands of the cell [50-52].

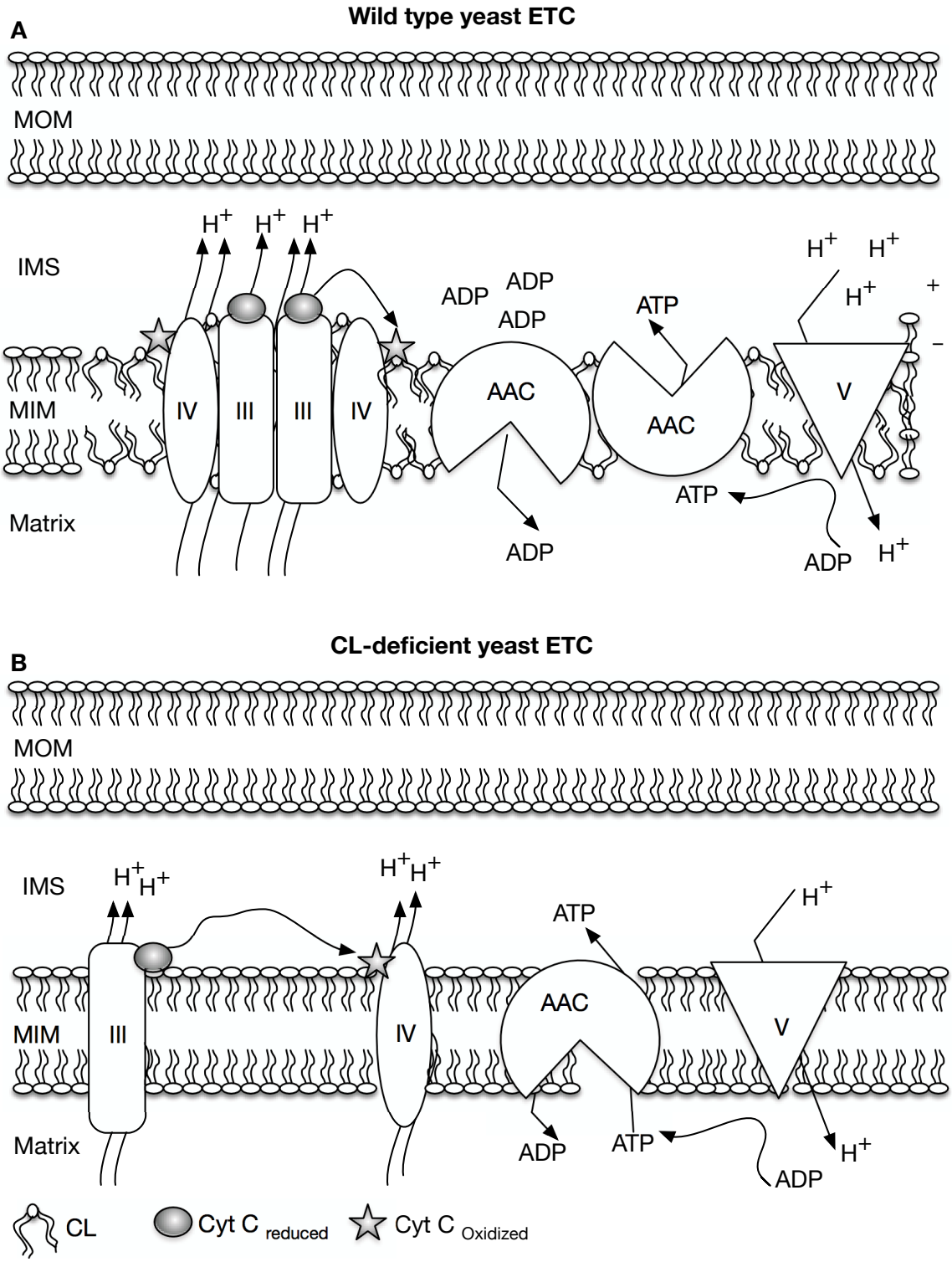
A
Wild type yeast ETC
MOM
IMS
MIM
Matrix
H+
IV
III
III
IV
ADP
ADP
ADP
AAC
AAC
ATP
V
ATP
ADP
ADP
B
CL-deficient yeast ETC
MOM
IMS
MIM
Matrix
III
IV
AAC
ATP
V
ADP
ATP
ADP
CL
Cyt C reduced
Cyt C Oxidized

Figure 1.5. CL facilitates the supramolecular organization of the ETC. A. In wild-type yeast, two subunits each of complex III and cytochrome oxidase (complex IV) form a higher-order structure with the aid of CL. The proximity of these two complexes is thought to reduce the electron leakage by potentially reducing the distance travelled by cytochrome c, which shuttles in a reduced and oxidized state between complex IV and III, respectively. CL, apart from being essential for the dimerization and activity of ADP-ATP carrier (AAC), is also hypothesized to form micro-domains within the MIM, which may harbor the entire bioenergetic machinery in proximity, thus increasing its efficiency and reducing the leakage of electrons to form reactive oxygen species (ROS). **B.** In CL deficient yeast, the supra-molecular organization of ETC is lost. Although this does not inhibit ATP generation under normal conditions, oxidative phosphorylation (OXPHOS) gets uncoupled from ATP synthesis at times of stress and increased energy demand.

Analysis of Barth syndrome patient lymphoblasts (which have mutations in *TAZ*) revealed increased accumulation of IV monomer, lower I/III2 levels and reduced expression of complex I, indicating the importance of the CL reacylation process in the formation of these supercomplexes [53].

Complex V (ATP Synthase) of the ETC, in co-operation with CL, was shown in fruit-fly flight-muscle mitochondria to reduce the inherent free energy associated with highly curved membranes and stabilize mitochondrial cristae [54]. ATP synthase dimerization, and its subsequent organization into a higher-order ribbon-like complex around the curved cristae, was lost in flies with inactivated CL synthase (*CLS*) or *TAZ1* genes [54]. Electron micrographs of flight muscle mitochondria from these flies showed aggregation of MIM and loss of cristae morphology, similar to alterations in human lymphoblast mitochondria from patients with mutations in the human *TAZ* gene [54]. Therefore, although CL is not absolutely required for ETC activity and ATP production under normal conditions, under stress or when ETC has to function at its maximum capacity to fulfill the energy requirements of fruit-fly flight muscles, CL is required to maintain ETC efficiency and it does that by organizing the ETC into supramolecular structures [45].

1.7 ROLE OF CL IN THE REGULATION OF APOPTOSIS

Cells can undergo apoptosis by extrinsic or intrinsic pathways. The extrinsic pathway requires binding of Fas or tumor necrosis factor-α to their respective cell surface ligands and the subsequent activation of caspase 8 and 10, which in turn results in the cleavage of pro-caspase-3 and Bid to caspase-3 and truncated Bid (t-bid). The intrinsic pathway

involves MOM perforation and the release of pro-apoptotic factors including cytochrome-c from mitochondria to the cytoplasm to facilitate apoptosis [28,55]. In some cells, the extrinsic pathway alone is not enough for apoptosis to proceed, and the release of pro-apoptotic factors from the mitochondria to boost the extrinsic apoptotic signal has been shown to play a prominent role in this process [28,55].

CL is essential for MOM pore formation as it has been shown to translocate, with the help of the CL-binding protein nucleoside diphosphate kinase or Mt-CK [32,56,57], from the MIM to MOM during the early stages of apoptosis [58]. CL provides docking sites on the MOM for the pro-apoptotic factors caspase 8 and Bid [59,60]. CL-associated caspase-8 cleaves Bid to proapoptotic t-bid, which along with CL recruits and aids in the oligomerization of Bax and Bak proteins at the MOM. Bax and Bak oligomerization is thought to be essential for the perforation of the MOM [61]. Bid has also been shown to aid in redistributing CL from the MIM to the MOM, and thereby interfering with the organization of cristae and ETC function, and further worsening mitochondrial dysfunction in the dying cell [62,63].

In addition to providing docking sites for MOM-perforating proteins, CL also regulates the release of cytochrome c from the mitochondria to the cytoplasm to drive apoptosis. Cytochrome c is a soluble protein that, under normal conditions, is membrane associated through electrostatic interaction with the negative phosphate group of CL and hydrophobic interactions with the acyl chains of CL [64,65]. The latter association of cytochrome c with CL increases its peroxidase activity and, in the presence of excess hydrogen peroxide, mature CL containing four unsaturated acyl chains is highly

susceptible to peroxidation [28,55,66]. Oxidized CL is less efficient in binding cytochrome c, therefore, CL oxidation causes the release of cytochrome from the mitochondria to cytosol [67,68]. CL peroxidation is essential for the release of other pro-apoptotic factors from the mitochondria including Smac/Diablo, Endo G, Omi/HtrA2, and apoptosis inducing factor (AIF) [66].

1.8 BARTH SYNDROME (BTHS) OVERVIEW

BTHS is an X-chromosome linked pediatric "orphan" disease with a prevalence of 1:400,000 live births, but is believed to be under-diagnosed with a potentially higher prevalence of 1:140,000 live births [69]. The disease is caused by mutations in the evolutionarily conserved *TAZ* gene. In humans, *TAZ* is comprised of 11 exons and is located on the X chromosome [70,71]. To date, approximately 120 different mutations have been identified in the *TAZ* gene that cause Barth syndrome. They are not concentrated to a hot spot but are instead spread across all 11 exons of the gene. The majority of these mutations are missense mutations and small insertions or deletions. Frame-shift, exon-intron splice-site mutations, large exon deletions and complete gene deletion have also been documented in affected infants and carrier mothers. Majority of these mutations have been shown to cause complete loss of tafazzin function, therefore, failure to remodel *de novo* synthesized CL to mature CL by mutant tafazzin is believed to cause BTHS.

Cardiomyopathy, mainly dilated cardiomyopathy, occurs in 70% of individuals diagnosed with BTHS. However, BTHS considered a multi-system disease as patients exhibit a

myriad of symptoms such as, but not restricted to, neutropenia, recurrent infections, mouth ulcers, myopathy, exercise intolerance, delayed motor milestones, abnormal fatigue, mild learning disabilities, growth delay, delayed puberty, and aciduria [69,72]. If BTHS goes undiagnosed, sudden cardiac arrest due to ventricular arrhythmia, or bacterial septicaemia due to neutropenia, leads to fatalities in most infants within the initial few years after birth. Although there is no known cure, the disease can be effectively managed with standard heart-failure medications, antibiotics and Granulocyte-Colony Stimulating Factor injection to fight recurrent infections by raising neutrophil counts [69,72]. However, in severe cases, heart transplantion, ventricular-assist devices to prevent arrhythmia and prophylactic antibiotic treatment to coincide with periods of neutropenia were used to manage the disease, with different degrees of success [69,72]. Unfortunately, since there is no correlation between the type or location of the mutation with the clinical severity of the disease, it is not easy to predict the prognosis of the disorder by *TAZ* gene sequencing [69,72]. Despite symptom management that has extended the lifespan for most BTHS patients, quality of life and lifespan are still not near the norm. There is a need for a deeper understanding of BTHS if we are to move toward more effective treatments.

1.9 PHOSPHOLIPID AND MITOCHONDRIAL ULTRASTRUCTURAL ALTERATIONS IN BTHS

Analysis of the fatty acyl species composition of CL in yeast, fly and humans showed that mono-/di-unsaturated fatty acyl species are more enriched than saturated species [73]. The major forms of CL unsaturated fatty acyl chains were C18:2 / C18:1. More

specifically, the predominant fatty acyl species in CL of human hearts, human lymphoblast, *Saccharomyces* and *Drosophila* are tetralinoleoyl (C18:2; L4-CL), C18:1, C16:1/C18:1, and C16:1/C18:2, respectively [73]. However, human and other mammalian brain are an exception, as brain contains a diverse array of CL acyl chains including short aliphatic chains as well as polyunsaturated fatty acids including arachidonic and docosahexaenoic acids [74]. At present it is not known if CL with different acyl chain compositions differ functionally, but it is clear that mutation of tafazzin affects the maintenance of mature CL in humans, mouse, yeast, fruit-fly and zebrafish [75-79]. Phospholipid analysis in heart, skeletal muscle, lymphocytes, fibroblasts and cultured lymphoblast from BTHS patients showed increased MLCL levels and a concomitant 75% decrease in CL mass [80]. The rate of incorporation of linoleic acid, but not other fatty acids, into CL and PG was significantly reduced in patient fibroblasts [80]. When CL fatty acyl species profile was determined in skeletal muscle, left ventricle, right ventricle, and platelets from BTHS patients, the predominant L4-CL species was missing and the majority of CL contained saturated acyl species [75]. Interestingly, MLCLAT1 over-expression in lymphoblasts immortalized from Barth syndrome patients could substitute for loss of tafazzin by restoring L4-CL level to those observed in non-patient cells [22]. Currently, albeit not widely available, estimation of elevated MLCL to CL ratio in blood specimens along with *TAZ* gene sequencing is the most accurate and effective way to diagnose BTHS [69].

Electron micrographs of lymphoblasts from BTHS patients showed abnormal clusters of giant and fragmented mitochondria with MIM adhesions and subsequent loss of intra-

cristae space [81]. Coupled with aberrations in MIM morphology and cristae structure, the expression of ETC complexes (I, IV and V), stability and assembly of respiratory supercomplexes (I/III2/IV) that reside on the inner membrane were all compromised in BTHS patient lymphoblasts [49,53]. In agreement with these alterations, a decrease in mitochondrial respiration and ATP synthesis was observed; however, this decrease was offset by a compensatory increase in mitochondrial mass [82]. Further, mitochondria produced slightly more reactive oxygen species (ROS) than normal, and BTHS cells failed to undergo Fas ligand stimulated apoptosis as they failed to recruit caspase-8 to MOM, which in turn blocked downstream steps of the mitochondrial component of the extrinsic apoptotic pathway [82]. Since these cells can undergo apoptosis through caspase-8-independent pathways, at present, the importance of this block in extrinsic apoptotic pathway and its effects on viability/sensitivity to stress of BTHS cells is not known [82].

1.10 BTHS PATHOGENESIS

CL is at the front and centre of the molecular pathogenesis of BTHS, but the molecular mechanisms that cause multisystem failure in this disease are not well understood (Schlame & Ren 2006). At present it is not clear if reduced CL mass or failure to produce mature CL is important for BTHS pathogenesis (Schlame & Ren 2006). Recent studies in yeast lacking tafazzin showed that un-remodeled CL is not functionally different from mature CL, as the former was equally efficient in maintaining mitochondrial OXPHOS and mitochondrial morphology [83]. This observation is at odds with the widely held view that inability to make mature CL results in alterations in mitochondrial respiratory-complex stability, OXPHOS and morphology, ultimately leading to multi-system

dysfunction in BTHS. However, in mammals, as evidenced by abundant L4-CL in heart and skeletal muscle than in other tissues [84], maintenance of mature CL might be crucial for the sustained generation of ATP in these aforementioned tissues as they depend on mitochondria for their energy production (Schlame & Ren 2006). Loss of L4-CL in these tissues might initiate the pathogenesis of cardiomyopathy and skeletal-muscle weakness in BTHS (Schlame & Ren 2006). Furthermore, mature CL might be specifically required for yet-to-be identified mitochondrial functions in both yeast and mammals [83]. In yeast and fly tafazzin mutants, preventing the initiation of CL remodeling by either deleting *CLD1* or iPLA2, respectively, prevented CL loss and MLCL accumulation, and that in turn was shown to restore growth in ethanol medium under heat stress in yeast, and prevent male sterility in flies [83,85]. This experimental evidence suggests that mitochondrial dysfunction due to loss of tafazzin function is caused by reduced CL mass and MLCL accumulation, and not by the change in the fatty acyl composition of CL [83,86].

Complete loss of tafazzin function in differentiated cardiomyocytes and undifferentiated embryonic stem cells of *D. melanogaster* leads to loss of CL in both cell types, but BTHS-like alterations in MIM (aggregation of inner membranes, aberrant cristae, etc.) were seen only in embryonic stem cells that differentiated to cardiomyocytes. This finding implies that BTHS might be a developmental disease, and that embryonic factors might act as modifiers of pathogenesis [2,52]. The same study also showed that certain types of mitochondria with dense cristae organization, like *Drosophila* flight muscle mitochondria but not heart-muscle mitochondria (loose cristae), are more prone to

morphological alterations when CL levels are decreased (Acehan et al. 2009). These alterations are suspected to be pronounced during periods of higher energy demands, indicating that physiological factors might affect the clinical outcome of BTHS [52,87].

To date, it is impossible to predict the outcome of BTHS due to a lack of known genotype-phenotype correlation. Clinical manifestation of the disease has been shown to vary even within the same family, implying there are modifier genes that alter the severity of the disease [88,89]. A concomitant mutation in LIM domain binding 3 gene (LDB3) was identified in a BTHS patient with severe cardiomyopathy. It was proposed that LDB3 mutations (which cause left ventricular wall thinning) might have exaggerated the patient's cardiomyopathy, and acted as a negative phenotypic modifier of *TAZ* deficiency [89,90]. However, the putative modifier effect of LDB3 on the BTHS phenotype has to be further characterized. Mutations in cardiac sodium-channel type V and alpha-subunit gene (SCN5A) are associated with arrhythmias and left ventricular wall thinning; therefore, it is hypothesized to also act as a modifier of BTHS phenotype. These observations highlight the need to identify and characterize modifier genes in cells lacking tafazzin function to fully understand the pathogenesis and clinical manifestations of this disease [89].

1.11 TAFAZZIN

The human tafazzin gene consists of 11 exons, of which exons 5, 6 and 7 can undergo differential splicing resulting in four major splice variants: full-length (FL), exon 5 lacking (Δ5), exon 7 lacking (Δ7), and both exon 5 and 7 lacking (Δ5Δ7) mRNAs

[84,91,92]. At present, there are conflicting reports on which major variant is the predominant mRNA in humans. A recent study analyzing the proportion of *TAZ* mRNAs in blood samples of normal and BTHS patients showed that Δ5 mRNA is the most abundant isoform in both cases [92], but an earlier study estimated that Δ7 mRNA is the most expressed isoform [84]. Regardless, analysis of the ability of the major human *TAZ* splice variants to compensate for loss of tafazzin function in *taz1*Δ mutant yeast showed that only the Δ5 splice variant is able to completely restore mature CL, MLCL/CL ratio, CL mass and mitochondrial respiration. The FL variant could partially rescue CL mass and mature CL but not the other phenotypes [84,93,94]. Heterologous expression of the human *TAZ* splice variants in tafazzin-deficient *Drosophila* showed that the Δ5 mRNA could restore mature CL, MLCL/CL ratio, CL mass, fertility and mitochondrial respiration but not the skeletal-muscle related climbing phenotype, which could only be complemented by the expression of FL variant [20]. The *Drosophila* studies showed that the Δ5 and FL variants can remodel CL to mature CL, but the FL variant seems to possess additional and or unique function(s) since its expression alone could specifically restore the climbing phenotype [92]. Further, these studies showed that the other *TAZ* splice variants reported are either catalytically inactive or that they possess undiscovered functions that are only pertinent in mammals [92]. Importantly, these experiments implied that tafazzin function is evolutionarily conserved from yeast to humans, and that both *D. melanogaster* and *S. cerevisiae* could be valuable tools to study BTHS.

1.12 TAFAZZIN IS A TRANSACYLASE THAT TRANSFERS ACYL CHAINS BETWEEN PHOSPHOLIPIDS

Fatty acyl chains in CL are usually restricted to one or two species, including linoleate (C18:2) in mammalian hearts, palmitoleate (C16:1) and oleate (C18:1) in yeast, and oleate (C18:1) and linoleate (18:2) in fruit flies [73]. It is now well established in many systems that *de novo* synthesized CL undergoes fatty acyl remodeling to achieve this fatty acyl configuration [73,75-79]. Like BTHS in humans, deletion of *TAZ* homologues in mice, zebrafish, yeast and fruit flies all lead to decreases in unsaturated CL, as well as decreases in CL level with concomitant increases in MLCL levels [73,75-79]. These findings, and the observation that *TAZ* is closely related to glycerolipid acyltransferases as it contains an evolutionarily conserved HX4D (histidine followed by an aspartate separated by 4 amino acids) catalytic acyltransferase motif [19], clearly hinted that tafazzin might remodel *de novo* synthesized CL.

Rat liver and human lymphoblast mitochondria were shown *ex vivo* to possess the ability to transfer fatty acyl chains from PC and PE to CL. When rat liver mitochondria were incubated with [^{14}C]linoleoyl-PC and tetraoleoyl-CL (O4-CL), the latter lipid was completely remodeled to tetralinoleoyl-CL (L4-CL) through successive transfer of linoleoyl groups from PC to O4-CL generating the intermediates LO3-CL, L2O2-CL and L3O-CL [95]. This experiment showed that all the acyl chains of CL were amenable to remodeling and that the enzyme catalyzing acyl transfer from PC to CL, unlike acyltransferases, does not require Co-enzyme A (CoA) activated acyl chains for its activity [95]. Importantly, BTHS patient lymphoblast mitochondria, when compared to

these from normal patient lymphoblasts, showed marked reductions in the ability to transfer oleoyl groups (predominant acyl species in lymphoblast CL) from radiolabelled oleoyl-PC to MLCL, indicating that mutation in *TAZ* hinders CL remodeling [1,95]. Conclusive experimental evidence for the enzymatic function of tafazzin came from *in vitro* enzymatic studies with purified *Drosophila* full-length tafazzin [1]. The purified protein efficiently transferred linoleoyl chains from 1-palmitoyl-2-[^{14}C]linoleoyl-PC to MLCL to produce CL and lyso-PC (LPC), and stimulated the reverse reaction catalyzing the transfer of acyl chains from CL to LPC. These reactions did not require CoA-activated acyl chains, and the addition of acyl-CoA did not stimulate acyl transfer [1]. *Drosophila* tafazzin preferred mono-unsaturated species over poly-unsaturated acyl species like arachidonic acid [1]. Human TAZ protein, when expressed in *taz1*Δ yeast cells, generated CL enriched in palmitoleate and oleate (yeast can only synthesize fatty acids with one double bond), consistent with an enriched specificity for fatty acyl groups that are unsaturated [84,93,94]. Although the transfer of acyl groups between PC and CL was the most efficient reaction *in vitro*, the enzyme could also transfer acyl groups between variety of phospholipids (PE and CL, PC and PE, and PC and PA). The combined observations collectively led to the conclusion that the function of tafazzin in cells is as a transacylase that catalyzes the transfer of acyl chains between PC/PE and CL [1].

In yeast, the *CLD1* gene product is known to specifically deacylate saturated acyl species from *de novo* CL to generate MLCL, and deletion of the *CLD1* gene led to a 2.4-fold increase in abundance of saturated acyl species in CL, indicating its importance in CL remodeling [11]. However, in mice, deletion of iPLA2γ led to only minor decreases in

mature CL [21], and in *Drosophila* the abrogation of iPLA2 activity prevented MLCL accumulation but did not affect CL remodeling [85]. Recently, it was shown that secreted PLA2, cytosolic PLA2 and calcium independent PLA2 can degrade CL to MLCL or dilyso-CL *in vitro* [96]. Therefore, at this time, the role of other phospholipases in CL remodeling cannot be ruled out, however, elegant *in vitro* enzymatic studies with purified *Drosophila* tafazzin in liposomes and artificial mitochondrial membranes (lipid composition similar to mitochondria) showed that acyl specificity is conferred by the lipid composition and the physical property of the membranes where transacylations occur [97]. Epand and colleagues showed that tafazzin reacts with only a small fraction of lipids, and that its enzymatic activity is most efficient in artificial membranes that contain non-bilayer lipids like CL [97]. From these findings they hypothesized that the presence of non-bilayer lipids might drive tafazzin transacylase activity by reducing the packing order of the membrane, resulting in better mixing of lysolipid-like MLCL with its acyl donor PC (which packs tightly) [97]. Further, *in vivo* the localization of non-bilayer lipids in curved mitochondrial membrane structures like cristae junctions, and in contact sites between MOM and MIM with loosely packed membranes, would favor the transfer of unsaturated acyl species to MLCL and LPC to generate phospholipids that do not pack tightly and are able to stabilize the local physical property of the membrane [97]. This effect would restrict tafazzin activity to segregated regions within the mitochondria, and thus all of the *de novo* synthesized CL should somehow come in contact with these regions to be remodeled [97]. Yeast Taz1 has been shown to physically associate with ATP synthase; interestingly, this protein binds CL and in co-operation with CL is required for the maintenance of highly curved cristae membrane structures [45,54]. It is possible that the physical association of Taz1 with ATP synthase could facilitate the

quick reshuffling of CL fatty acyl composition to stabilize cristae structures. In light of these findings, it is suspected that tafazzin could exchange acyl groups to adapt the lipid composition to suit the needs of a specific membrane structure and in effect it may serve as a "membrane chaperone" [97].

1.13 TAFAZZIN DEFICIENCY IN *Saccharomyces cerevisiae*

Transacylase activity of purified yeast Taz1 has not been directly confirmed, however, estimation of transacylase activity by the production of CL and PC from MLCL and LPC respectively was markedly reduced in isolated mitochondria from *taz1*Δ yeast [1]. Inactivation of *TAZ1* resulted in a decrease in CL mass with the remaining CL having saturated acyl species, and an accumulation of MLCL as was seen in BTHS cells [78]. The preceding findings, specific localization of Taz1 in yeast mitochondria and the ability of human tafazzin to complement for the loss of *TAZ1* confirmed that the transacylase function of tafazzin is conserved from yeast and humans [84,93,94].

Loss of remodeled CL in BTHS patients led to severe defects in mitochondrial morphology characterized by giant abnormal mitochondria with MIM adhesions and loss of cristae structures [81]. In yeast, deletion of *TAZ1* led to occasional swollen mitochondria and mitochondria with elongated and hypertrophied cristae structures [98], however, a recent analysis of mitochondrial defects in *crd1*Δ (cannot make *de novo* CL) and *taz1*Δ yeast showed that alterations in morphology were more subtle, with mitochondria containing longer MOM and cristae membranes when compared to wild-type yeast [83]. In addition, the minor alterations in mitochondrial membrane length in

these CL mutants seemed to be strain dependent [83]. Further, the above study also showed that only the wild-type W3031-a yeast cells do not possess any defects in mitochondrial morphology when compared to the other laboratory wild-type yeast cells. The above study underlines the importance of carefully choosing the yeast strain to study mitochondrial defects and given that the W3031-a yeast strain is free of inherent mitochondrial morphology defects this strain could be a valuable model system to study mitochondrial biology.

CL is proposed to be a glue that organizes the assembly of various components of ETC and AAC into a higher-order supramolecular structures to facilitate efficient transfer of electrons between the energy-generating machinery of mitochondria [45,48]. In humans, loss of tafazzin function caused disruptions in the organization of bioenergetic machinery into supramolecular structures [53]. In *taz1*Δ yeast, ETC complex IV was shown to more easily disassociate from III2IV and III2IV2 super complexes [49], but this was not observed in other studies [45,83,98]. Therefore, the role of remodeled CL in the supramolecular organization of the ETC is not clear.

The rate of oxygen consumption is proportional to the amount of ADP phosphorylated to ATP; estimation of oxygen consumption after the addition of known amounts of ADP (state III respiration) and after the exhaustion of added ADP (state IV respiration) in isolated mitochondria is used to assess mitochondrial respiration [45,94]. In normal mitochondria, due to limitations in electron transfer, state IV respiration is lower than state III respiration [45,94]. The ratio of state III over state IV respiration (RCR, or respiratory control ratio) is a measure of OXPHOS coupling and MIM stability [45,94].

Negligible RCR means that electron transfer is uncoupled from ATP synthesis, with potential leakage of electrons from the IMS to the matrix causing a loss of proton gradient across the MIM [45,94]. In both *crd1*Δ and *taz1*Δ yeast, RCR was lower than in wild-type cells, but OXPHOS was uncoupled only when these mutants were heat stressed by growth at 40˚C [50,51,83,94]. The efficiency of phosphorylation could be estimated by the measuring the amount of oxygen atoms reduced per ADP converted to ATP (ADP:O ratio) (Ma 2004; Koshkin & Greenberg 2002; Koshkin & Greenberg 2000). Estimation of ADP:O ratio in CL mutants showed reduced values, with the efficiency of ATP generation more pronounced in *crd1*Δ cells than *taz1*Δ cells [83,94]. Estimation of respiration after OXPHOS is uncoupled from ATP generation, by the addition of an uncoupler like CCCP (2-[2-(3-Chlorophenyl) hydrazinylyidene] propanedinitrile), showed that maximum electron transport capacity was unaffected in *taz1*Δ cells and was only moderately reduced in *crd1*Δ yeast [83]. These results are in agreement with the finding that *taz1*Δ yeast cells are viable in growth conditions (non-fermentable carbon sources like ethanol, lactate and glycerol) that require mitochondrial ATP generation. However, growth of *taz1*Δ yeast cells was severely hampered in non-fermentable media when cells were stressed by growth at 37˚C [78,83]. Interestingly, loss of Taz1 function led to increased ROS generation when these cells were grown in ethanol medium at 37˚C [99]. Moreover, this increase in ROS could not be attributed to defects in ROS scavenging under these growth conditions [99]. These findings showed that Taz1 function, although necessary for mitochondrial energy production when under heat stress, is not an absolute requirement for the maintenance of OXPHOS and MIM stability under normal conditions.

1.14 *Saccharomyces cerevisiae*: A MODEL SYSTEM TO STUDY TAFAZZIN BIOLOGY

Yeast with its simpler CL metabolism and tractable tools for genetic manipulation has helped to shed some light on the pathophysiology of BTHS by establishing genotype-phenotype correlations for tafazzin mutations [83,100].

Until recently, it was not clear if the loss of CL mass and the corresponding increase in MLCL, or the lack of remodeled CL, were the cause of the mitochondrial abnormalities observed in BTHS patients and in the various models of tafazzin deficiency [2]. In yeast, saturated acyl species from *de novo* CL synthesis are specifically deacylated by Cld1 to generate MLCL, which is then reacylated to remodeled CL by Taz1 [11,100]. There are no redundant or parallel pathways affecting CL remodeling. Deletion of the *CLD1* gene causes accumulation of saturated acyl species in CL. Analysis of OXPHOS showed that ADP:O ratio, RCR, state III and IV respiration and electron transport capacity were not affected in *cld1*Δ mutant, implying that remodeled CL is not an absolute requirement for OXPHOS function [83]. Further, concomitant deletion of *CLD1* in *taz1*Δ cells prevented MLCL accumulation, restored growth at 37˚C in medium with ethanol as sole carbon source [83], and rescued all OXPHOS defects [83]. Collectively, these findings led to the conclusion that the absolute mass changes in CL and MLCL, and not the defect in remodeling CL, is required for OXPHOS function of yeast mitochondria. However, in mammals, the CL deacylase that generates MLCL is not known, and its identification might be complicated by the potential involvement of multiple phospholipases in CL turnover [21,101]. Therefore, at this moment it is not possible to dissect the individual role of *de novo* CL, mature CL, and MLCL in mitochondrial function in mammals.

To date, 36 missense *TAZ* mutations have been reported in BTHS; of these, many are predicted to produce mutated proteins [100,102]. However, until recently the molecular mechanisms of how these mutant polypeptides lose their function was not known. Claypool and colleagues identified that the majority of these BTHS mutations occur at either identical or conserved residues that are between human and yeast tafazzin [102]. Further, overexpression of Taz1 from three individual *TAZ1* plasmid constructs that contained conserved human *TAZ* amino acid residue substitutions instead of the yeast were able to reverse MLCL accumulation in *taz1*Δ yeast [102]. These findings validated the conserved biochemical function of human and yeast tafazzin and lend credibility to the study of loss-of-function mechanisms of BTHS missense mutations in yeast [102]. Of 21 BTHS mutants studied, 20 were non-functional (failed to reverse MLCL abundance) when overexpressed in *taz1*Δ yeast [100]. Among these, three mutants altered a putative membrane anchor domain of Taz1, which anchors the peptide to the IMS leaflet of MOM and MIM [103]. Peptides with these mutations had lower expression and were shown to mislocalize to the matrix. A concomitant deletion of the IMS quality-control protein Yme1 improved their expression; however, in its absence the mutant peptides formed detergent-resistant aggregates [100,103]. Interestingly, *in vitro* mitochondria import assays indicated that Yme1 deletion improved the import of both wild-type and mutant Taz1 peptides and, importantly, in its absence the transacylase activity of wild-type Taz1 was significantly reduced [100]. These findings implied that the proteolytic function of Yme1 is necessary for quality-control to weed out aberrant Taz1 to ensure its catalytic efficiency. Of the other non-functional mutations, a majority of them were located in and around the putative acyl transferase motifs of Taz1 producing catalytically dead proteins

[100]. In addition, point mutations that produced polypeptides with defective assembly, thermosensitivity and reduced catalytic function were also identified [100]. In summary, these studies in yeast identified the multiple loss-of-function mechanisms for BTHS missense mutations and in the process elucidated the biology of Taz1 by identifying a putative membrane anchor region that might be necessary for its proper localization. It also showed the importance of the mitochondrial quality-control protein Yme1 for Taz1 assembly and activity.

1.15 MURINE MODEL OF BTHS

Tafazzin expression in mouse was abolished by using a tetracycline-inducible (tet-on) shRNA system to knockdown *Taz* expression [104,105]. *Taz* mRNA levels were reduced in cardiac and skeletal-muscle by 85-95% when the *Taz* shRNA was expressed by the addition of doxycycline to the diet [104,105]. Although inhibition of *Taz* expression resulted in MLCL accumulation and loss of mature L4-CL by 2 months of age in skeletal and cardiac muscles, mitochondrial abnormalities such as vacuolated cristae, MIM adhesions and mitophagy were noticed only in skeletal-muscle but not in cardiomyocyte mitochondria [104,105]. In agreement with this finding, *in vivo* cardiac function measured by echocardiography was normal at 2 months of age [104,105]. Mitochondrial abnormalities and cardiac function were significantly compromised only as the mice aged to 8 months, and this pattern does not recapitulate the early onset of neonatal cardiomyopathy in BTHS [104,105]. However, a higher dose of doxycycline was shown to induce *Taz* mRNA knockdown as early as embryonic day 10.5 (E 10.5) and was associated with mitochondrial defects such as vacuolated cristae, reduced cristae density,

and a reduction in mitochondrial size in hearts [76]. Careful histological analyses of E10.5 hearts also showed ventricular traberculations and left ventricular wall thinning or compaction as is seen in BTHS patients [76]. Interestingly, unlike the majority of BTHS patients, none of these mice survived beyond the newborn stage and in utero deaths of pups were significantly higher in doxycyline fed mothers than in controls [76]. Although the mechanistic details are not clear, this study emphasized that BTHS is a developmental disorder and that tafazzin is important for heart development [76].

CHAPTER 2. RATIONALE AND OBJECTIVES

In BTHS, and in the multiple models of tafazzin deficiency, mutations in *TAZ* inhibit the remodeling of *de novo* CL to mature CL. This inhibition results in reduced CL mass with the CL present having more saturated fatty acyl chains, and an increase in the level of the tafazzin substrate MLCL. This altered CL metabolism causes mitochondrial dysfunction as observed through aberrant mitochondrial structure, decreased organization of the ETC, and decreased energy production. Further, how mitochondrial dysfunction results in the myriad of symptoms seen in BTHS patients is not well understood.

The *S. cerevisiae* yeast system allows facile and tractable genetic manipulations allowing genome-wide screens to be performed, uncovering new genotype-phenotype correlations. My aim was to use this system to identify genes whose inactivation impacts the fitness of yeast cells that had lost tafazzin function. From the genes identified, and their known functions, I characterized processes that affect cell health and fitness in the absence of tafazzin, to further our understanding of the precise cellular processes that could impact BTHS.

CHAPTER 3. MATERIALS AND METHODS

3.1. REAGENTS

Reagents for molecular biology came from different sources, custom oligonucleotides were acquired from Integrated DNA Technologies (IDT), HiFi Taq DNA polymerase from Invitrogen was used to perform PCR amplifications, and all the restriction enzymes and T4 DNA ligase used in cloning procedures were purchased from New England BioLabs. Plasmids from bacteria were purified using the QIAprep Spin Miniprep Kit from Qiagen. Genomic DNA was purified from yeast with the Yeast DNA Extraction Reagent (Y-DER) Kit from Pierce. DNA fragments and PCR amplicons used for ligation were cleaned with the GeneCleanII Kit from Bio-101. For phospholipid labelling ^{32}P orthophosphoric acid was purchased from PerkinElmer. Phospholipids were resolved by thin layer chromatography (TLC) on LK5 silica gel 150 A TLC plates from Whatman. N-[3-triethylammoniumpropyl]-4-[p-diethylaminophenylhexatrienyl] pyridinium dibromide (FM4-64) from Molecular Probes was used to assess yeast vacuolar morphology. Most yeast and bacterial growth media were purchased from Difco except for Synthetic Complete (SC) media (SC and SC-uracil), which were from Sunrise Science products. Complete protease-inhibitor tablets with or without EDTA were from Roche. Nourseothricin (NAT) or ClonNAT was from Werner BioAgents. The yeast strain CWY-152 (W3031-α *OM45-GFP*::*TRP1)* used to assess mitophagy was a kind gift from Dr. Kanki at Kyushu University School of Medical Sciences, Japan. Native 3-12% precast Bis-Tris PAGE gels from Invitrogen were used to resolve mitochondrial proteins. For a complete list of the yeast strains used in this study see **Table 1.**

Table 1 Yeast strains used in this study.

Strain	Genotype	Source
BY4741 (CBY 300)	*MAT***a** *his3Δ1 leu2Δ0 met15Δ0 ura3Δ0*	EUROSCARF
CBY 301	BY4741 *yme1Δ::KANMX4*	EUROSCARF
Y2454 (CBY 302)	*MATα mfa1Δ::MFA1pr-HIS3 can1Δ0 his3Δ1 leu2Δ0 ura3Δ0 lys2Δ0*	[106]
CBY 303	Y2454 *taz1Δ::NATMX4*	This study
CBY 304	BY4741 *crd1Δ::KANMX4*	EUROSCARF
W3031-a (CWY 150)	*MAT***a** *leu2-3,112 trp1-1 can1-100 ura3-1 ade2-1 his3-11,15*	Thermo Scientific
W3031-α (CWY 151)	*MATα leu2-3,112 trp1-1 can1-100 ura3-1 ade2-1 his3-11,15*	Thermo Scientific
CWY 152	W3031-α *OM45-GFP::TRP*	[107]
CWY 153	W3031-a *taz1Δ::NATMX4*	This study
CWY 154	W3031-α *yme1Δ::KANMX4*	This study
CWY 155	W3031-a *taz1Δ::NATMX4 yme1Δ::KANMX4*	This study
CWY 156	W3031-a *OM45-GFP::TRP*	This study
CWY 157	W3031-a *OM45-GFP::TRP taz1Δ::NATMX4*	This study
CWY 158	W3031-a *OM45-GFP::TRP yme1Δ::KANMX4*	This study
CWY 159	W3031-a *OM45-GFP::TRP yme1Δ::KANMX4 taz1Δ::NATMX4*	This study

3.2. MEDIA

Yeast were normally grown in rich medium containing 1% bacto-yeast extract, 2% bacto-peptone, 2% carbon source and 2% agar (included to make solid medium). The fermentable carbon source dextrose, or the non-fermentable carbon source lactate, was added to the yeast extract peptone mixture (YP) to make YP with dextrose (YPD) or YP with lactate (YPL), respectively. Synthetic defined (SD) medium or minimal medium typically contained 2% dextrose, 0.67% bacto-yeast nitrogen base and only these amino acids (20 mg/L adenine sulfate, 20 mg/L L-histidine HCl, l00 mg/L L-leucine, 30 mg/L L-lysine, 20 mg/L L-methionine, 20 mg/L L-tryptophan, and 20 mg/L uracil) to account for auxotrophies that often occur in our laboratory yeast strains. In certain experiments, such as in SGA analysis, some amino acid(s) (SD - histidine) are excluded to facilitate selection of yeast cells. When G418 was required in SD medium, the medium contained 1% monopotassium glutamate, 0.17% yeast nitrogen base devoid of both ammonium sulphate & amino acids, 2% dextrose and the required amino acid supplements. SD medium containing 2% dextrose and 0.17% yeast nitrogen base without ammonium sulphate & amino acids (SD-N) was used to induce mitophagy. SC medium usually contained 2% dextrose, 0.67% bacto-yeast nitrogen base, 85.6 mg/L of the following amino acids and supplements: L-alanine, L-arginine HCl, L-asparagine, L-aspartic acid, L- cysteine HCl, glutamine, L-glutamic acid, glycine, L-histidine HCL, myo-inositol, L-isoleucine, L-lysine HCl, L-methionine, L-phenylalanine, L-proline, L-serine, L-threonine, L-tryptophan, L-tyrosine, uracil, and L-valine, 21 mg/L adenine, 173.4 mg/L L-leucine, and 8.6 mg/L para-aminobenzoic acid. However, in experiments that forced yeast to undergo mitochondrial respiration, the dextrose in SC was substituted with 2%

lactate (SC medium with lactate). SC medium lacking uracil (SC-uracil) was used to select for yeast transformed with pRS416-based plasmids. Bacteria used for cloning and propagation of yeast plasmids were grown in Luria Bertani (LB; contains 10g/L tryptone, 5g/L yeast extract, 10g/L sodium chloride) broth or on LB solid medium (with 2% agar). Ampicillin (100mg/L) was included in LB medium to select for colonies with plasmids after transformation.

3.3. YEAST TRANSFORMATIONS

Yeast cells were transformed with plasmid DNA or PCR amplicons of genomic DNA as described [108] using the lithium acetate/polyethylene glycol method. Cells were grown in 5-10 ml of YPD medium at 25˚C until they reached mid-log phase (0.5 OD_{600}). After that, they were harvested by centrifugation at 3000 rotations per minute (rpm) for 5 min in an eppendorf microfuge. The pellet was then resuspended in 50 µL of 100 mM lithium acetate, 10 mM Tris-HCl pH 8.0 and 0.1 mM EDTA (LiAc/TE). The DNA to be transformed (1-3 µg) and heat-denatured herring sperm DNA (50 µg) were added to the resuspended pellet, mixed by inversion and then incubated at room temperature. After 5 min, 300 µL LiAc/TE containing 40% polyethylene glycol 3400 was added to the above mixture and thoroughly vortexed before the contents were transferred to 14-ml culture tubes (Bio-Rad). The tubes were then incubated in a water bath at 42˚C for 1 hour with intermittent gentle shaking. At the end of the incubation period, the cell suspension was centrifuged for 30 sec at 14000 rpm, the resulting pellet was washed once with 10 mM Tris-HCl pH 8.0 and 0.1 mM EDTA (TE) and then resuspended in 100 µL of TE. The entire mixture was plated evenly on suitable solid medium containing selective agar

medium (SC -uracil solid medium for transformation with pRS416-based plasmids) or YPD medium (for targeted gene disruptions). The cells were incubated at 25˚C for 2-4 days except in the case of targeted gene disruptions, wherein the cells were incubated overnight before they were replica plated onto appropriate selective medium.

3.4. CONSTRUCTION OF W3031-a *taz1*Δ::*NATMX4* (CWY-153), BY2454 *taz1*Δ::*NATMX4* (CBY-303) AND W3031-α *yme1*Δ::*KANMX4* (CWY-154) YEAST STRAINS

The *TAZ1* gene in CWY-153 and CBY-303 cells was disrupted and replaced with a NAT-resistance marker by homologous recombination using a PCR-generated *taz1*Δ*::NATMX4* gene disruption cassette [109]. The primer pair F-taz_M (5'-*TCT TTT AGG GAT GTC CTA GAA AGA GGA GAT TTT TTA GAA GCC TA*A CAT GGA GGC CCA GAA TAC CC) and R-taz_M (5'-*ATC ATC CTT ACC CTT TGG TTT ACC CTC TGG AGG CAG AAA CTT TTG CAG* TAT AGC GAC CAG CAT TCA C) was used to amplify the *NATMX4* gene from the plasmid pAG25 (EUROSCARF). Each primer contained at their 5' ends 44 (F-taz_M; italicized) or 47 (R-taz_M; italicized) nucleotides identical to the regions adjacent to *TAZ1* translational start and stop sites. At their 3' ends they contained a 20-nucleotide stretch of *NATMX4* specific sequence. This arrangement resulted in a PCR product that contained the *NATMX4* cassette with extensions homologous to the regions proximal to the translation start and stop sites of the *TAZ1* gene. The PCR amplicon was purified with the GeneCleanll Kit (Bio-101) and then transformed (see **section 3.3**) into W3031-a (CWY-150) and BY2454 (CBY-302) yeast strains, and transformants were plated on YPD solid and grown overnight at 25˚C to allow homologous recombination. To select for transformants with a disrupted *TAZ1* coding

sequence, the resulting lawn of cells was replica plated to YPD solid medium containing ClonNAT (100mg/L, Werner BioAgents). Genomic DNA from these transformants was purified using Y-DER (yeast DNA extraction reagent) Kit (Pierce) and then used for PCR amplification with primers TAZ5 flanking forward (5'-CCATTGTCTCTCCAATTGGTG) and TAZ3 flanking reverse (5'-TCATGCTTTAGGTCAGCCTGA) that bound (- 367 bp) upstream and downstream (+408 bp) of the *TAZ1* coding sequence, respectively. The generated PCR product comprised a NdeI site if it harbored the wild-type *TAZ1* coding sequence and this site was abolished and replaced by a XmaI site if disrupted by the *taz1*Δ*::NATMX4* cassette. Therefore, PCR amplicons generated from the transformants were subjected to restriction enzyme digestion with XmaI (New England Biolabs) or NdeI (New England Biolabs) to confirm the successful disruption of the *TAZ1* coding sequence.

The CWY-154 strain was generated in a similar manner with the gene disruption cassette *yme1*Δ*::KANMX4* PCR amplified from genomic DNA purified from CBY-301 (BY4741 *yme1*Δ*::*KANMX4) cells using primers Yme1F (5'-AGCAAGCACAGCTTAAAGGA) and Yme1R (5'-ATGAAGCAAAAGCGAAACCG). To enable homologous recombination between the disruption cassette and the wild-type *YME1* allele of CWY-151 (W3031-α), the primers were designed such that they were homologous to the upstream and downstream flanking regions of the *YME1* coding sequence. The PCR-generated *yme1*Δ*::KANMX4* was then used to transform the CWY-151 strain, and transformants were selected on solid medium containing G418 (200 mg/L, Invitrogen). To confirm *YME1* open reading frame (ORF) disruption, genomic DNA purified from transformants was used to amplify the flanking regions of *YME1* coding sequence using

primers cYme1F (5'-GTTAAATCTCTACCTTGCGTTTTTGA) and cYme1R (5'-TGCTGGTGTTATGAAGCAAAAGC) that bind upstream and downstream of the translation start and stop codons, respectively. Successful disruption of *YME1* generated shorter PCR products (1.86 Kbp) compared to amplicons (2.47 Kbp) generated from transformants with wild-type *YME1*.

3.5. CONSTRUCTION OF pRS416 PLASMID EXPRESSING *TAZ1*

To express *TAZ1* exogenously from its own promoter, its coding sequence along with its upstream (-340 bp from translation start site) and downstream (+200 bp from stop codon) flanking regions was PCR-amplified and subcloned to the pRS416 plasmid. The primers TazF_BglII_8140454 (5'-GGAAGATCTATTTTGTCACCTCGTAGGAGC) and TazR_XhoI_815730 (5'-CCGCTCGAGCAAGGCCTTTTCTGGTCTTT) that include the BglII and XhoI restriction enzyme sequence overhangs, respectively, were used to PCR-amplify the specified DNA insert from genomic DNA extracted from CWY-150. The PCR product was digested with BglII and XhoI and then ligated into the pRS416 plasmid already linearized with BamHI and XhoI. The ligation was carried out overnight at 14˚C with the aid of T4 ligase.

The ligation mixture (1μL) was then mixed with electro-competent DH10B *Escherichia.coli* cells (Invitrogen) in a 0.1-cm electroporation cuvette and then electroporated at 1.56 kV using a Bio-Rad Genepulser II. After that, 1 ml of SOC medium (0.5% yeast extract, 2% tryptone, 10 mM NaCl, 2.5 mM KC1, 10 mM $MgCl_2$, 20 mM $MgS0_4$, 20 mM glucose) was added to the cells before they were transferred to 14-ml

culture tubes (Bio-Rad). The tubes were incubated at 37˚C under constant shaking, and after 30 min, their contents were evenly spread on LB solid medium containing 100mg/L ampicillin and incubated overnight at 37˚C. Resultant colonies containing the pRS416 *TAZ1* plasmid were grown for 16 hrs in 3 ml of LB broth containing 100mg/L ampicillin. Plasmids were isolated from these cultures using a QIAprep Spin Miniprep Kit (Qiagen) and assessed for the successful generation of pRS416 *TAZ1* plasmid. This was confirmed by the release of the *TAZ1* open reading frame containing insert from the isolated plasmids after restriction enzyme digest with SacI and XhoI. The *TAZ1* gene was sequenced to ensure polymerase fidelity.

3.6. SYNTHETIC GENETIC ARRAY (SGA) ANALYSIS

In *S. cerevisiae,* there are about 5000 non-essential genes; deletion of any one these genes from a haploid yeast cell does not affect its viability. At present, approximately 4700 mutants (deletion-collection) each carrying a single non-essential-gene deletion is available as an ordered array from EUROpean *Saccharomyces cerevisiae* archive for functional analysis (EUROSCARF). In each deletion-collection mutant, the deleted gene is replaced by a dominant kanamycin-resistance selectable marker (*KANMX4)*. A query strain carrying a nourseothricin-resistance marker (*NATMX4*) that replaces the ORF of a gene of interest is then generated. SGA analysis, with the aid of robotics, facilitates large-scale mating between the query strain and each of the deletion-collection mutants to generate an array of 4700 diploid cells each a haploid for the gene of interest and a non-essential yeast gene. Since the disrupted genes in question are replaced with antibiotic-resistance markers, double mutants can be easily selected on medium containing both

G418 (200 mg/L, Invitrogen) and ClonNAT (100 mg/L, Werner BioAgents). Among the 4700 double mutants so produced, some may not be viable, or may grow much more slowly than normal, indicating a synthetic lethal or synthetic sick interaction between the genes. This type of result generally indicates that the proteins encoded by the two genes either act in single large complex or they function in parallel compensatory pathways. Identification of such genetic interactions has been successfully used in the past to define gene function [106].

SGA analysis was conducted as previously described [106]. The query strain CBY-303 was generated by replacing the *TAZ1* coding region with the *NATMX4* cassette in *MATα* Y2454 yeast cells by PCR-based gene replacement as described above (**section 3.4**). This strain was then robotically crossed with each of the *MAT***a** deletion-collection mutants and the array of generated diploids was selected on plates with YPD solid medium containing both G418 and ClonNAT. Meiosis was induced in these diploids by robotically transferring them to sporulation medium (2% agar, 1% potassium acetate, 0.1% yeast extract, 0.05% glucose, supplemented with uracil, histidine, and leucine). After 5 days of sporulation at 22˚C, *MAT***a** haploid spores that derived from mating between the query strain and the deletion-collection strains were specifically selected by incubating the spores in SD medium lacking histidine and arginine but containing canavanine (SD - His/Arg, canavanine 50 mg/L) for 2 days at 30˚C. The *MATα* query and the *MAT***a** deletion-collection mutants are histidine auxotrophs and do not grow in the absence of histidine. However, the query strain carries the *HIS3* gene under the control of the a-factor gene activated promoter (*MFApr*) such that *HIS3* gene is only expressed in *MAT***a** cells. Therefore, growth in SD medium without histidine will only support the growth of

*MAT***a** haploid spores that resulted from mating between the query and one of deletion-collection mutants. In addition, unlike the deletion mutants, the query strain has a defective arginine permease gene (*can1*Δ) and therefore cannot take up arginine or its analogue canavanine from the growth medium. When canavanine instead of arginine is present in the growth medium, *CAN1* cells, with permease activity incorporate it into cells causing lethality. Therefore, inclusion of canavanine (50 mg/L) in the haploid selection medium provides further insurance that only haploid spores and not *CAN1/can1*Δ diploids are selected for further analysis. After another round of selection in haploid selection medium, the cells were robotically transferred to SD solid medium containing G418 (SD - His/Arg, G418 200 mg/L, canavanine 50 mg/L) and incubated for one day before they were finally transferred to solid medium containing both G418 and ClonNAT (SD - His/Arg, G418 200 mg/L, ClonNAT 100 mg/L, canavanine 50 mg/L) and incubated for two days at 30˚C. The double-mutant haploid arrays produced in this way were manually screened for lethality and growth defects and validity of the observed genetic interactions was checked by random spore analysis and/or tetrad analysis.

3.7. RANDOM SPORE ASSAY TO CONFIRM *TAZ1* AGGRAVATING GENE DELETIONS

Of the 159 genes that showed genetic interaction with *TAZ1,* 35 (**Table 2**), based on their having a role in the mitochondria, were selected for random spore assays. The CBY-303 strain was manually mated with each of 35 single-gene mutants from the deletion-collection and the resulting diploids were selected on YPD solid medium containing (G418 200 mg/L, ClonNAT 100 mg/L). The diploids were suspended at approximately 2×10^7cells/ml in sporulation broth (1% potassium acetate, 0.1% yeast extracts, 0.05%

glucose, supplemented with uracil, histidine, and leucine) and then allowed to sporulate for 5-6 days. The spores were harvested and suspended at approximately 5×10^8cells/ml in distilled water containing 100µg/ml zymolase 100T and incubated for 15 min at 30˚C to completely digest the yeast spore cell wall. After that, 0.5-ml aliquots were transferred to 1.5-ml Eppendorf tubes and then pelleted at 14,000 g for 30 sec, the supernatant was disposed of and the pellets were resuspended in 1 ml of distilled water, centrifuged as before and then resuspended in 0.1 ml of fresh distilled water. This mixture was vigorously vortexed for 2 min, since the spores are far more hydrophobic than vegetative cells; they clump together and also adhere to polypropylene walls of the 1.5 ml Eppendorf tubes. The vegetative cells were discarded by several washings in distilled water before the adhered spores were resuspended by the addition of 1 ml of water containing 0.01% Nonidet P-40 (Sigma) and sonicated in ice for 1-3 min. The purified spores were diluted and about 200 spores were evenly plated on solid medium containing SD -His/Arg, SD - His/Arg, G418 200 mg/L, and SD - His/Arg, G418 200 mg/L, ClonNAT 100 mg/L and allowed to grow at 30˚C. The resultant colonies were counted after 3-5 days manually and with the help of Quantity One software (Bio-Rad VersaDoc). Spores that carried double mutants with true genetic interaction with *TAZ1* typically did not grow in SD - His/Arg, G418 200 mg/L, ClonNAT 100 mg/L medium.

Table 2. List of genes selected for random spore analysis.

Standard Name	Systematic Name	Saccharomyces Genome Database description [110]
Mitochondrial quality-control		
YTA12	*YMR089C*	Mitochondrial inner membrane m-AAA protease; mediates degradation of misfolded or unassembled proteins; also required for correct assembly of mitochondrial enzyme complexes
YME1	*YPR024W*	Catalytic subunit of the i-AAA protease complex; responsible for degradation of unfolded or misfolded mitochondrial gene products; also has a role in intermembrane space protein folding; mutation causes an elevated rate of mitochondrial turnover
Mitochondrial iron metabolism		
ISA2	*YPR067W*	Protein required for maturation of mitochondrial [4Fe-4S] proteins; localizes to the mitochondrial intermembrane space
GGC1	*YDL198C*	Mitochondrial GTP/GDP transporter; essential for mitochondrial genome maintenance; has a role in mitochondrial iron transport; member of the mitochondrial carrier family
ISA1	*YLL027W*	Protein required for maturation of mitochondrial [4Fe-4S] proteins; functions in a complex with Isa2 and possibly Iba57; *ISA1* deletion causes loss of mitochondrial DNA and respiratory deficiency; depletion reduces growth on nonfermentable carbon sources; functional ortholog of bacterial A-type ISC proteins
ETC components / ETC biogenesis		
ATP18	*YML081C-A*	Subunit of the mitochondrial F1F0 ATP synthase; F1F0 ATP synthase is a large, evolutionarily conserved enzyme complex required for ATP synthesis; termed subunit I or subunit j; does not correspond to known ATP synthase subunits in other organisms
AEP3	*YPL005W*	Peripheral mitochondrial inner membrane protein; may facilitate use of unformylated tRNA-Met in mitochondrial translation initiation; stabilizes the bicistronic mRNA containing two subunits of ATP synthase.
ATP17	*YDR377W*	Subunit f of the F0 sector of mitochondrial F1F0 ATP synthase; F1F0 ATP synthase is a large, evolutionarily conserved enzyme complex required for ATP synthesis
SUE1	*YPR151C*	Protein required for degradation of unstable forms of cytochrome c; located in the mitochondria

Standard Name	Systematic Name	Saccharomyces Genome Database description [110]
Maintenance of Mito-DNA / respiration / oxidative stress		
IDP1	*YDL066W*	Mitochondrial NADP-specific isocitrate dehydrogenase; catalyzes the oxidation of isocitrate to alpha-ketoglutarate; not required for mitochondrial respiration and may function to divert alpha-ketoglutarate to biosynthetic processes
CEM1	*YER061C*	Mitochondrial beta-keto-acyl synthase; possible role in fatty acid synthesis; required for mitochondrial respiration
MHR1	*YDR296W*	Protein involved in homologous recombination in mitochondria; required for recombination-dependent mtDNA partitioning; involved in stimulation of mitochondrial DNA replication in response to oxidative stress
GND1	*YHR183W*	6-phosphogluconate dehydrogenase (decarboxylating); catalyzes an NADPH regenerating reaction in the pentose phosphate pathway; required for growth on D-glucono-delta-lactone and adaptation to oxidative stress
ECM31	*YBR176W*	Ketopantoate hydroxymethyltransferase; required for pantothenic acid biosynthesis, converts 2-oxoisovalerate into 2-dehydropantoate
Mitochondrial protein import		
OCT1	*YKL134C*	Mitochondrial intermediate peptidase; cleaves destabilizing N-terminal residues of a subset of proteins upon import, after their cleavage by mitochondrial processing peptidase (Mas1-Mas2); may contribute to mitochondrial iron homeostasis
MBA1	*YBR185C*	Membrane-associated mitochondrial ribosome receptor; forms a complex with Mdm38 that may facilitate recruitment of mRNA-specific translational activators to ribosomes; possible role in protein export from the matrix to inner membrane
TOM5	*YPR133W-A*	Component of the TOM (translocase of outer membrane) complex; responsible for recognition and initial import of all mitochondrially directed proteins; involved in transfer of precursors from the Tom70 and Tom20 receptors to the Tom40 pore
Arginine metabolism		
ORT1	*YOR130C*	Ornithine transporter of the mitochondrial inner membrane; exports ornithine from mitochondria as part of arginine biosynthesis

3.8. TETRAD ANALYSIS TO CONFIRM GENETIC INTERACTION BETWEEN *TAZ1* AND *YME1*

Tetrad analysis was performed to determine the validity and strength of the negative genetic interaction between *TAZ1* and *YME1*. Yeast strains CWY-153 (W3031-a *taz1*Δ::*NATMX4*) and CWY-154 (W3031-α *yme1*Δ::*KANMX4*) were mated on YPD solid medium at 25˚C. The resulting diploids were selected on YPD solid medium containing G418 200 mg/L and ClonNAT 100 mg/L for 2 days. After that, cells were sporulated for 5-6 days at 22˚C in sporulation medium (2% agar, 1% potassium acetate, 0.1% yeast extracts, 0.05% glucose, supplemented with leucine, tryptophan, uracil, adenine and histidine at 50% of normal requirement). With an inoculation needle, a matchstick-head-size clump of spores was suspended in 50 μL of zymolase 100T solution (0.5 mg/ml zymolase in 1M sorbitol). This mixture was incubated at 30˚C to enable the partial digestion of the yeast spore cell walls, and after 10 min placing the tube on ice stopped the digestion. The spore mixture was then diluted with distilled water to 0.5-1 ml before transfer to YPD solid medium. Under a micro-dissection microscope, intact ascii, each containing 4 spores, were teased with a micro-dissection needle and placed at distinct positions within the YPD plate. The separated spores were then allowed to germinate into haploid colonies for 2-3 days at 25˚C. The resulting colonies were then replica-plated onto YPD solid medium containing G418 200 mg/L and ClonNAT 100 mg/L and incubated for 2 days. There, growth was determined and their sensitivity to G418 and ClonNAT was used to infer the genetic makeup of each haploid strain. The haploid strains from the tetrad dissection were also assessed for growth by spot dilution assays (**section 3.10**) on solid YPD or SC medium containing 2% lactate. The *taz1*Δ *yme1*Δ haploid spores grew much slower than both single-mutant and wild-type cells. One of

these strains, CWY-155 (W3031-a *taz1*Δ*::NATMX4 yme1*Δ*::KANMX4*), was chosen for further analysis.

3.9. CONSTRUCTION OF YEAST STRAINS FOR Om45-GFP ASSAY

Yeast strains carrying a chromosomal version of *OM45*-GFP were utilized to monitor mitophagy [107]. The strain CWY-152 (W3031-α *OM45-GFP*::*TRP1),* a gift from Dr. Kanki (Kyushu University School of Medical Sciences, Japan), was used through standard yeast mating and tetrad dissections to replace the *YIL136W* gene (encodes Om45) with GFP tagged *OM45-GFP*::*TRP1* allele in *taz1*Δ *yme1*Δ cells and in *taz1*Δ and *yme1*Δ single mutants. To generate a *MAT***a** version of wild-type yeast with *OM45-GFP*::*TRP1,* CWY-152 was mated with wild-type CWY-150 (W3031-a). The diploids were selected on SD medium lacking tryptophan (SD-trp) and then were sporulated, and the resulting spores were dissected and allowed to germinate on YPD medium as described above (**section 3.8**). Haploid colonies that grew on SD-trp solid medium were selected and confirmed for Om45-GFP tagging by observing mitochondrial GFP fluorescence using the GFP filter fitted to a Zeiss Axiovert 200M microscope. To determine mating type (*MAT***a** *or MATα*), colonies that showed mitochondrial GFP fluorescence were then subjected to yeast mating halo assay. The selected colonies were patched on YPD solid medium and then replica-plated on to YPD solid medium containing 0.05% Triton X-100 already spread with a lawn of *MAT***a** or *MATα* tester strains. If the selected haploid colony replica were a *MAT***a** cell*,* it would inhibit the growth of *MATα* tester lawn, producing a halo around it. This mating-type assay identified five *MAT***a** colonies, and after further testing for Om45-GFP fluorescence, one,

CWY-156 (W3031-a *OM45-GFP*::*TRP1*), was selected for mitophagy assay and for the generation of CWY-158 (W3031-a *yme1*Δ*::KANMX4 OM45-GFP*::*TRP1*) cells. Yeast strains CWY-157 (W3031-a *taz1*Δ*::NATMX4 OM45-GFP*::*TRP1*), CWY-159 (W3031-a *taz1*Δ*::NATMX4 yme1*Δ*::KANMX4 OM45-GFP*::*TRP1*) and CWY-158 (W3031-a *yme1*Δ*::KANMX4 OM45-GFP*::*TRP1*) were generated as described for CWY-156 cells. The CWY-152 strain was mated with CWY-153 and CWY-155 to generate CWY-157 and CWY-159 cells, respectively. The CWY-156 was mated with CWY-154 to generate CWY-158 cells. Appropriate selection media (SD-trp, ClonNAT 100 mg/L; SD-trp, G418 200 mg/L; and, SD-trp, G418 200 mg/L, ClonNAT 100 mg/L) were used to select for *OM45-GFP*::*TRP1* containing haploid colonies with *taz1*Δ *yme1*Δ or single-gene mutations.

3.10. SPOT ASSAY

Growth potential of yeast strains used in this thesis was estimated using the spot assay on appropriate medium at either 25˚C or 37˚C. Briefly, yeast were grown to early stationary phase 0.9-1.0 OD_{600} at 25˚C in YPD or YPL or SC medium, the cultures were then diluted to 0.45 OD_{600} and then serially diluted (1:10) four times in a 96-well culture plate and spotted on to appropriate solid medium using a replica pinner. The plates were incubated at either 25˚C or 37˚C for 3-5 days, after which they were imaged using a Bio-Rad VersaDoc.

3.11. STEADY-STATE ANALYSIS OF PHOSPHOLIPIDS

Yeast phospholipids were obtained from crude preparations of mitochondria and analyzed by one dimensional TLC as previously described [103,111]. Briefly, 3 ml cultures of indicated yeast strains were initiated at 0.025 OD_{600} in either YPD or YPL broth in the presence of 10 μCi ^{32}Pi/ml (labelled orthophosphoric acid from PerkinElmer). The cultures were allowed to grow for 5-6 generations at 30˚C to achieve steady-state ^{32}P incorporation into each phospholipid class to reflect its relative mass compared to total phospholipids. The cells were harvested and suspended in 300 μL of MTE buffer (0.65 M mannitol, 20 mM Tris, pH 8.0 and 1mM EDTA) containing 1 mM PMSF and appropriate concentration of complete protease inhibitors (Roche). In the presence of 200 μL of 0.5-mm acid-washed glass beads, the cells were then mechanically fractured by high-speed vortexing for 1 hour. Unbroken cells and glass beads were first sedimented by centrifugation at 300 g for 5 min at 4˚C; the resulting supernatant was then centrifuged at 13,000 g for 5 min at 4˚C to a obtain crude mitochondrial fraction. Lipids were extracted from equal amounts of crude mitochondrial preparation (as determined by liquid scintillation) by the Folch method. Briefly, 1.5 ml of 2:1 chloroform/methanol were added to the extract and agitated for 1 hour at room temperature, and after that 0.3 ml of distilled water was added to this mixture, vortexed and centrifuged at 2200 rpm for 20 min to separate the aqueous and organic phases. To the organic phase, 0.25 ml of 1:1 methanol/distilled water was added, vortexed to mix the phases, and the mixture was centrifuged as before to collect the organic phase, which was then dried under a stream of liquid nitrogen. The dried samples were resuspended in chloroform, and loaded onto pre-washed (with 1:1 chloroform/methanol) and pre-treated (with 1.8% boric acid in absolute

ethanol) LK5 silica gel 150 A TLC plates (Whatman). Lipids were separated for approximately 2 hours by placing the TLC plates in a chromatography tank containing 30/35/7/35 (v/v/v/v) chloroform/ethanol/water/triethylamine. After the first run, the plates were removed from the tank, dried completely in a fume hood and then re-run for the second time in the same direction to achieve adequate resolution. Dried TLC plates were wrapped in plastic wrap and exposed to X-Omat Blue film (Kodak) to visualize phospholipids by autoradiography. To quantitate the steady-state levels of phospholipids, the same TLC plates were exposed to phosphor imager screen (Bio-Rad) for 30 min before it was scanned and quantified by the Storm scan system (Molecular Dynamics) and Image-Quant software, respectively.

3.12. SDS-PAGE AND WESTERN BLOTTING

A Mini-PROTEAN3 unit (Bio-Rad) was utilized as per manufacturer's directions to perform both SDS-PAGE and protein transfer to PVDF (GE Healthcare) membranes. Briefly, proteins were denatured in sample buffer (150 mM Tris-HCl, pH 8.8, 6% SDS, 25% glycerol, 6 mM EDTA, 0.5% 2-mercaptoethanol, and 0.05% bromophenol blue) and then resolved using 10% SDS-PAGE (0.375 M Tris-HCl, 0.08% sodium dodecyl sulphate, 10% acrylamide, 0.2% ammonium per sulphate and 20µL TEMED) by the application of constant current at 100 volts. The separated proteins were then wet-transferred to PVDF in 25 mM Tris-HCl, 200 mM glycine, 10% methanol at 20 volts and 90 mA overnight. To maintain equal protein loading between samples, protein concentration was determined for cell extracts before SDS-PAGE using the Coomassie (Bradford) protein assay kit (Pierce). The membranes were then allowed to sit for an hour

under constant shaking in blocking buffer (5% milk, 3% bovine serum albumin, 0.1% tween 20 in PBS). The blots were then incubated with an appropriate dilution of primary antibody (1:5,000 dilution for anti-Cox2 from MitoSciences, and 1:10,000 anti-GFP from Clontech) in blocking buffer under constant shaking overnight at 4˚C. The following day, the membranes were washed thrice (10 min wash each with 0.1% tween 20 in PBS) before they were incubated with 1:10,000 dilutions of either anti-rabbit or anti-mouse horseradish peroxidase conjugated secondary antibodies (Cell Signalling) in blocking buffer for an hour. After the excess antibodies were washed off with 0.1% Tween 20 in PBS (three washes, 10 min each), proteins were detected by enhanced chemiluminescence (GE Healthcare or Millipore) as directed by the manufacturer. To ensure equal protein loading after western blotting, the membrane was stripped (100 mM β-mercaptoethanol, 2% sodium dodecyl sulphate, 62.5 mM Tris-HCl, pH 6.8) for 1 hour at 55˚C and then re-probed with anti-phosphoglycerate kinase 1 sera (Pgk1) (MitoSciences) overnight at 1:5,000 dilution in blocking buffer.

3.13. MICROSCOPY

All yeast cells, unless specified, were viewed using the plan-neofluor 100x oil immersion objective lens fitted to a Zeiss Axiovert 200M microscope. The images were captured by a Zeiss Axio Cam HR camera and analyzed using Zeiss Axiovision 4.6 software. Yeast vacuoles were visualized with the DIC (differential interference contrast) filter, GFP signal was detected with the help of GFP filter, and the rhodamine and fluorescein isothiocyanate (FITC) filters were used to track vacuolar morphology with FM4-64 and vacuolar acidification with quinacrine, respectively. Before viewing under the

microscope, the cells were typically concentrated to 50 µL in PBS and then spotted on charged glass slides (Superfrost, Fisher Scientific).

3.14. Om45-GFP MITOPHAGY MONITORING ASSAY

Yeast *OM45* encodes a MOM protein (Om45) and it is expressed in stationary-phase cells grown in medium with a non-fermentable carbon source. C-terminal GFP tagging of the chromosomal *OM45* (Om45-GFP) does not affect its normal mitochondrial localization; however, mitophagy results in Om45-GFP accumulation in the vacuole. Hence, tracking Om45-GFP signal from the mitochondria to the vacuole upon nitrogen starvation (mitophagy induction) is used to assess mitophagy by microscopy. GFP, unlike most other proteins, is relatively resistant to vacuolar degradation and persists as free GFP after the degradation of tagged protein (Om45). Therefore, after nitrogen starvation, estimation of free GFP versus Om45-GFP levels by western blotting with anti-GFP sera was used to determine mitophagy efficiency, as was previously shown [107].

Mitophagy in CWY-156, CWY-157, CWY-158 and CWY-159 yeast strains was assessed with minor modifications to the protocol detailed by Kanki and colleagues [107]. The indicated strains were first grown in 2 ml of YPD medium; once they reached 0.5 OD_{600} they were harvested by centrifugation, washed twice in distilled water and then resuspended in 6 ml of YPL at 0.2 OD_{600}. They were then incubated at 25˚C under constant shaking until they reached stationary-phase (0.8-1.5 OD_{600}). After that, a sample of cells (3 ml) from each strain was collected and marked as before nitrogen starvation. These samples were immediately pelleted and washed once with GTE (20% glucose, 50

mM Tris-HCl pH 7.4 and 1 mM EDTA) buffer before they were stored at -70˚C. The remaining culture was washed thoroughly in distilled water three times to remove traces of YPL medium and resuspended in 3 ml of SD-N medium lacking nitrogen. After 24 hrs, the cells were harvested by centrifugation, marked as after nitrogen starvation and then processed as described above. One ml of GTE buffer containing 1 mM PMSF and appropriate concentration of complete protease inhibitors (Roche) was added to the cell pellets saved above. The cells were then lysed using a bead beater (Bio-Spec) in the presence of 0.2 ml of 0.5-mm acid-washed glass beads. The glass beads and unbroken cells were pelleted by centrifugation at 300 g for 5 min at 4˚C; the resulting supernatant was then denatured in sample buffer. The denatured proteins were then resolved by 10% SDS-PAGE and transferred to PVDF membranes as described before. The blots were then subjected to western blotting with (1:10,000) GFP anti-sera (ClonTech) to estimate the levels of Om45-bound and free GFP in samples from before and after nitrogen starvation.

To assess mitophagy by fluorescence microscopy, the indicated strains were grown as described for Om45-GFP western blotting albeit in 2-ml culture volumes. Cells before and after starvation were harvested by low speed centrifugation at 1000 g for 1 minute and then resuspended in 50 µL of PBS. To visualize Om45-GFP signal, 3 µL samples were spotted on glass slides, covered with coverslips and viewed under a Zeiss Axiovert 200M microscope through the GFP filter. The images were captured with a Zeiss Axio Cam HR coupled to Zeiss Axiovision 4.5 software**.** The accumulation of GFP signal in the vacuole after starvation was confirmed by superimposing the images of the vacuoles captured under the DIC filter over the GFP images.

3.15. ELECTRON MICROSCOPY

Yeast strains CWY-150 (W3031-a), CWY-153 (W3031-a *taz1*Δ*::NATMX4*), CWY-154 (W3031-α *yme1*Δ*::KANMX4*) and CWY-155 (W3031-a *taz1*Δ*::NATMX4 yme1*Δ*::KANMX4*) were grown in 5 ml of SC medium containing 2% lactate to early stationary-phase (0.9-1.0 OD_{600}). The cells were then harvested and washed with 1 ml of distilled water before they were suspended in 1 ml of 1.5% $KMnO_4$. This mixture was kept under constant shaking on an orbital shaker. After 20 min, the cells were pelleted at 14000 g for 1 min and then washed twice in 1 ml of distilled water. The resulting pellet was incubated in 1ml of 1% sodium periodate for 15 min under constant shaking. At the end of the incubation, the cells were pelleted as before and washed once with distilled water. One ml of 1% NH_4Cl was added to the washed cells and they were kept under constant shaking for another 10 min before they were washed and suspended in 0.5 ml of PBS. The $KMnO_4$-fixed cells were gradually dehydrated by washes in increasing concentrations of ethanol. Dried samples were then infiltrated with LR White Resin, and then embedded onto capsules and left to dry at 60˚C for 2 days. Once the resin hardened, thin sections were cut using a LKB Huxley ultramicrotome. To assess mitochondrial morphology, the sections were viewed and captured using a JEOL JEM 1230 Transmission Electron Microscope at 80kV and Hamamatsu ORCA-HR digital camera, respectively. Mitochondrial morphological alterations such as altered mitochondrial shape, mitochondrial size, altered MIM structure, vacuolated MIM and MIM adhesions were quantitated by manually counting at least 150 mitochondria for each strain studied. Mitochondria containing any one of these aberrations were counted as aberrant

mitochondria, however, mitochondria without the above alterations but with an elongated shape were tabulated separately as elongated mitochondria.

3.16. VACUOLAR MORPHOLOGY ASSESSMENT WITH FM4-64 TRAFFICKING

FM4-64 (Sigma), a lipophilic stain that reaches the vacuole via endocytosis, was used to visualize vacuolar morphology in wild-type and mutant yeast strains. Mid-logarithmic phase cells grown in YPD at 25˚C or 37˚C were concentrated to 2-4 OD_{600} in 500 µL of SC medium (pre-warmed to 37˚C to resuspend cultures grown at 37˚C) containing 1.6 µM FM 4-64 and incubated for 10 min at 25˚C or 37˚C. After 10 min, the cells were washed twice with YPD medium (pre-warmed YPD was used for cells grown at 37˚C) and then transferred to fresh YPD and incubated under constant shaking for 120 min at 25˚C or 37˚C. At the end of incubation, 3 µL samples of live cells from each of the strains were spotted on a glass slide to visualize FM 4-64 (excitation/emission maxima ~ 515/640 nm) fluorescence using the rhodamine filter fitted to a Zeiss Axiovert 200M microscope.

3.17. VACUOLAR ACIDIFICATION STATE ASSESSMENT USING QUINACRINE ACCUMULATION

A healthy vacuole maintains an acidic pH in its lumen; hence, accumulation of quinacrine (a weak base) in vacuolar lumen was used as described before to assess its acidification state [112,113]. Wild type and mutant yeast strains were grown in YPD medium at 37˚C to mid-log phase and then washed twice with pre-warmed HEPES-buffered YPD at pH 7.6. The cells were then resuspended in HEPES-buffered YPD at pH 7.6 containing 200 µM quinacrine and incubated at room temperature for 5 min. At the end of incubation the

cells were washed in 50 mM PBS containing 2% glucose at pH 7.6, and 3 μL samples of cells from each strain were spotted onto glass slides and quinacrine fluorescence was determined using the fluorescein isothiocyanate (FITC) filter fitted to a Zeiss Axiovert 200M microscope.

3.18. ESTIMATION OF PROTEIN CARBONYL CONTENT

A protein carbonyl assay kit (BioVision #K830-100) was used to estimate the carbonyl content in proteins. This kit estimates the amount of protein-bound 2,4-dinitrophenylhydrazone (DNP) formed by the conversion of added 2,4-dinitrophenylhydrazine (DNPH) to DNP by protein carbonyl groups. Wild-type and mutant yeast strains were grown in 25 ml of YPL medium to mid-log phase at 25˚C and then shifted to 37˚C. When the cultures reached 0.9-1.0 OD_{600}, the cells were harvested by centrifugation at 1000 g for 10 min at 4˚C. After that, they were washed once in 25 ml of ice cold GTE (20% glucose, 50 mM Tris-HCl pH 7.4 and 1 mM EDTA) before they were resuspended in 1 ml of ice-cold GTE with complete protease inhibitors (Roche). Upon the addition of approximately 0.5 ml of 0.5-mm acid-washed glass beads to the GTE-washed cells they were mechanically broken by high-speed vortexing 6 times for 30 sec separated by 30-sec incubations in ice. Whole-cell extracts were then obtained after the removal of unbroken cells by centrifugation at 300 g for 5 min at 4˚C.

Yeast extract (0.5-1 mg of protein) from each of the strains was dissolved in 0.1 ml of distilled water to a concentration of 10 mg/ml protein and used for protein carbonyl content determination. The samples were first treated with 10% streptozocin for 10 min at

room temperature to remove nucleic acid contamination. After that, 0.1 ml of DNPH was added to each sample and they were incubated in the dark for 10 min at room temperature. At the end of the incubation period, 0.03 ml of 100% trichloro acetic acid was added to the samples and the tubes were placed on ice for 5 min, after which the precipitated proteins were pelleted by centrifugation at 14,000 g for 2 min. The pellet was then washed twice with 0.5 ml of ice-cold acetone before the proteins were re-solubilized by the addition of 0.2 ml of 6 M guanidine. After the removal of insolubilized material by brief centrifugation, 0.1-ml samples were transferred to 96 well plates to measure the formation of DNP at 375 nm using a plate reader (Infinite 200Pro, Tecan). A sample of distilled water (0.1 ml) with no cell extracts and AGE-BSA (BioVision) was also reacted with DNPH to serve as background and positive controls, respectively. Once the plate reader measured the DNP formation, 0.05 ml samples were taken from each sample well and then subjected to protein content determinations using the BCA assay kit (BioVision K812-1000). The corrected OD (sample OD 375 nm - background OD 375 nm) was used to estimate the carbonyl content in each sample by using the following formula as described before [99,114].

C = [(corrected OD 375 nm) /6.34) X (200)] nmol/well

CP = nmol carbonyl per mg protein

$= (C/P) \times 1000 \times D$

Where:

6.364 = mM extinction coefficient for 96-well plate (= 22 mM-1 cm-1 × 0.2893 cm path length in well)

C = nmol Carbonyl in sample well

P = protein from standard curve estimated by BCA kit × 40 = µg/well

D = dilution or concentration step applied to sample

1000 = factor to convert µg to mg

3.19. ISOLATION OF YEAST MITOCHONDRIA

One-liter cultures of yeast strains were grown in YPL medium at 30˚C until they reached an OD_{600} of 1-2. The cells were harvested by centrifugation at 2500 g for 5 min at room temperature and mitochondria were isolated by differential centrifugation as detailed previously [115]. Briefly, harvested cells were washed once in distilled water, resuspended in 30 ml of freshly prepared TD buffer (100 mM Tris-sulphate, pH9.4, 10 mM DTT) and incubated for 5 min at 30˚C with gentle shaking. These cells were then collected by centrifugation (2500g for 5 min) and resuspended in SP buffer (1.2 M sorbitol, 20 mM potassium phosphate, pH 7.4); after that, spheroplasts were generated by treatment with zymolase 100T (1.5 mg/g cells) for 30-60 min at 30˚C with gentle shaking. Spheroplasts were harvested by centrifugation at 2500 g for 5 min at 4˚C and then washed twice with 40 ml of ice-cold SP buffer. After the washes, the spheroplasts were resuspended in 60 ml of ice-cold SH buffer (0.6 M sorbitol, 20 mM HEPES-KOH, pH 7.4) containing 1 mM PMSF and appropriate concentration of complete protease inhibitors (Roche). The suspension was transferred to a large-piston glass homogenizer (Potter-Elvehjem-Type Tissue Grinders) and homogenized with 25 strokes; the homogenized mixture was then subjected to centrifugation twice at 2500 g for 5 min at 4˚C. The supernatants from the previous steps were pooled together in a fresh 50-ml glass tube and pelleted by centrifugation at 12,000g for 10 min at 4˚C. Using a small-scale

glass homogenizer, the pellet was first carefully resuspended in 1 ml of SH buffer and then resuspended in 25 ml of ice cold SH buffer. This suspension was further centrifuged at 2500g for 5 min at 4˚C; the supernatant was saved and then pelleted at 12,000 g for 10 min at 4˚C. The resulting pellet (mitochondria) was resuspended in 0.5 ml of SH buffer and divided into samples containing 0.1-0.3 mg protein (estimated by Coomassie (Bradford) Protein Assay Kit, Pierce). The samples were flash frozen in liquid nitrogen and stored at -70˚C until further analysis.

3.20. BLUE-NATIVE PAGE (BN-PAGE)

The status of yeast respiratory-chain supercomplexes was assessed by BN-PAGE as described previously with minor modifications [116]. Frozen mitochondria (0.2 mg of protein) were thawed and suspended in 0.04 ml of 50 mM NaC1, 5 mM 6-aminohexanoic acid, 50 mM imidazole/HC1, pH 7.0. To solubilize membranes, 10% solution of dodecylmaltoside (DDM) at a detergent/protein ratio of 2 g/g was added to this mixture followed by incubation for 20 min in ice. The suspension was centrifuged at 20,000 g for 20 min at 4˚C, the supernatant with solubilized protein was saved, 1 μL of 5% Coomassie blue G-250 (Pierce) was added to the supernatant and then separated on a 3-12% precast Bis-Tris Native PAGE (Invitrogen, BN1001BOX) using a XCell sure lock Mini-Cell gel running tank (Invitrogen) by the application of constant current at 150 V for approximately 2 hours in a cold room. To improve detection of faint protein bands and to maximize protein transfer to PVDF membranes, the dark cathode buffer with 0.02% Coomassie blue G-250 was replaced with light cathode buffer (0.0002% Coomassie blue

G-250) once the proteins reached one-third of the running distance in BN-PAGE. A diluted sample of ferritin, which runs as two visible (brown) bands with molecular masses of 440 kDa and 880 kDa (matches the mass of ETC Complex IV monomer and ETC III2IV2 supercomplex) was separated along with the samples by BN-PAGE to serve as a molecular marker [117]. The proteins were then transferred to PVDF membranes using a semi-dry electroblotting apparatus in the presence of electrode buffer containing 5 mM Tricine, 7.5 mM imidazole, pH 7.0 at 4˚C for 90 min. The blot was then probed by western blotting with 1:5000 dilutions of anti-Cox2 antibody (Mito Sciences) to detect the status of yeast respiratory-chain super complexes.

CHAPTER 4. RESULTS

4.1. YEAST LACKING TAZ1 HAVE LOW CL LEVELS, ACCUMULATE MLCL AND GROW POORLY IN NON-FERMENTABLE MEDIUM AT 37˚C

To create an *S. cerevisiae* model of BTHS, the *TAZ1* coding sequence in the wild-type (W) yeast was replaced with a nourseothricin antibiotic-resistance marker *(NATMX4)* by homologous recombination. To determine if the loss of *TAZ1* leads to the expected decrease in the level of CL and increase in MLCL, wild-type (CWY 150), *crd1*Δ (CBY 304) and *taz1*Δ (CWY 153) yeast cells were labeled with radioactive phosphorus (^{32}P, as orthophosphoric acid) to steady-state by growth for 5-6 generations in either YPD or YPL medium at 30˚C. Radiolabelling to steady-state results in the level of ^{32}P incorporation into each phospholipid class being reflective of its relative mass compared to other phospholipids. Mitochondria were then isolated and lipids were extracted by chloroform extraction, resolved by TLC and visualized by autoradiography. The *taz1*Δ mutant, when grown in YPD or YPL medium, accumulated the CL precursor MLCL when compared to W cells (**Figure 4.1 A**). The levels of CL did not differ between W and *taz1*Δ mutant in YPD medium but was significantly lower in the *taz1*Δ mutant when grown in YPL medium (**Figure 4.1 A**). The identity of the CL band on the chromatogram was determined based on the known mobility for CL in the TLC solvent used, and confirmed by the phospholipid profile of *crd1*Δ mutant that cannot synthesize CL from PG.

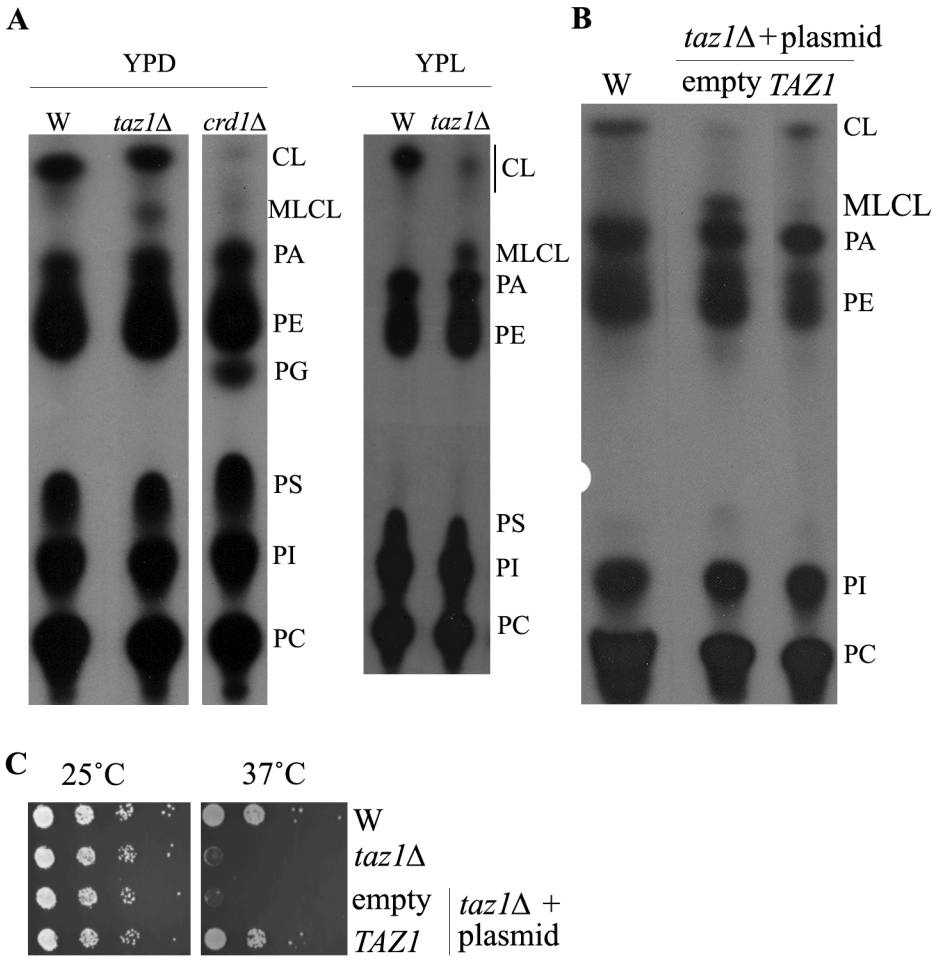
A
YPD
YPL
W
taz1Δ
crd1Δ
W
taz1Δ
CL
MLCL
PA
PE
PG
PS
PI
PC
CL
MLCL
PA
PE
PS
PI
PC
B
taz1Δ+plasmid
W
empty TAZ1
CL
MLCL
PA
PE
PI
PC
C
25°C
37°C
W
taz1Δ
empty TAZ1
taz1Δ + plasmid

Figure 4.1. Taffazin-deficient yeast have low levels of CL, accumulate MLCL and grow poorly in respiring conditions at 37˚C. A&B. The indicated yeast strains were suspended in YPD or YPL at 0.025 OD_{600} in the presence of 10 μCi $^{32}P_i$ / ml and were grown for 5-6 generations at 30˚C to achieve steady-state labeling of phospholipids. At the end of the growth period, phospholipids were extracted from mitochondria, separated by TLC and visualized by autoradiography. **A.** Representative TLC shows that *taz1*Δ cells accumulate its remodeling precursor MLCL in both YPD and YPL. However, lower CL levels were noticed in the *taz1*Δ mutant than W cells when grown in YPL medium but not in YPD. The *crd1*Δ mutant, which lacks the enzyme to synthesize CL from PG is completely devoid of CL and accumulates its precursor PG. **B.** Exogenous expression of *TAZ1* under the control of its own promoter was able to rescue CL levels and reverse the accumulation of MLCL in *taz1*Δ cells. **C.** Growth assay of wild-type and *taz1*Δ strains in non-fermentable medium with lactate as carbon source at 25˚C and 37˚C. Indicated strains were grown to early stationary-phase 0.9-1.0 OD_{600}, cultures were diluted to 0.45 OD_{600} and then serially diluted (1:10) and spotted on SC medium with 2% lactate as carbon source and grown for 3-5 days at 25˚C or 37˚C. Yeast lacking tafazzin grew poorly at 37˚C and this defect could be rescued by the exogenous expression of *TAZ1* from a plasmid. **Abbreviations used: W** - wild-type yeast.

As expected, the *crd1*Δ mutant lacked CL and accumulated the CL synthetic precursor PG (**Figure 4.1 A**). Expression of *TAZ1* from the pRS416 plasmid (low copy, generally 1-3 copies/cell) under the control of its own promoter was able to restore the CL level in *taz1*Δ mutant to wild-type levels and prevented the accumulation of MLCL (**Figure 4.1 B**). Transformation of an empty pRS416 plasmid in the *taz1*Δ mutant failed to restore CL and MLCL levels (**Figure 4.1 B**). The *TAZ1* gene deletion results in an accumulation of its substrate MLCL, and a growth-medium-dependent decrease in CL.

BTHS is characterized by abnormal and dysfunctional mitochondria. These changes to the mitochondria are suspected to cause many of the symptoms related to the disease, although exactly how is not clear [2]. To determine if inactivation of *TAZ1* affects yeast mitochondrial function, I assessed the ability of this mutant to grow in non-fermentable medium where the sole source of ATP is from mitochondrial respiration. To this end, W and *taz1*Δ cells, and *taz1*Δ cells transformed with an empty control plasmid or with a plasmid containing *TAZ1* coding sequence, were grown to early stationary-phase in YPL liquid medium and then serially diluted and spotted onto SC solid medium containing 2% lactate as the carbon source and grown for 3-5 days at 25˚C and 37˚C. Yeast cells lacking *TAZ1* grew at a normal rate at 25˚C but showed decreased growth at 37˚C. This phenotype was reversed in the *taz1*Δ mutant carrying the plasmid containing the *TAZ1* gene but not with the empty plasmid (**Figure 4.1 C**). This result indicates that loss of *TAZ1* in yeast leads to mitochondrial dysfunction when yeast cells are grown at 37˚C in SC medium with 2% lactate as the sole carbon source.

4.2. SGA ANALYSIS TO IDENTIFY GENES THAT AFFECT THE FITNESS OF *taz1*Δ CELLS

In this study, SGA analysis was performed with a *TAZ1*-deficient yeast strain (CBY303). The SGA analysis allowed for the construction of cells in which the *TAZ1* gene was inactivated along with each non-essential yeast gene, creating a panel of ~4700 double mutants. These double mutants were analyzed for those that resulted in a decrease in cell growth in fermentable medium (YPD), a condition where cells lacking only the *TAZ1* gene grow at a normal rate. The screen was performed twice, and the two screens together identified 159 genes that aggravated the fitness of *taz1*Δ yeast cells. Of these, 35 are nucleus-encoded genes that have a known function in the mitochondria, and these were prioritized because Taz1 resides in mitochondria and mitochondrial dysfunctional is a conserved hallmark of tafazzin deficiency from yeast to humans. Of these 35 genes, 18 (**Table 2**) were selected for further analysis because they have a phenotype similar to the known phenotypes associated with aberrant CL metabolism in yeast, are part of processes known to physically associate with CL, or were identified in both SGA screens. This list contained genes that play a role in ETC biogenesis, mitochondrial DNA maintenance, mitochondrial protein import, oxidative stress, mitochondrial quality-control, or solute transport. To rule out false positive results due to the high-throughput nature of the SGA screen, and the ability of yeast cells to accumulate second-site suppressors during the screen, the 18 double mutants were recreated using standard yeast genetics mating techniques and random spore assay to determine their ability to decrease growth.

This analysis identified 6 of 18 genes, namely *YME1, TOM5, ISA2, GGC1, SUE1* and *ORT1,* that when inactivated in a *taz1*Δ mutant decreased growth (**Table 3**). The role of *YME1* was further characterized, as its inactivation alone has phenotypes similar to that of cells with an inactivated *TAZ1* gene, and there are no known links between its function and that of *TAZ1,* and its further study may provide novel insight into the biological role of *TAZ1*.

The SGA screen indicated that deletion of *YME1* in *taz1*Δ cells causes a growth defect in the double mutant. *YME1* is a mitochondrial quality-control protease that degrades misfolded mitochondrial IMS and MIM proteins, and also functions as a chaperone in the folding of ETC complex IV subunit Cox2 [118]. Yme1 is a homo-oligomer with a molecular mass of ~1000 kDa and belongs to a family of ATP- and Zn^{2+}-dependent proteases containing a C-terminal proteolytic domain and an ATPase Associated with diverse cellular Activities (AAA) domain [118]. Yme1 has a single transmembrane domain scanning the MIM. The protease domain of Yme1 faces the IMS of the mitochondria and its N terminus is in the mitochondrial matrix [118]. Since yeast contain a second mitochondrial AAA protease with a matrix-facing protease domain (m-AAA), Yme1 is often referred to as i-AAA protease [118]. Loss of *YME1* function in yeast was previously shown to cause growth defects in non-fermentable medium at 37˚C [119].

Table 3. *TAZ1* gene has negative genetic interactions with these following genes.

Standard Name	Systematic Name	Saccharomyces Genome Database description [110]
Mitochondrial quality-control		
YME1	*YPR024W*	Catalytic subunit of the i-AAA protease complex; responsible for degradation of unfolded or misfolded mitochondrial gene products; also has a role in intermembrane space protein folding; mutation causes an elevated rate of mitochondrial turnover
Arginine metabolism		
ORT1	*YOR130C*	Ornithine transporter of the mitochondrial inner membrane; exports ornithine from mitochondria as part of arginine biosynthesis; human ortholog is associated with hyperammonaemia-hyperornithinaemia-homocitrullinuria (HHH) syndrome
ARG3	*YJL088W*	Ornithine carbamoyltransferase; also known as carbamoylphosphate: L-ornithine carbamoyltransferase; catalyzes the biosynthesis of the arginine precursor citrulline.
CPA1	*YOR303W*	Small subunit of carbamoyl phosphate synthetase; carbamoyl phosphate synthetase catalyzes a step in the synthesis of citrulline, an arginine precursor; translationally regulated by an attenuator peptide encoded by *YOR302W* within the *CPA1* mRNA 5'-leader.
CPA2	*YJR109C*	Large subunit of carbamoyl phosphate synthetase; carbamoyl phosphate synthetase catalyzes a step in the synthesis of citrulline, an arginine precursor
ARG1	*YOL058W*	Arginosuccinate synthetase; catalyzes the formation of L-argininosuccinate from citrulline and L-aspartate in the arginine biosynthesis pathway; potential Cdc28 substrate.
Mitochondrial iron metabolism		
ISA2	*YPR067W*	Protein required for maturation of mitochondrial [4Fe-4S] proteins; functions in a complex with Isa1 and possibly Iba57; localizes to the mitochondrial intermembrane space, overexpression of ISA2 suppresses *GRX5* mutations.
GGC1	*YDL198C*	Mitochondrial GTP/GDP transporter; essential for mitochondrial genome maintenance; has a role in mitochondrial iron transport.

Standard Name	Systematic Name	Saccharomyces Genome Database description [110]
Mitochondrial iron metabolism		
*FRE4**	*YNR060W*	Ferric reductase, reduces a specific subset of siderophore-bound iron prior to uptake by transporters; expression induced by low iron levels.
*SIT1**	*YEL065W*	Ferrioxamine B transporter; member of the ARN family of transporters that specifically recognize siderophore-iron chelates; transcription is induced during iron deprivation and diauxic shift; potentially phosphorylated by Cdc28
Mitochondrial protein import		
TOM5	*YPR133W-A*	Component of the TOM (translocase of outer membrane) complex; responsible for recognition and initial import of all mitochondrially directed proteins; involved in transfer of precursors from the Tom70p and Tom20p receptors to the Tom40p pore

* Indicates not tested by random spore analysis.

Further, alterations to mitochondrial morphology (punctate and/or swollen mitochondria) have also been reported for *yme1*Δ yeast [119]. In addition, stable shRNA (small hairpin RNA) knockdown of *YME1L* (the human ortholog of yeast *YME1*) in human embryonic kidney 293 cells caused altered mitochondrial morphology with aberrant cristae, defective assembly and accumulation of ETC complex subunits in the MIM, apoptosis resistance and an increased susceptibility of mitochondria to oxidative stress [120]. These alterations in both yeast and human cell lines lacking the i-AAA protease function are remarkably similar to alterations seen in *taz1*Δ yeast and BTHS patient lymphoblast mitochondria. Therefore, I chose to explore the role of *YME1* in tafazzin-deficient yeast for this thesis. Moreover, during the course of this work others have shown that *YME1* has a role in regulating Taz1 function by ensuring the removal of unfolded Taz1 as it is being imported into the mitochondria [100].

4.3. *YME1* DELETION AGGRAVATES THE GROWTH OF *taz1*Δ YEAST

The genetic interaction between *YME1* and *TAZ1* was further confirmed by tetrad analysis. To this end, the *YME1* gene was replaced with a kanamycin-resistance marker (*KANMX4*) by homologous recombination. The *yme1*Δ mutant (CWY 154) with the *KANMX4* cassette was then mated with *taz1*Δ yeast (CWY 153) where the *TAZ1* gene had been replaced by the *NATMX4* cassette. The resulting diploid cells were forced to undergo meiosis and the haploid spores from each ascus (each meiotic ascus contains 4 spores) were separated and allowed to grow as individual colonies on YPD for 3 days. The genetic make-up of each of the resulting colonies was determined by their growth resistance to nourseothricin, G418, or both. A *taz1*Δ *yme1*Δ mutant contains both *NATMX4* and *KANMX4* markers that confer resistance to nourseothricin and G418

respectively; therefore, the *taz1*Δ *yme1*Δ double mutant will be resistant to the presence of both antibiotics. Tetrad analysis showed that the double mutants grew very slowly compared to the wild-type and single mutants in YPD at 25˚C (**Figure 4.2 A**). The double-mutant colonies from tetrads were further tested for their growth phenotype by a second growth assay in YPD medium at 25˚C. Serial dilutions (1:10) of the various yeast strains were spotted on YPD solid medium and allowed to grow for 3-5 days at 25˚C. The *taz1*Δ *yme1*Δ (CWY 155) cells grew poorer than the single-gene-deletion strains, providing further confirmation that *YME1* deletion aggravates the growth of *taz1*Δ yeast (**Figure 4.2 B**).

4.4. THE *taz1*Δ *yme1*Δ CELLS HAVE AN EXACERBATED GROWTH DEFECT IN NON-FERMENTABLE MEDIUM

Similar to *taz1*Δ cells, yeast cells lacking Yme1 function have been shown to grow poorly at 37˚C in medium containing a non-fermentable carbon source [121]. To determine if this growth defect is exacerbated in cells lacking both Taz1 and Yme1 functions, I compared the growth of *yme1*Δ cells with wild-type, *taz1*Δ, and *taz1*Δ *yme1*Δ yeast strains in SC medium with 2% lactate as the sole carbon source. To this end, 1:10 serial dilutions of each yeast strain were spotted onto solid medium and allowed to grow for 3-5 days either at 25˚C or 37˚C. As previously reported the *yme1*Δ cells grew normally at 25˚C, but similar to the *taz1*Δ mutant, their growth was severely decreased compared to wild-type cells at 37˚C (**Figure 4.3**). The *taz1*Δ *yme1*Δ yeast had a growth defect at 25˚C, and failed to grow at 37˚C. This same phenotype was observed for the *taz1*Δ *yme1*Δ cells on glucose medium, where glycolysis supplies the majority of cellular energy. Therefore,

the growth defect of *taz1*Δ *yme1*Δ cells appears to be independent of the source of cellular ATP.

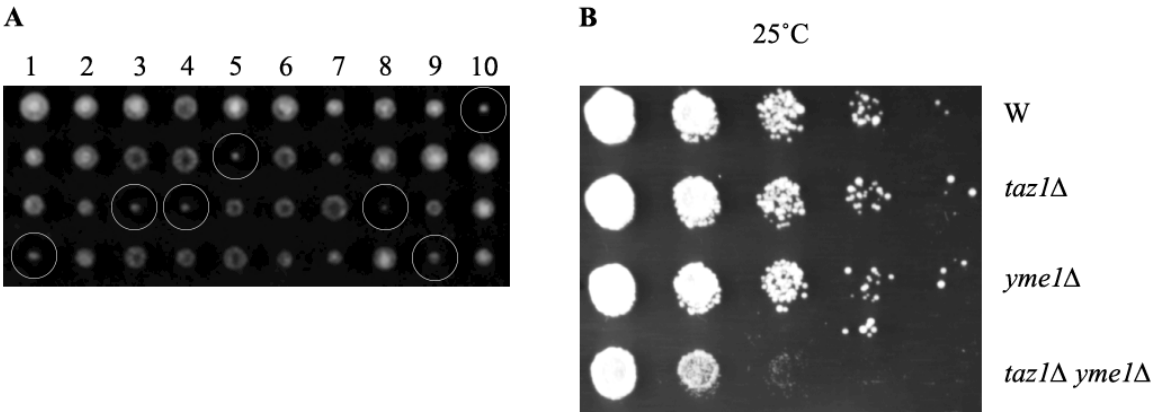

Figure 4.2. ***TAZ1*** **and** ***YME1*** **double-mutant cells are synthetically sick. A.** Tetrad separation of meiotic spores from a cross between *taz1*Δ and *yme1*Δ yeast shows slow-growing *taz1*Δ *yme1*Δ mutants (indicated by white circles) in fermentable YPD medium. Each column has four colonies arising from a single tetrad (ascus) that resulted from the cross between *taz1*Δ and *yme1*Δ cells. The single mutants *taz1*Δ and *yme1*Δ carry nourseothricin- and kanamycin-resistance markers respectively. Growth resistance to the addition of both the antibiotics G418 and nourseothricin confirmed the genetic make-up of the double-mutant colonies. **B.** Spot assay shows that *taz1*Δ *yme1*Δ double mutants are synthetically sick in YPD medium. Indicated strains were grown to early stationary-phase 0.9-1.0 OD_{600} and then resuspended in SC medium at 0.45 OD_{600}. This dilution was then serially diluted (1:10) and spotted on YPD solid medium and grown for 3-5 days at 25˚C. **Abbreviations used: W** - wild-type yeast.

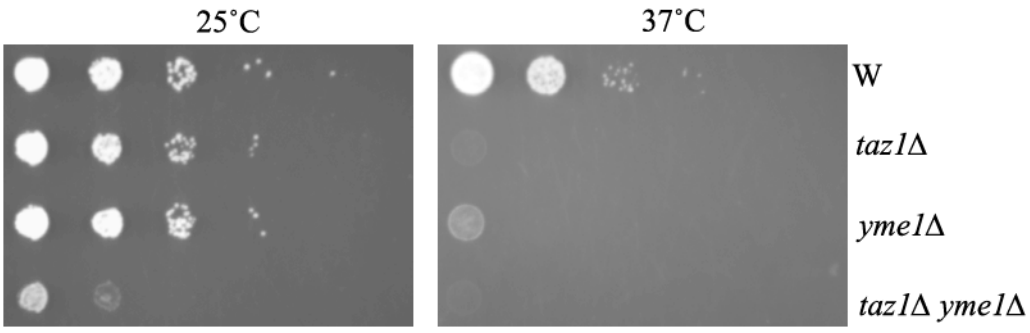

Figure 4.3. Growth assay of *taz1*Δ and *yme1*Δ mutant yeast cells show that they are both growth defective in non-fermentable medium at 37˚C. Indicated strains were grown to early stationary-phase 0.9-1.0 OD_{600} and then suspended in minimal medium at 0.45 OD_{600}. This dilution was then serially diluted (1:10) and spotted on SC solid medium with 2% lactate and grown for 3-5 days at 25˚C and 37˚C.
Abbreviations used: W - wild-type yeast

4.5. THE *taz1*Δ *yme1*Δ CELLS DID NOT SHOW SIGNIFICANT CHANGES IN CL OR MLCL LEVELS COMPARED TO *taz1*Δ AND *yme1*Δ SINGLE MUTANTS

A conserved hallmark of loss of tafazzin function is the accumulation of MLCL and a decrease in CL. To address if the *taz1*Δ *yme1*Δ yeast exacerbated this imbalance in CL metabolism, or altered other aspects of mitochondrial phospholipid levels that could result in a sicker cell (as Yme1 contributes to turnover of the main enzyme in mitochondria that synthesizes PE) [122], the phospholipid levels of W (CWY 150), *taz1*Δ (CWY 153), *yme1*Δ (CWY 154) and *taz1*Δ *yme1*Δ (CWY 155) yeast were analyzed by labeling cellular phospholipids with ^{32}P to steady-state. TLC separated individual phospholipids and their relative levels were determined by detection using a STORM phosphor-imager and analysis using Image quant software. CL and MLCL levels were not considerably different between the *taz1*Δ *yme1*Δ yeast and the single *taz1*Δ mutant (**Figure 4.4**). The decreased growth of *taz1*Δ *yme1*Δ cells does not appear to be due to gross changes in mitochondrial phospholipid levels.

4.6. THE *taz1*Δ *yme1*Δ MUTANT IS CHARACTERIZED BY SEVERE MITOCHONDRIAL ABNORMALITIES

The loss of tafazzin function causes abnormal mitochondrial morphology with MIM adhesions, cristae that are vacuolated, and defective cristae arrangement [98]. The *yme1*Δ cells also harbor punctate mitochondria that lack reticulated cristae structures, and some swollen mitochondria were also observed in these cells [123].

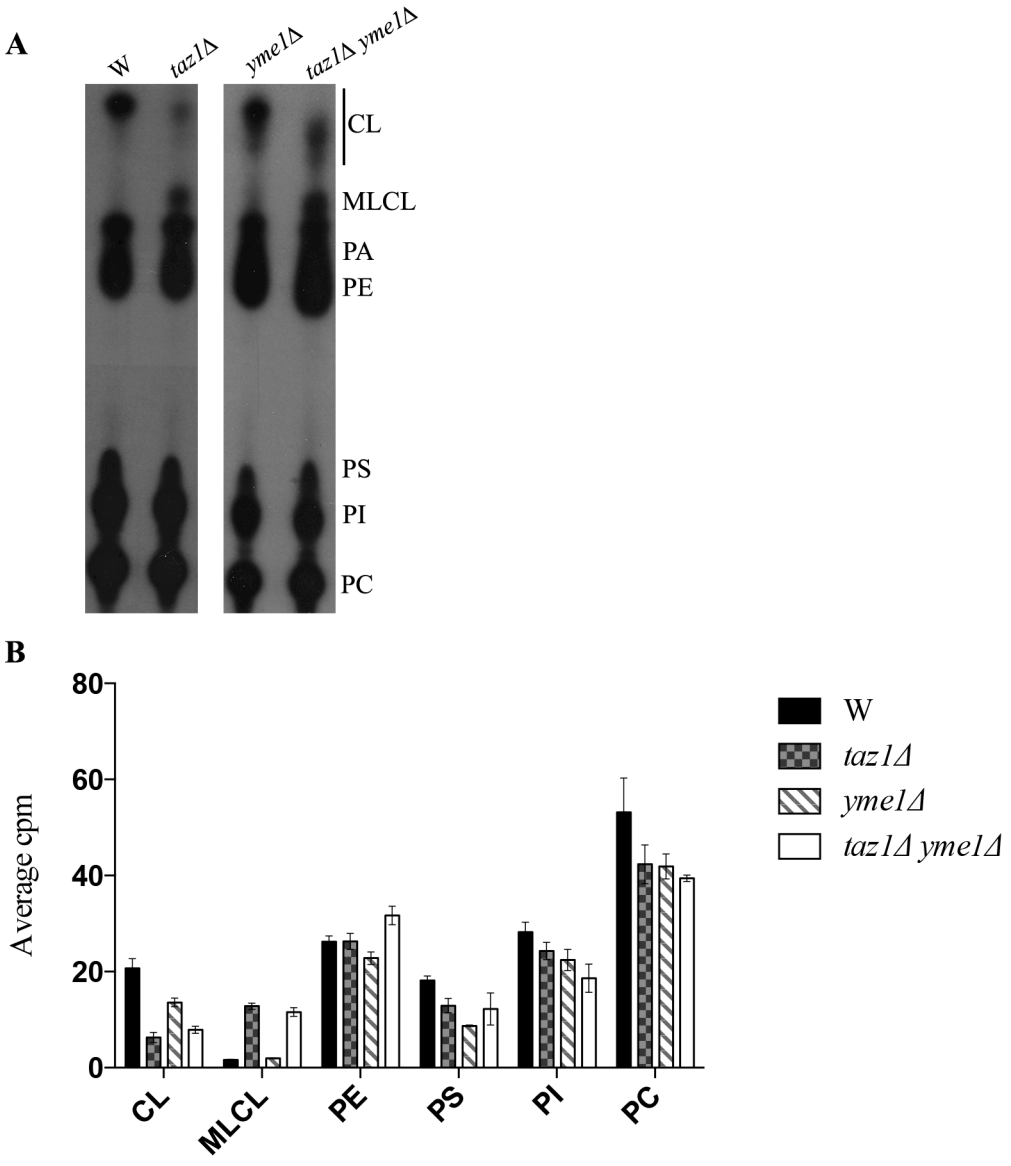

Figure 4.4. Double-mutant *taz1*Δ *yme1*Δ yeast did not show any significant changes to steady-state CL and MLCL levels when compared to *taz1*Δ mutants. A. Shows a representative TLC autoradiogram of the steady-state phospholipid levels of various yeast strains. The indicated yeast strains were suspended in YPL medium at 0.025 OD_{600} in the presence of 10 μCi $^{32}P_i$ / ml and were grown for 5-6 generations at 30˚C to achieve steady-state labeling of phospholipids. At the end of the growth period, phospholipids were extracted from mitochondria, separated by TLC and visualized by autoradiography. **B.** Shows the quantitation data of steady-state phospholipid levels from two independent experiments using a STORM phosphor-imager.

To determine whether *taz1*Δ *yme1*Δ cells have mitochondrial morphology defects that are more extreme than those of either single mutant alone, electron microscopy (EM) was performed (**Figure 4.5**). The yeast were grown in SC medium with 2% lactate at 25˚C to early stationary-phase to induce the proliferation of mitochondria, and were fixed and processed for EM as detailed in the methods (Section 3.15). Approximately 150-250 mitochondria were counted for each strain, and their morphologies were noted to quantify morphological differences (**Figure 4.5 B**). The W (CWY 150) yeast mitochondria were normal, with a defined reticulated network (**Figure 4.5 A panel a**). The *taz1*Δ (CWY 153) yeast contained a significant proportion of elongated mitochondria, but no other significant morphological defects were apparent (**Figure 4.5 A panel b & 4.5 B**). The loss of Yme1 (CWY 154) from yeast led to abnormally shaped mitochondria with vacuolated cristae, and a loss of reticulation in many of the mitochondria (**Figure 4.5 A panel c & 4.5 B**). Alterations to mitochondrial shape and cristae arrangement were more pronounced in *taz1*Δ *yme1*Δ cells (CWY 155), and there were a greater proportion of cells harboring aberrant mitochondria compared to *yme1*Δ yeast (**Figure 4.5 A panel d & 4.5 B**). Interestingly, the giant mitochondria were also seen in in *taz1*Δ *yme1*Δ cells, often found in close proximity to the vacuole (**Figure 4.5 A panel d**). Further, many of the *taz1*Δ *yme1*Δ cells had large multi-vacuolar structures, and appeared very sick (**Figure 4.5 A panel d**). These observations indicate that deletion of *YME1* in *taz1*Δ yeast causes severe defects to mitochondrial morphology resulting in a larger proportion of cells with giant mitochondria that lacked cristae, with a subset of these lying adjacent to the vacuole.

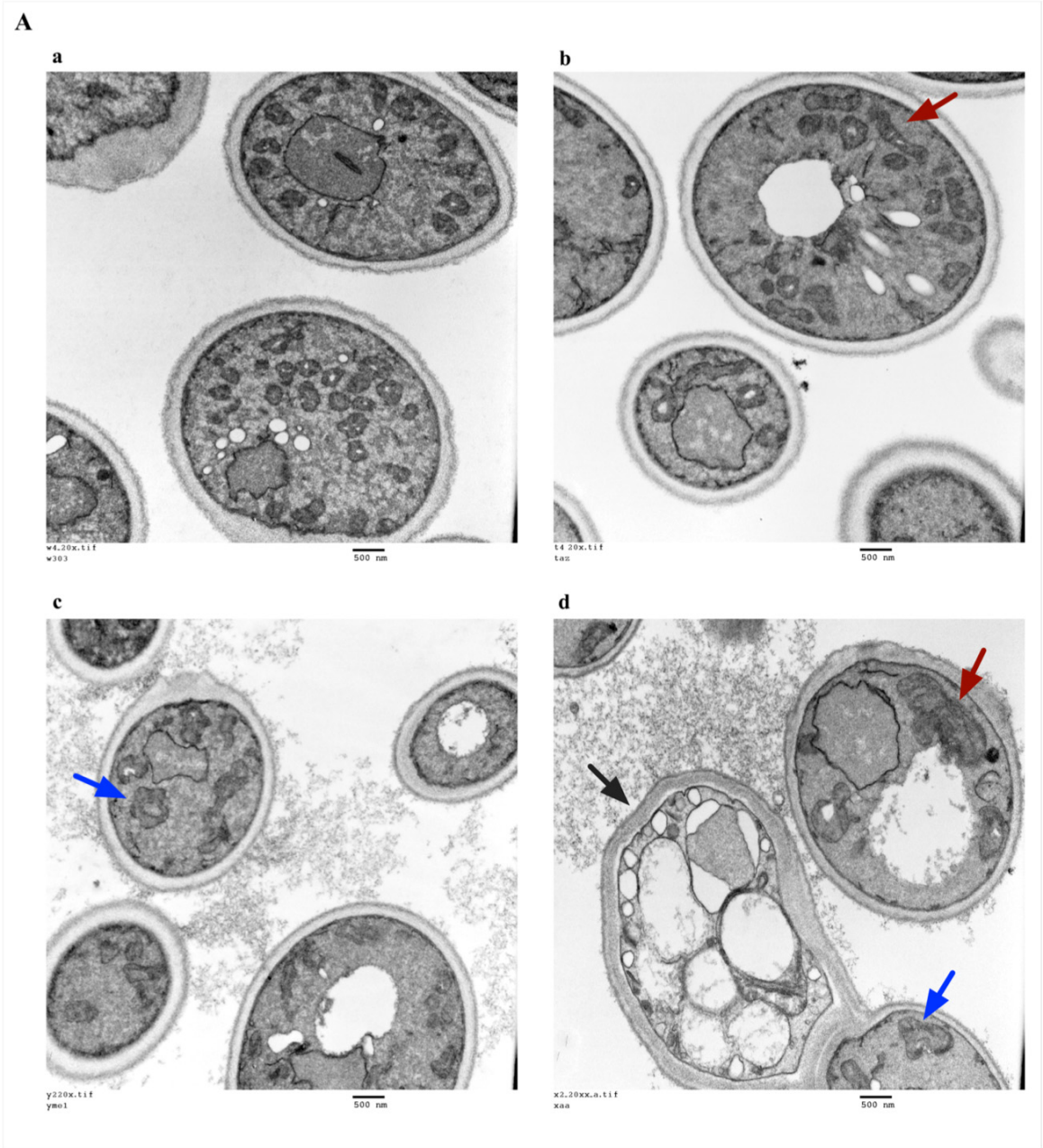
A
a
w4.20x.tif
w303
500 nm
b
t4 20x.tif
taz
500 nm
c
y220x.tif
ymo1
500 nm
d
x2.20xx.a.tif
xaa
500 nm

B

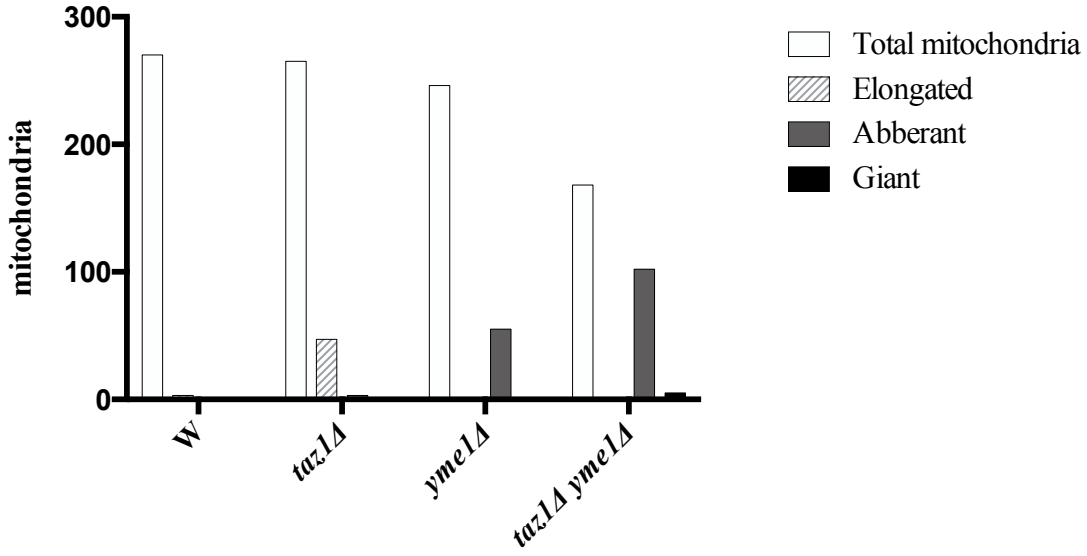

	Total mitochondria	Elongated	Abberant	Giant
W	270	3	0	0
taz1Δ	265	47	3	0
yme1Δ	246	1	55	0
taz1Δ yme1Δ	168	0	102	5

Figure 4.5. Electron microscopy reveals severe mitochondrial morphological abnormalities in *taz1*Δ *yme1*Δ double-mutant yeast. A. Wild-type (W) and mutant strains were grown to early stationary-phase (0.9-1.0 OD_{600}) in SC medium with 2% lactate and then processed for electron microscopy as described in section 3.15. **A.** Panels **a** & **b** show a representative capture from wild-type and *taz1*Δ yeast and both these strains harbored predominantly healthy mitochondria with an increase in the presence of healthy but elongated mitochondria (indicated by a red arrow) in *taz1*Δ yeast (also see **figure 4.5 B –** bar graph and tabulation). Both *yme1*Δ and *taz1*Δ *yme1*Δ yeast harbored abnormally shaped mitochondria with loss of cristae structures (panels **c** & **d**, see blue arrows). However, the defects were more pronounced (see **figure 4.5 B –** bar graph and tabulation) in *taz1*Δ *yme1*Δ cells, which also harbored cells with giant mitochondria (indicated by a red arrow) and further, many of the cells were not intact or dying (panel **d,** see black arrow**)** with no visible mitochondria.

4.7. MITOPHAGY IS INEFFICIENT IN *taz1*Δ *yme1*Δ CELLS

Autophagy is a process that begins when cellular components and organelles are encapsulated by a double-membrane structure called the autophagosome. The encapsulated contents are then delivered to the vacuole or lysosome for degradation and recycling to meet the energy demands of the cells under starvation. Selective or cargo-specific autophagy is the selective uptake of organelles like mitochondria (mitophagy) or peroxisomes (pexophagy) by autophagosomes for degradation [124]. Unlike non-selective autophagy that occurs under starvation, selective autophagy can occur even in nutrient-rich conditions to suit the physiological requirements of the cell [124]. Mitophagy occurs in yeast cells to reduce the number of mitochondria as cells enter late stationary-phase, when the energy demands of the cell are less [125]. Accumulation of aberrant mitochondria is a source of increased ROS production, and unchecked accumulation of such mitochondria poses a risk to cell survival. Failure to remove damaged mitochondria by mitophagy is detrimental to yeast cell survival [126].

My EM analysis revealed that the *taz1*Δ *yme1*Δ (CWY 155) yeast cells accumulated a significant number of aberrant mitochondria; in some instances these aberrant structures were swollen, completely lacked the reticulated cristae network, and were in close proximity to the vacuolar membrane, suggesting that these large mitochondria might be undergoing mitophagy and/or were unable to complete mitophagy. This finding prompted me to determine if mitophagy can proceed effectively in *taz1*Δ *yme1*Δ cells compared to either single-deletion alone and to wild-type cells.

I used a well-characterized mitophagy assay that tracks vacuolar uptake and degradation of a GFP-tagged MOM protein Om45-GFP [107]. Under normal growth conditions there is very little mitophagy occurring in yeast cells; however, upon nitrogen starvation mitophagy is induced. The W and mutant yeast cells were grown to early stationary-phase to induce the expression of Om45-GFP. Fluorescence microscopy of the yeast cells at this stage showed that in all the yeast strains tested, the GFP signal was predominantly at the mitochondria, indicating that mitophagy was not occurring (**Figure 4.6 A panels a-h**). Cells were then washed and resuspended in nitrogen free medium (SD-N) and incubated at 25˚C for 24 hrs to induce mitophagy. Fluorescence microscopy after incubation in SD-N medium revealed that in more than 90% of wild-type (CWY 156) and *taz1*Δ (CWY 157) cells the GFP signal was predominantly at the vacuole, indicative of mitophagy occurring in these cells (**Figure 4.6 A panels i-l**). Although the bulk of GFP signal was observed in the vacuoles of *yme1*Δ (CWY 158) cells, GFP signal from outside the vacuole still persisted in some of these mutants implying a mild defect in mitophagy (**Figure 4.6 A panels m/n**). However, in the *taz1*Δ *yme1*Δ yeast cells (CWY 159), after incubation in nitrogen starvation medium, the GFP signal was predominantly observed from mitochondria not engulfed by the vacuole implying faulty mitophagy in these cells (**Figure 4.6 A panels o/p**).

Once mitochondria are taken up by the vacuole, Om45-GFP is cleaved to Om45 and free GFP. Unlike most proteins, free GFP is relatively stable in the vacuole. The difference in the amount of free GFP versus Om45-GFP was therefore used to estimate the efficiency of mitophagy. Western blotting with GFP anti-sera showed that before nitrogen

starvation, free GFP could not be detected in any of the yeast strains tested, and only Om45-GFP was seen (**Figure 4.6 B**).

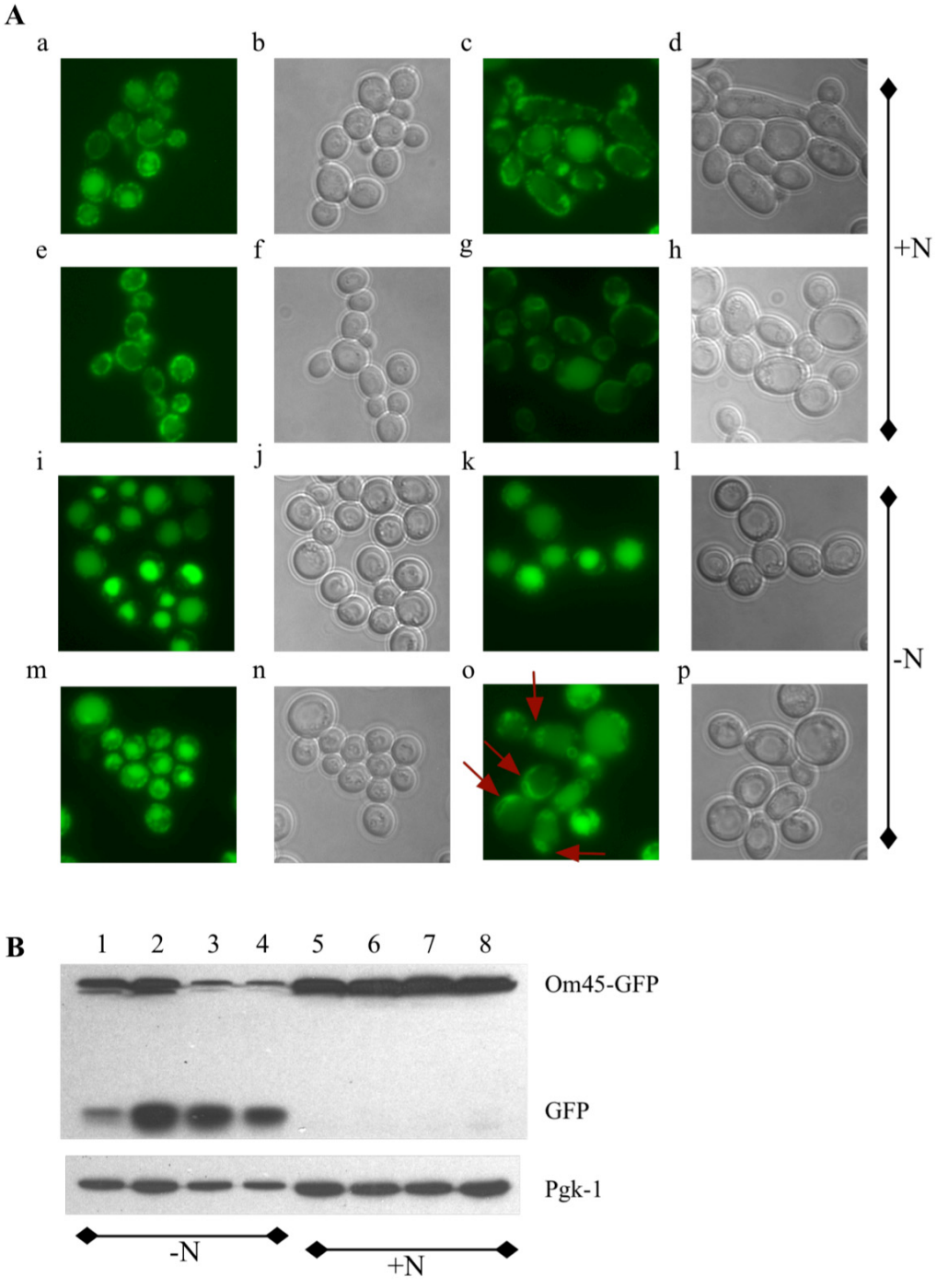
A
a
b
c
d
e
f
g
h
+N
i
j
k
l
m
n
o
p
-N
B
1
2
3
4
5
6
7
8
Om45-GFP
GFP
Pgk-1
-N
+N

Figure 4.6. Mitophagy is inefficient in *taz1*Δ *yme1*Δ yeast. A & B. *YIL136W* gene is tagged with a GFP epitope in all of the indicated strains and these cells were grown in YPL medium to 0.8-1.5 OD_{600}. The cells were then washed twice in distilled water and a sample of cells was saved and processed for microscopy and western blotting prior to resuspension and growth in SD-N medium. After 24 hours of growth in SD-N medium the cells were harvested and processed for fluorescence microscopy and for western blotting with anti-GFP antibodies. **A.** Shows representative fluorescence and differential interference contrast (DIC) microscopy indicating the cellular localization of Om45-GFP in various yeast cells before [wild-type (**a/b**), *taz1*Δ **(c/d),** *yme1*Δ **(e/f) and** *taz1*Δ *yme1*Δ **(g/h)**] and after [wild-type (**i/j**), *taz1*Δ **(k/l),** *yme1*Δ **(m/n)** and *taz1*Δ *yme1*Δ **(o/p)**] 24 hours of nitrogen starvation. After nitrogen starvation, Om45-GFP is predominantly localized to the vacuole (an indication of mitophagy) in the majority of the cells of all the yeast strains except *taz1*Δ*yme1*Δ yeast (arrows indicate cells with GFP signal outside the vacuole). **B.** An anti-GFP antibody was used to perform western blotting to ascertain the levels of Om45-GFP and free GFP in the indicated yeast cells before and after nitrogen starvation. Western blotting indicated lower levels of free GFP in *taz1*Δ *yme1*Δ cells when compared to wild-type and single mutants, indicating inefficient mitophagy in these cells. An antibody against Pgk1 was used to assess protein loading among the different lanes.

Lanes 1-4: After Nitrogen starvation for one day, lane 1: *taz1*Δ *yme1*Δ, lane 2: *yme1*Δ, lane 3: *taz1*Δ, lane 4: wild-type**.**

Lanes 5-8: Before Nitrogen starvation, lane 5: *taz1*Δ*yme1*Δ, lane 6: *yme1*Δ, lane 7:*taz1*Δ, lane 8: wild-type.

Abbreviations used: +N-growth medium with Nitrogen, **-N**-growth medium without Nitrogen.

However, after nitrogen starvation both free GFP and Om45-GFP could be detected by western blot in all the yeast strains analyzed; however, the amount of free GFP in *taz1*Δ *yme1*Δ yeast cells was significantly lower than in wild-type, *taz1*Δ and *yme1*Δ cells (**Figure 4.6 B**). Further, in *yme1*Δ cells the amount of Om45 bound GFP when assessed by western blotting is higher in this mutant (**Figure 4.6 B, lane 2**) when compared to other yeast cells. The above finding further strengthens the implication that *yme1*Δ cells are mildly defective in mitophagy. To summarize, loss of Taz1 function allows for mitophagy to occur, loss of Yme1 function causes a mild defect in mitophagy. However, loss of function of both proteins results in a more pronounced defect in mitophagy.

4.8. THE *taz1*Δ *yme1*Δ CELLS DO NOT SHOW AN INCREASE IN PROTEIN CARBONYL CONTENT COMPARED TO *taz1*Δ CELLS

ROS damage to mitochondria can result in mitophagy. To determine if there were changes in ROS-mediated damage to *taz1*Δ *yme1*Δ cells (CWY 155) compared to wild-type (CWY 150), *taz1*Δ (CWY 153), or *yme1*Δ (CWY 154) cells, the protein carbonyl content was determined (**Figure 4.7**). Increased ROS generation introduces carbonyl groups to the side chains of amino acid residues in proteins; therefore, measuring the cellular protein carbonyl content is a direct measure of ROS-induced damage, and an indirect measure of ROS production [114]. The amount of carbonyl moieties attached to cellular proteins is estimated by measuring the levels of protein-bound 2,4-dinitrophenylhydrazone (DNP), formed by the conversion of 2,4-dinitrophenylhydrazine to DNP by protein carbonyl groups [99,114].

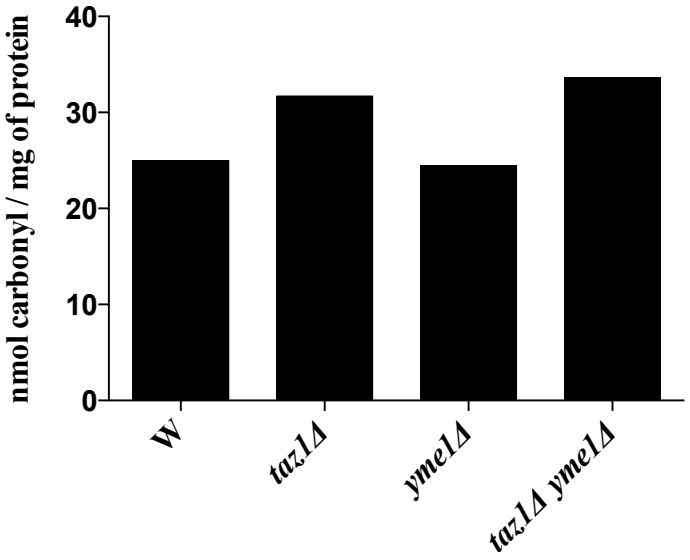

Figure 4.7. The *taz1*Δ *yme1*Δ mutant does not show an increase in protein carbonyl content compared to *taz1*Δ cells. Oxidative stress causes the introduction of carbonyl groups to side chains of amino acid residues in proteins. Protein carbonylation was measured by the spectrophotometric estimation of protein-bound 2,4-dinitrophenylhydrazone (DNP) formed by the conversion of 2,4-dinitrophenylhydrazine to DNP by protein carbonyl groups. Yeast cells were grown to 0.9-1.0 OD_{600} in YPL medium, after which proteins were extracted and estimated for carbonyl content using a protein carbonyl content assay kit (BioVision). The carbonyl content was then normalized to amount of protein in each sample and expressed as nmol carbonyl / mg of protein. The protein content in all the samples was measured by the bicinchoninic acid assay [127] using a BCA assay kit (BioVision).

To determine the degree of protein carbonylation, cells were harvested after they were grown to early stationary-phase in YPL medium at 37˚C. Yeast cell lysates were prepared and used to determine the amount protein carbonylation, which is expressed as nmol of protein carbonyl groups detected per mg of protein. The *taz1*Δ mutant has previously been shown to contain increased protein carbonyl content when grown in medium with a non-fermentable carbon source [99], and in my study the protein carbonyl content was also observed to increase in *taz1*Δ yeast cells (**Figure 4.7)**. The amount of protein carbonyl content in *taz1*Δ *yme1*Δ cells was also increased compared to that in wild-type and *yme1*Δ cells, but was similar to that observed increased in *taz1*Δ cells (**Figure 4.7**). Therefore, the accumulation of aberrant mitochondria due to inefficient mitophagy in *taz1*Δ *yme1*Δ cells does not exacerbate protein carbonylation in these cells beyond that observed in *taz1*Δ cells.

4.9. HIGHER-ORDER ASSOCIATION OF ETC III AND IV INTO III2IV2 SUPERCOMPLEXES IS NOT DEFECTIVE IN *taz1*Δ *yme1*Δ CELLS

Formation of ETC complexes requires CL for efficient assembly and stability [48]. In yeast, two monomers of ETC III have been shown to associate either with one or two monomers of complex IV to form III2IV2 and III2IV supercomplexes [46,48]. Supercomplex stability is important for the maintenance of ETC efficiency during cell stress to prevent ROS generation by preventing the escape of electrons from the ETC to the matrix or the IMS [45,50]. To determine if the increase in protein carbonylation in *taz1*Δ and *taz1*Δ *yme1*Δ cells is due to a decrease in ETC supercomplex formation, DDM-solubilized mitochondrial membranes were subjected to BN-PAGE followed by a western blotting with antibodies against Cox2, a subunit of complex IV (**Figure 4.8**). The loss of

TAZ1 function caused an accumulation of free ETC IV monomer with a concomitant decrease in III2IV2 levels (**Figure 4.8**). Surprisingly, although *yme1*Δ deletion by itself did not affect the formation of supercomplexes, inactivation of *YME1* in *taz1*Δ yeast cells was able to prevent the accumulation free complex IV and restore the formation of III2IV2 supercomplexes to wild-type levels (**Figure 4.8**). This finding implies that the increase in protein carbonylation observed in *taz1*Δ *yme1*Δ cells compared to wild-type cells is not due to an inability of these cells to maintain III2IV2 supercomplexes. An inability to maintain III2IV2 supercomplexes was surmised to be the reason that *taz1*Δ yeast cells displayed an increase in protein carbonylation compared to wild-type cells [99]. Although this still may be the case, the fact that protein carbonylation is increased to a similar extent in *taz1*Δ *yme1*Δ and *taz1*Δ cells, while III2IV2 supercomplex formation appear to be intact in *taz1*Δ *yme1*Δ cells and less intact in *taz1*Δ cells, suggests that the loss of Yme1 protease activity could be conducive for the physical association of complex III with complex IV in yeast cells lacking mature CL.

4.10. THE *taz1*Δ *yme1*Δ YEAST STRAIN IS SENSITIVE TO H_2O_2

In mitochondria, superoxide is generated when a impaired electron that had escaped the ETC reacts with molecular oxygen [128,129]. The superoxide can then react with iron to produce the potent reactive hydroxyl radical or it can react with lipids and proteins to produce lipid peroxides and protein carbonyls respectively [128].

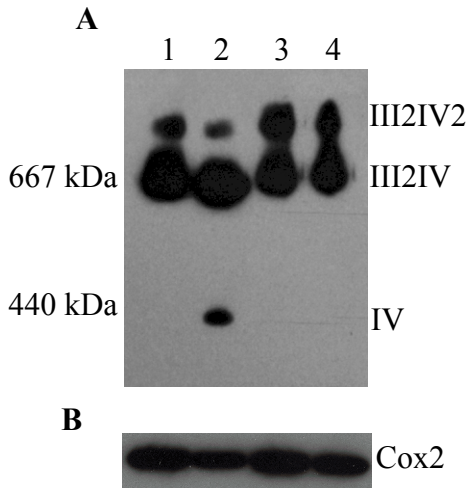

Figure 4.8. Supramolecular association of ETC III and IV into III2IV2 supercomplex is hampered in *taz1*Δ cells, and restored by *YME1* deletion. A. Shows a representative BN-PAGE gel that was transferred to nitrocellulose membrane and probed with an antibody against Cox2. Briefly, mitochondria were isolated and solubilized with DDM from the indicated strains. Proteins were then separated by BN-PAGE in the presence of Coomassie blue dye in the gel as described in section 3.20, and transferred to a PVDF membrane, which was probed with anti-sera against Cox2 to ascertain the formation of III2IV2 and III2IV ETC supercomplexes. Cox2 is one of the subunits of ETC IV; hence anti-sera against it is effective in assessing the efficiency of complex IV to associate with III to form higher-order supercomplexes. *TAZ1* deletion increases the accumulation of free IV monomer with a concomitant reduction in the formation of III2IV2 supercomplex. Interestingly, deletion of *YME1* from *taz1*Δ yeast (lane 4) restores III2IV2 supercomplex formation, preventing the accumulation of IV monomer. **B.** To assess the level of Cox2, equal amounts of mitochondrial extracts were separated under denaturing conditions (SDS-PAGE) and an antibody against Cox2 was used to determine the levels of Cox2 by western blot.

Lanes: 1: wild-type, 2: *taz1*Δ 3: *yme1*Δ, 4: *taz1*Δ *yme1*Δ**.**

In yeast, superoxide dismutases (SOD) located in both the cytosol and mitochondria quickly convert the superoxide to H_2O_2 to prevent the formation of potent reactive species like hydroxyl [128]. H_2O_2 is then detoxified to water by the actions of multiple enzymes such as catalase or glutathione-thioredoxin redox systems in the cytosol and by the peroxiredoxin-thioredoxin-glutathione redox system coupled to cytochrome c peroxidase in the mitochondria [128].

Based on my observation that there was a similar increase in ROS production in *taz1*Δ and *taz1*Δ *yme1*Δ cells, but the double-mutant exhibited a growth defect under the same growth condition, I determined if this 'sick' phenotype observed for the double-mutant is due to impaired ROS scavenging. Growth was determined in YPL medium in the presence or absence of 2.5 mM H_2O_2 at 25˚C and 37˚C (**Figure 4.9**). In the presence of 2.5 mM H_2O_2 the double-mutant (CWY 155) barely grew at 25˚C (**Figure 4.9 A**). H_2O_2 also decreased growth of the *yme1*Δ mutant (CWY 154) but not to the extent observed for *taz1*Δ *yme1*Δ cells, while the growth of the *taz1*Δ yeast strain (CWY 153) was also hindered in the presence of H_2O_2 but was on par with decreased growth observed in wild-type cells (CWY 150) (**Figure 4.9 A**). At 37˚C the *taz1*Δ *yme1*Δ failed to grow even in the absence of H_2O_2 while the growth of the other strains was not hindered under this condition (**Figure 4.9 B**), and the addition of H_2O_2 did not aggravate the growth phenotype when compared to 25˚C (**Figure 4.9 B**). These observations show that inactivation of the *TAZ1* gene does not alter sensitivity to H_2O_2, while inactivation of *YME1* resulted in a slight increase in sensitivity to H_2O_2. Inactivation of both *TAZ1* and *YME1* together resulted in a dramatic increase in H_2O_2 sensitivity, implying that there is a defect in H_2O_2 scavenging.

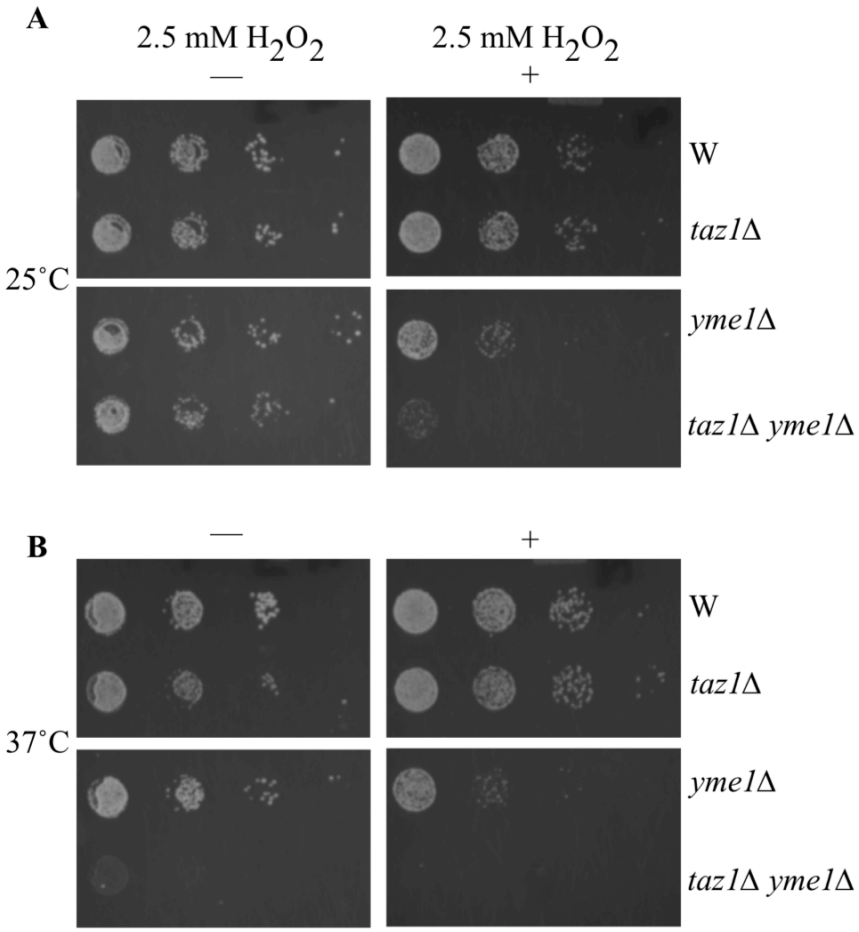

Figure 4.9. Double-mutant *taz1*Δ *yme1*Δ yeast strain is sensitive to H_2O_2. Yeast strains were grown to early stationary-phase 0.9-1.0 OD_{600} in SC medium and then suspended in the same medium to 0.45 OD_{600}, then serially diluted (1:10) and spotted on YPL medium with or without 2.5 mM H_2O_2 and grown for 3-5 days at 25˚C and 37˚C. **A.** The presence of 2.5 mM H_2O_2 in the growth medium affects the growth of both *yme1*Δ and *taz1*Δ *yme1*Δ cells. However, the growth defect is more pronounced in yeast lacking both *TAZ1* and *YME1*. **B.** The *taz1*Δ *yme1*Δ mutant fails to grow at 37˚C in YPL medium even in the absence of 2.5 mM H_2O_2.

4.11. VACUOLAR MORPHOLOGY AND ACIDIFICATION IS NORMAL IN *taz1*Δ *yme1*Δ YEAST CELLS

Complete loss of CL in *crd1*Δ yeast cells causes loss of vacuolar acidification and swollen vacuoles when these cells are grown in YPD at 37˚C [113]. It is not known if loss of either *TAZ1* or *YME1* causes defects in vacuolar morphology or acidification, and if this is exacerbated when both genes are inactivated. Further, autophagic degradation has been shown to be faulty in yeast with defective vacuolar acidification [130]. The Om45-GFP mitophagy assay indicated that the loss of *YME1* function modestly hinders mitophagy, and that deletion of the *TAZ1* gene in this mutant further exacerbates this defect. To determine if either aberrant vacuolar morphology and/or the loss of vacuolar acidification contribute to the mitophagy defect in the *taz1*Δ *yme1*Δ yeast, vacuolar morphology and its acidification state were visualized by labeling the vacuole with FM4-64 and quinacrine, respectively.

FM4-64 is a lipophilic dye that is inserted into the plasma membrane and then transported by the endocytic pathway to the vacuole. As FM4-64 accumulates in the vacuolar membrane it is routinely used to monitor vacuolar morphology. Yeast cells (strains CWY 150, 153, 154 and 155) were grown in YPD medium either at 25˚C or 37˚C and incubated with FM4-64 for 2 hours. At the end of the incubation time FM4-64 fluorescence was visualized using fluorescence microscopy. Vacuolar morphology was normal at both 25˚C and 37˚C in all the yeast strains tested (**Figure 4.10 A&B)**. The multilobular nature of the vacuole was more pronounced in all the strains grown at 37˚C than the cells cultured at 25˚C (**Figure 4.10 A&B)**.

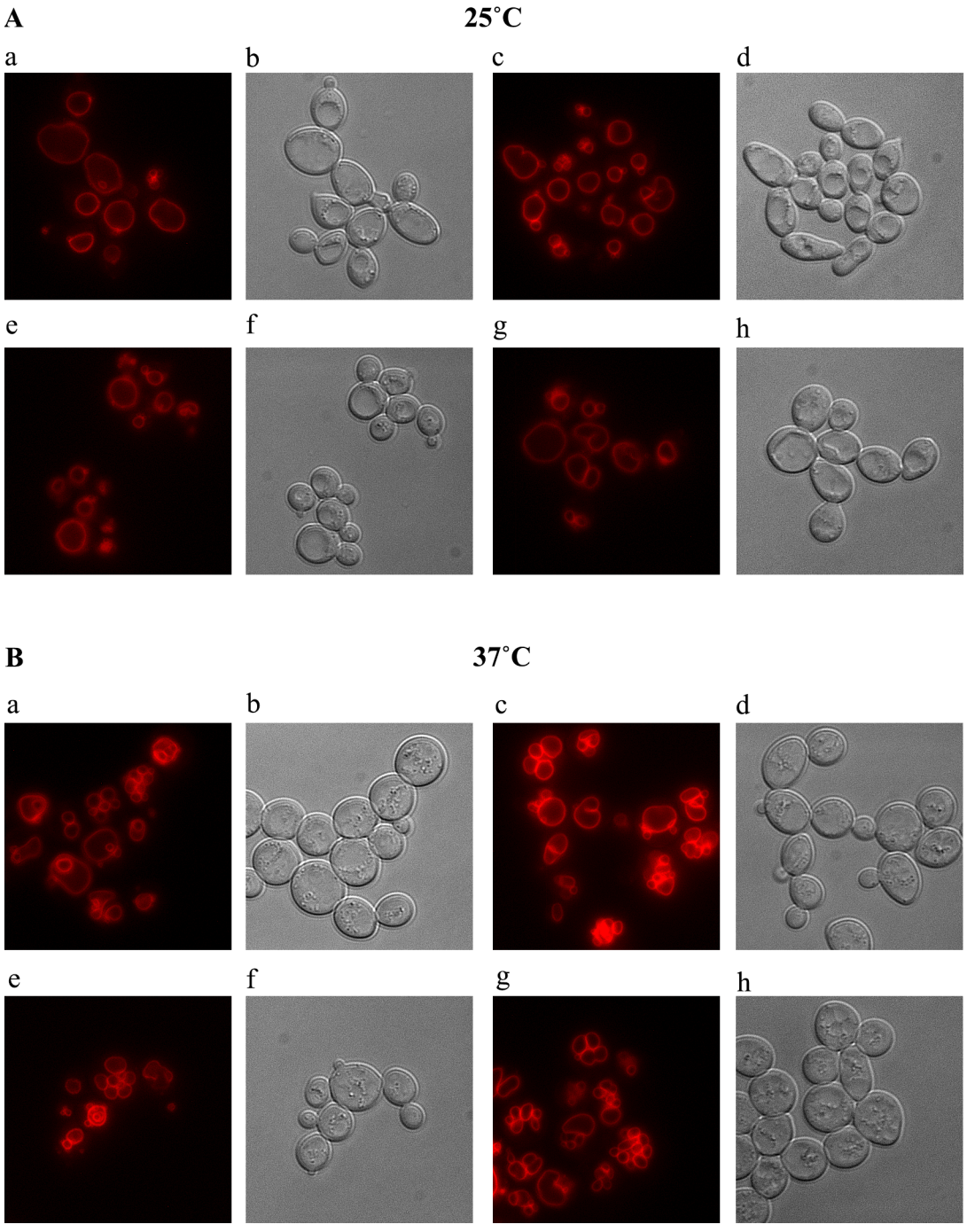
A
25˚C
a
b
c
d
e
f
g
h
B
37˚C
a
b
c
d
e
f
g
h

Figure 4.10. Vacuolar morphology assayed by FM4-64 staining is normal in mutant yeast. A&B. FM4-64, a lipophilic vital stain that reaches the vacuole and the endosomal membranes by endocytosis, was used to visualize the vacuolar morphology of the indicated strains. Briefly, log-phase cells grown in YPD at 25˚C (**A**) or 37˚C (**B**) were incubated with 1.6 μM FM 4-64 for 10 min at 25˚C (**A**) or 37˚C (**B**). The cells were then washed twice with fresh YPD medium and then transferred to YPD for incubation under constant shaking for 120 min at 25˚C (**A**) or 37˚C (**B**). At the end of incubation, samples from each of the cultures were spotted on a glass slide to visualize FM 4-64 fluorescence using a rhodamine filter set. FM4-64 staining of wild-type yeast (**a**), *taz1*Δ **(c),** *yme1*Δ **(e)** and *taz1*Δ *yme1*Δ **(g)** yeast cells. Panel's **b, d, f** and **h** show the DIC images of wild-type, *taz1*Δ, *yme1*Δ and *taz1*Δ *yme1*Δ yeast cells.

Quinacrine is a weak base that can easily diffuse across cellular membranes and accumulates in acidic compartments of the cell [112,131]. The vacuole maintains an acidic pH in its lumen; hence the accumulation of quinacrine, or a lack thereof, in this compartment can be used to determine if there is an increase in the pH of the vacuole [112]. Cells were grown in YPD medium at 37˚C to mid-log phase and then incubated with quinacrine for 5 min, washed and observed under a fluorescence microscope for quinacrine accumulation in the vacuolar lumen. The vacuoles of all the yeast strains (CWY 150, 153, 154 and 155) tested accumulated this weak base in its lumen to similar degrees (**Figure 4.11)**. These results indicate the single *taz1*Δ and *yme1*Δ mutants, and the *taz1*Δ *yme1*Δ double-mutants, do not have defects in their vacuolar morphology or its acidification.

4.12 OTHER GENES OF INTEREST IDENTIFIED BY *taz1*Δ SGA SCREEN

Functional work to determine why inactivation of *YME1* results in a growth defect in yeast cells also lacking the *TAZ1* gene was the main focus of this work. However, the SGA screen also identified other genes whose inactivation resulted in a growth defect in cells lacking the *TAZ1* gene. Some of these genetic interactions were confirmed by me using standard yeast genetics techniques, while others not confirmed by me have appeared in the literature or are found in databases that track genetic interactions in yeast. Each of these genetic interactions is mentioned here as a reference for future work on the biological function of Taz1.

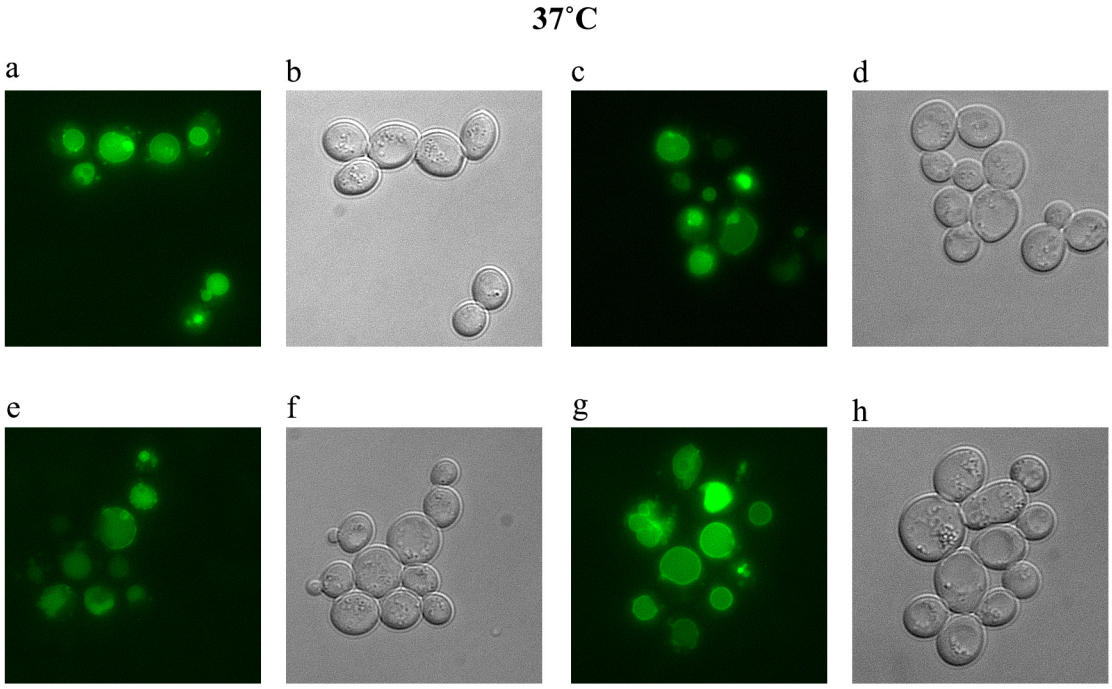

Figure 4.11. The single mutants *taz1*Δ and *yme1*Δ and the *taz1*Δ*yme1*Δ yeast strains do not have defects in vacuolar acidification. Quinacrine was used to assess the vacuolar acidification state of all the strains used in this study. This dye can diffuse easily across cellular membranes and since it is a weak base it accumulates in cellular compartments with a lower pH. A healthy vacuole maintains an acidic pH in its lumen and hence the accumulation of quinacrine or a lack thereof in its lumen can indicate its acidification state. Mid-log phase cells grown in YPD medium at 37˚C were washed twice in pre-warmed HEPES buffered YPD at pH 7.6 and then incubated at room temperature for 5 min in HEPES buffered YPD at pH 7.6 with 200 µM quinacrine. After that, the cells were washed in 50 mM PBS with 2% glucose at pH 7.6. The cells were then visualized for quinacrine fluorescence in the vacuolar lumen under a microscope. Quinacrine accumulation in the vacuolar lumen of wild-type (**a**), *taz1*Δ **(c),** *yme1*Δ **(e)** and *taz1*Δ *yme1*Δ **(g)** yeast cells. Panels **b, d, f** and **h** show the DIC images of wild-type, *taz1*Δ, *yme1*Δ and *taz1*Δ *yme1*Δ yeast cells.

A closer look at the SGA data implied that six of the structural genes of the arginine biosynthetic process that functions in the cytoplasm and mitochondria (*ORT1, ARG1, ARG3, CPA1, CPA2* and *CPA1* attenuator peptide) might have genetic interactions with *TAZ1*. Random spore analysis indeed confirmed that when *ARG1* was deleted from *taz1*Δ yeast cells it caused an aggravating effect on the growth of the double-mutant cells. The remaining genetic interactions need to be confirmed. Collectively, these genetic interactions imply that the maintenance of arginine metabolism is important for yeast cell fitness in cells that have no Taz1 function.

My SGA analyses also indicated that deletion of genes involved in iron metabolism, namely *ISA1, SIT1* and *FRE4*, decreased the growth of *taz1*Δ cells (**Table 3)**. Both *ISA1* and *ISA2* encode mitochondrial proteins that are required for the maturation of [4Fe-4S] proteins. *GGC1* encodes a mitochondrial GTP/GDP transporter that is also known to import iron from the IMS to the matrix where the maturation of [4Fe-4S]-containing proteins occurs. Random spore analysis indicated that both *ISA2* and *GGC1*, but not *ISA1*, decreased growth of cells with an inactivated *TAZ1* gene. Iron uptake in yeast is dependent on a family of iron siderophore transporters that import ferrous ion-containing siderophores into the cell. These siderophores are then acted upon by a family of ferric reductases that reduce them to free ferric ions to be used by the cell. SGA analyses indicated that deletion of either *SIT1* (siderophore transporter) or *FRE4* (ferric reductase) in *taz1*Δ cells affected the growth of the double mutant. These observations, in conjunction with the genetic interaction of *TAZ1* with *ISA2* and *GGC1*, imply that in the absence of *TAZ1,* maintenance of mitochondrial iron metabolism is necessary for cell viability. However, it should be noted that the genetic interaction between *TAZ1* and

SIT1, and *FRE4* and *TAZ1*, has not been confirmed by random spore analysis or tetrad analysis. Nonetheless, there appears to be an intriguing link between mitochondrial iron import and Taz1 function.

The TOM (translocase of outer membrane) complex is located in the MOM and is responsible for the initiation of the import of mitochondrial targeted proteins. Tom5 is part of this complex and my SGA screen and random spore analysis confirmed that inactivation of the *TOM5* gene decreases the growth of cells lacking the *TAZ1* gene. This genetic interaction has been confirmed and analyzed in detail by others, where it was determined that inactivation of Taz1 decreases mitochondrial protein import through the MOM [132].

Two large-scale studies [35,133] to characterize the genetic networks of yeast metabolism and yeast mitochondria found that *TAZ1* has a negative genetic interaction with *PYC2* (cytoplasmic pyruvate carboxylase isoform), *MIP1* (mitochondrial DNA polymerase gamma subunit required for mitochondrial genome maintenance), *GEP3* considered a putative GTPase regulating the assembly of mitochondrial ribosome small subunit and *PRO2* (gamma-glutamyl phosphate reductase; catalyzes the second step in proline biosynthesis). These genes were also identified by SGA analyses in my study but were not followed up for further confirmation by random spore or tetrad analysis (**Table 4**). However, I mentioned them here for future reference.

Table 4. Candidate genes that might have negative genetic interactions with *TAZ1*.

Standard Name	Systematic Name	Saccharomyces Genome Database description [110]
*PYC2**	*YBR218C*	Pyruvate carboxylase isoform; cytoplasmic enzyme that converts pyruvate to oxaloacetate; differentially regulated than isoform Pyc1; mutations in the human homolog are associated with lactic acidosis
*MIP1**	*YOR330C*	Mitochondrial DNA polymerase gamma subunit; conserved C-terminal segment is required for the maintenance of mitochondrial genome
*GEP3**	*YOR205C*	Protein required for mitochondrial ribosome small subunit biogenesis; null mutant is defective in respiration and in maturation of 15S rRNA; protein is localized to the mitochondrial inner membrane; null mutant interacts synthetically with prohibitin (Phb1).
*PRO2**	*YOR323C*	Gamma-glutamyl phosphate reductase; catalyzes the second step in proline biosynthesis

* Indicates not tested by random spore or tetrad analysis.

The interaction of *TAZ1* with *GEP3* is interesting because inactivation of *GEP3* has negative genetic interaction with prohibitins (IMS localized multimers that regulate the activity of m-AAA protease), which are known to genetically interact with the structural genes of CL biosynthesis and are proposed to organize mitochondrial membranes into CL rich compartments [38,134]. Therefore, the observed negative genetic interaction between *TAZ1* and *GEP3* implies that the failure to remodel *de novo* synthesized CL to mature CL could negatively impact the organization of CL rich domains within the mitochondrial membrane.

CHAPTER 5. DISCUSSION

The focus of this thesis was to use SGA analyses to identify genes which, when inactivated, cause growth defects in *taz1*Δ yeast cells. The genome-wide screen identified genetic interaction between *TAZ1* and *YME1* that encodes the IMS-localized quality-control protease Yme1. Further, negative genetic interactions were also noted between *TAZ1* and genes regulating most of the arginine biosynthetic pathway and genes controlling mitochondrial iron metabolism. However, *yme1*Δ yeast cells, like the *taz1*Δ mutant, grow poorly in growth medium that requires energy production from mitochondria at 37˚C [123] and were also shown to possess mitochondrial abnormalities [123] similar to what has been noted with the loss of tafazzin function in yeast and humans. Since, tafazzin and Yme1 single mutants share similar phenotypes, both proteins are likely to share biochemical function(s). Therefore, to identify these shared biochemical function(s), the focus of my thesis was directed towards characterizing the 'sick' phenotype of *taz1*Δ *yme1*Δ double-mutant yeast cells.

5.1. CHARACTERIZATION OF YEAST MODEL OF BTHS

The CL and MLCL mass of yeast lacking *TAZ1* was assessed. The *taz1*Δ mutant accumulated the CL remodeling precursor MLCL compared to wild-type cells when grown in medium containing either dextrose or lactate as the sole carbon source (**Figure 4.1 A**). However, the loss of CL mass was evident in *taz1*Δ yeast cells when they were grown in medium containing lactate, but not dextrose (**Figure 4.1 A**). This observation is consistent with the previous characterization of steady-state phospholipid levels in *taz1*Δ

yeast, which showed less than 10% reduction in CL mass compared to wild-type cells when they were estimated for stationary-phase cells grown in dextrose containing medium [78]. As previously shown the *taz1*Δ mutant used in this study grew poorly in medium with non-fermentable carbon source like lactate at 37˚C (**Figure 4.1 B**) [78]. In summary, the steady-state CL and MLCL mass and growth phenotype of the *TAZ1* deficient yeast cells used in this study were in agreement with previous characterization of *taz1*Δ yeast cells.

5.2. CHARACTERIZATION OF YEAST LACKING *TAZ1* AND *YME1*

Before the characteristics of the 'sick' phenotype of the *taz1*Δ *yme1*Δ double mutant were determined, the growth phenotype of *yme1*Δ yeast cells used in this study was determined in medium with 2% lactate as the carbon source at 25˚C and 37˚C. As previously reported [123], the *yme1*Δ cells grew poorly in this medium at 37˚C (**Figure 4.3**). Electron microscopy revealed that the majority of *yme1*Δ cells contained normal mitochondria, but also that 25% of the total mitochondria accounted for were abnormally shaped with loss of reticulated cristae structures (**Figure 4.5**). These observations are in agreement with the previous studies [119,123] of yeast lacking *YME1*; however, cells used in this thesis did not contain giant mitochondria or mitochondria that were pinched within the vacuolar membrane, which is a characteristic of mitochondria undergoing mitophagy. In *taz1*Δ cells, approximately 20% of the total mitochondria were elongated but did not show any alterations in their MIM cristae structures (**Figure 4.5**). This observation is contradictory to one study [98] that reported abnormal mitochondria with cristae reticulations and MIM adhesion, but in agreement with a recent study [83] that assessed mitochondrial

morphology of tafazzin deficiency in various yeast strain backgrounds. This study reported that cells with the W3031-a genetic background did not possess any aberrant mitochondria, and that loss of tafazzin from these cells produced only mild alterations to mitochondrial morphology with elongated MOM membranes. In agreement with the above finding, I did not observe any aberrant mitochondria in the wild-type W3031-a cells used for this thesis. Mitochondrial morphology defects in the *taz1*Δ *yme1*Δ cells were more severe than in the *yme1*Δ cells, with approximately 60% of the total mitochondria abnormal, and moreover, a few cells possessed giant mitochondria that were in close proximity to the vacuole (**Figure 4.5**). Further, many of the t*az1*Δ *yme1*Δ cells when grown in non-fermentable medium had large multi-vacuolar structures, and appeared to be in the processes of dying, as they were not intact. It is not clear why loss of *YME1* function from *taz1*Δ cells exacerbates defects in mitochondrial morphology, but it is not due to gross changes to mitochondrial phospholipid levels. This conclusion was reached by comparing the steady-state phospholipid levels of all the yeast strains used in this study using radiolabelled ^{32}P.

Loss of both CL and PE affects mitochondrial biogenesis and cause synthetic lethality in yeast [40]. In this context, it is interesting that Yme1 regulate the turnover of proteins such as Psd1, Ups1 and Ups2, which are modulators of both PE and CL levels in yeast [122,135]. Psd1 catalyzes the conversion of PS to PE in the mitochondria, and both Ups1 and Ups2 reside in the IMS and are proteolytic targets of Yme1 [136]. Ups1 has been shown to transport PA from MOM to MIM to supply PA for CL synthesis [8], and Ups2 by an unidentified mechanism, has been shown to maintain normal PE levels in yeast

[136]. Therefore, I hypothesized that loss of *YME1* in *taz1*Δ cells might exacerbate the defects in CL metabolism caused by *taz1*Δ or it might result in the loss of both PE and CL, thereby causing defects in mitochondrial morphology. However, phospholipid analyses showed slightly elevated PE levels in *taz1*Δ *yme1*Δ cells when compared to single mutants (**Figure 4.4**). Furthermore, the levels of CL and MLCL were unchanged in the double-mutant when compared to the *taz1*Δ mutant. Interestingly, the PC levels of all the mutants were considerably lower when compared to those of wild-type cells. Yeast lacking *TAZ1* have been previously shown to contain lower mitochondrial PC levels compared to wild-type cells [12], but there are no previous reports of loss of PC in *yme1*Δ yeast cells. Further, loss of *YME1* in the *taz1*Δ context mildly exacerbates the loss of PC in this mutant. The above finding is interesting because PC is a major phospholipid and any changes to its levels could significantly alter the biology of the cell. Therefore, further analysis of PC metabolism and regulation in these mutants is warranted. Moreover, it should be noted that these findings of changes in phospholipid levels have to be followed up with detailed experiments, as I did not precisely quantitate the total amount of ^{32}P incorporation into phospholipids. The exact mechanism leading to severe mitochondrial abnormalities in *taz1*Δ *yme1*Δ cells is not clear, not involve gross changes in phospholipid levels. The mitochondrial ultrastructure defects in *yme1*Δ cells have been strongly linked to the aggregation of proteins that are components of the MICOS complex (Aim5, Aim13, Fcj1, Aim37), which is essential for maintenance of mitochondrial cristae junctions and organization of mitochondrial inner-membrane architecture [137]. Therefore, it is possible that a simultaneous loss of *YME1* in *taz1*Δ yeast cells could worsen the mitochondrial ultrastructural defects associated with this cell type.

Aberrant mitochondria are an increased source of ROS in the cell, and therefore, have to be promptly removed to sustain cell survival [126]. For this removal, mitophagy selectively targets damaged mitochondria to be degraded in the vacuole [125], and mitophagy plays a crucial role in clearing abnormal mitochondria to prevent uncontrolled ROS generation in yeast [126]. Since *taz1*Δ *yme1*Δ cells accumulate aberrant mitochondria and contain giant misshapen mitochondria proximal to the vacuole, the ability of these cells to undergo mitophagy was tested using the well-characterized Om45-GFP assay (**Figure 4.6**) [107,138]. All the yeast strains used in this study were able to undergo mitophagy, but the efficiency of mitophagy was drastically reduced in *taz1*Δ *yme1*Δ double-mutant cells. Therefore, Taz1 and Yme1 are together necessary for the maintenance of efficient mitophagy in yeast cells.

The mitochondrial protein Atg32 is selectively expressed in mitochondria destined for mitophagy, and its expression and specific interaction with autophagy scaffold protein Atg11 is crucial for selective uptake of mitochondria into the vacuole in yeast [139]. Recently, Yme1 has been shown to proteolytically process the C terminus of Atg32, and this step was necessary for Atg32 interaction with Atg11 [140]. Loss of Yme1 prevents Atg32 processing, which reduced its interaction with Atg11, resulting in a 70-80% reduction in mitophagy [140]. In this thesis, yeast-lacking Yme1 were found to only show a mild reduction in mitophagy, and only cells that lacked both Taz1 and Yme1 showed a drastic reduction in mitophagy. At present, the reason for this difference in the extent of mitophagy is not clear, but it could be due to the sensitivity of the mitophagy assay used. The above study used mitoPho8delta60 alkaline phosphatase assay (mitoPho8delta60 is a mitochondrion-targeted vacuolar alkaline phosphatase that becomes active when

mitochondria end up in the vacuole), and it is quantitative when compared to the semi-quantitative Om45-GFP assay used in this thesis [140]. Comparative mitophagy analyses using both the methods and detailed analysis of the processing state of Atg32 could decipher whether there is a difference in sensitivity between the assay methods and/or if there is a difference in the regulation of Atg32 processing. The Atg32 processing assay could also identify if the combined loss of both *TAZ1* and *YME1* exacerbates the Atg32 processing deficiency seen in *yme1*Δ cells. If this is the case, it could imply that the Yme1 protease activity towards Atg32 is regulated by mature CL and/or inhibited by MLCL. Respiratory growth and oxidative stress were shown to cause mitophagy by inducing Atg32 expression [141]. It will be interesting to compare and contrast the expression and localization of Atg32 in cells lacking both *TAZ1* and *YME1* with that in *yme1*Δ single mutants under these conditions. This experiment might tell us if the physiological functions of mature CL (maintenance of mitochondrial potential, morphology, protein import, etc.) have a role in expression, mitochondrial import, and localization of Atg32, and could explain the drastic reduction in mitophagy seen in *taz1*Δ *yme1*Δ cells compared to *yme1*Δ mutants.

In this thesis, I showed that loss of mature CL (*taz1*Δ mutant) does not abrogate mitophagy, but, we do not know the efficiency of mitophagy in yeast cells that cannot make any CL (*crd1*Δ). Determination of mitophagy efficiency in *crd1*Δ cells is important, because a specific role for CL in mitophagy has emerged in mammalian systems [142]. Recently, in rat cortical neurons, CL was shown to redistribute from the MIM to the MOM and then specifically bind to the microtubule-associated protein 1 light chain 3 (MAP1LC3/LC3) upon mitophagy induction by rotenone or 6-hydroxydopamine [142].

Preventing this interaction between externalized CL and the characteristic protein of the autophagosomal membrane (LC3) by introducing mutations in the CL-binding site of LC3 blocked the delivery of mitochondria to lysosomes via autophagosomes [142]. Further, in BTHS patient-derived fibroblasts, mitophagy was abrogated under oxidative stress [143]. Retroviral expression of human tafazzin in these patient-derived fibroblasts was able to restore both mature CL levels and mitophagy [143]. In these cells, under oxidative stress, mature oxidized CL was shown to redistribute to the MOM, and these mitochondria were marked for mitophagy [143]. However, in BTHS patient cells lacking functional tafazzin this process was absent [143]. These studies clearly indicate that in higher eukaryotes mature CL serves as an important marker to confer selectivity in mitophagy.

At present we do not know if CL redistribution occurs in yeast prior to mitophagy. Therefore, future studies to evaluate the externalization or a lack thereof of CL or oxidized CL (under oxidative stress) to the MOM upon mitophagy induction in yeast will be valuable to understand the role of CL in mitophagy. Yeast lacking *ATG32* are viable in medium with a non-fermentable carbon source and do not contain increased ROS levels. This implies the existence of alternative Atg32-independent mitophagy pathway(s) that can clear aberrant mitochondria that are produced under respiring growth conditions [139]. In light of mitophagy data in this thesis, I could speculate that mature CL specifically regulates components of this alternative pathway(s) or is required for its activity, or interestingly, CL redistribution itself may be a specific signal to induce mitophagy. To this end, identification of gene(s) whose deletion reverses the mitophagy phenotype seen in *taz1*Δ *yme1*Δ cells could provide mechanistic details on these Atg32-independent mitophagy pathways.

Loss of CL impairs vacuolar morphology and the ability to maintain an acidic vacuolar pH [113]. Maintenance of proper vacuolar morphology and acidification state is important for the ability to carry out autophagy [130]. To see whether vacuolar defects caused the drastic loss of mitophagy in the double-mutant yeast cells studied here, vacuolar morphology and its luminal pH were analyzed by FM4-64 and quinacrine staining, respectively. The *taz1*Δ *yme1*Δ strain did not show alterations in vacuole morphology or acidification (**Figures 4.10 & 4.11**). These assays were performed in medium containing dextrose to match the nitrogen-starvation conditions used to carry out the mitophagy assay. However, it will be interesting to note if the vacuolar health is compromised when *taz1*Δ *yme1*Δ cells are grown on medium with non-fermentable carbon sources such as lactate or ethanol. Therefore, at present, the role of a defective vacuole in abrogation of mitophagy in double-mutant yeast cells cannot be completely ruled out.

Abnormal mitochondria are an increased source of ROS production, and failure to clear these mitochondria increases the oxidative stress in the yeast cell [126]. Because I showed that *taz1*Δ *yme1*Δ mutant accumulates abnormal mitochondria and that are not efficiently cleared by mitophagy, oxidative damage in these cells was determined by measuring the amount of protein carbonylation. Protein carbonylation was increased in both the *taz1*Δ single-mutant cells and *taz1*Δ *yme1*Δ double-mutant cells but the accumulation of aberrant mitochondria in the latter yeast strain did not exacerbate its protein carbonyl content compared to that of *taz1*Δ cells. Previous estimation in yeast lacking either *TAZ1*

or *CRD1* have shown a doubling (~50 mM carbonyl/M protein) of protein carbonylation when compared to wild-type cells (~25 mM carbonyl/M protein) in YP medium with ethanol at 37˚C [99]. The carbonyl content did not double but increased from ~25 nmol carbonyl / mg protein in wild-type cells to ~35 nmol carbonyl / mg protein in both *taz1*Δ and *taz1*Δ *yme1*Δ mutants when grown in YPL at 37˚C (**Figure 4.7**), in agreement with previously estimated values under this assay condition [99]. Therefore, at present, it seems that the accumulation of aberrant mitochondria in *taz1*Δ *yme1*Δ mutant does not cause a more pronounced increase in ROS production than the increase determined in *taz1*Δ cells.

The ETC complexes III and IV associate to form supercomplexes. These higher-order complexes have been shown to be destabilized in both *taz1*Δ and *crd1*Δ mutants [45,49]. In yeast lacking *TAZ1,* complex IV has been shown to dissociate from complex III, and this dissociation is surmised to cause a leak of electrons from the latter complex to act as source of superoxides [49]. In my study, BN-PAGE assay showed that the supercomplex formation is destabilized in the *taz1*Δ mutant (**Figure 4.8**), supporting the notion that this destabilization might cause ROS overproduction. Surprisingly, loss of Yme1 function stabilized the supercomplex formation in *taz1*Δ cells (**Figure 4.8**). It is not clear how lack of Yme1 activity reverses the dissociation of complex IV from complex III. It should be noted that the amount of unassembled Cox2, which is one of the subunits of complex IV, is a proteolytic target of Yme1 [144], and the amount of unassembled Cox2 increased in *yme1*Δ yeast [144]. Further, Yme1 aids the folding of Cox2 in the absence of Cox18, which is the major chaperone of mitochondrially encoded Cox2 [145]. At present, how these functions of Yme1 affect the stable association complex IV with complex III is not

known and warrants further investigation. We do not know if dissociated complex IV is highly unstable resulting in degradation of Cox2 by Yme1. This idea seems highly unlikely, because we did not see lowering and restoration of Cox2 levels in *taz1*Δ and *taz1*Δ *yme1*Δ mutants, respectively (**Figure 4.8**). ROS damage to proteins measured by protein carbonyl content can either be caused by ROS overproduction or by ineffective ROS scavenging. A previous study has shown that the ROS scavenging system is intact in *taz1*Δ cells as the growth of these mutant cells is not hindered by the presence of oxidative stressors like H_2O_2 or paraquat in the growth medium [99]. It was concluded that the increase in protein carbonylation seen in *taz1*Δ cells is caused by ROS overproduction [99]. In this thesis, when growth of yeast cells was tested in the presence of 2.5 mM H_2O_2 loss of *YME1* resulted in a slight increase in sensitivity to H_2O_2, while inactivation of both *TAZ1* and *YME1* together resulted in a dramatic increase in H_2O_2 sensitivity, implying that there is a defect in H_2O_2 scavenging in these two mutants (**Figure 4.9**). Loss of *TAZ1* did not hinder growth in medium containing H_2O_2 a finding in agreement with the previous study indicating that H_2O_2 detoxification mechanisms are intact in this mutant [99]. In yeast, superoxide dismutases Sod1 (cytosol and IMS) and Sod2 (mitochondrial matrix) are known to initiate ROS scavenging by converting superoxide to H_2O_2, which is then detoxified by the catalases Cta1 (mitochondria and peroxisomes) and Ctt1 (cytosol), and by glutathione-thioredoxin redox systems in the cytosol and by the peroxiredoxin-thioredoxin-glutathione redox system coupled to cytochrome c peroxidase in the mitochondria [128,129]. At present, how loss of *YME1* causes H_2O_2 scavenging defects and how this phenotype is aggravated by the loss of Taz1 function is not clear. Although *yme1*Δ cells have been shown to be sensitive to H_2O_2 [146], the expression status and activity of these scavenging systems in the *yme1*Δ mutant

has not been studied. Future studies involving expression profiling and overexpression of the major players in ROS scavenging could identify the specific defect in ROS scavenging in *yme1*Δ and *taz1*Δ *yme1*Δ mutants. With this data we could speculate that loss of *YME1* from *taz1*Δ mutant cells negates ROS overproduction by possibly restoring respiratory-chain supercomplex stability, but *YME1* deletion causes an H_2O_2 scavenging defect, which ultimately affects cell survival under oxidative stress. Conversely, it is possible that the increased sensitivity of *taz1*Δ *yme1*Δ cells to H_2O_2 treatment is due to a lack of damaged mitochondrial removal through mitophagy, and not because of defects in ROS scavenging. In support of this argument, ROS have been shown to promote autophagy [147] by inhibiting the delipidation of LC3 [148], and H_2O_2 in particular causes mitophagy by inducing mitochondrial fragmentation in HeLa cells [149]. Failure to remove damaged mitochondria results in increased ROS generation ultimately resulting in cell death [126]. Since mitophagy is inefficient in *taz1*Δ *yme1*Δ cells, sensitivity to H_2O_2 could be due to the effect of accumulation of damaged mitochondria.

5.3. MAINTENANCE OF CELLULAR IRON METABOLISM IS CRUCIAL FOR YEAST LACKING *TAZ1*

In addition to *YME1,* SGA analysis also found that *TAZ1* has negative genetic interactions with genes regulating iron metabolism and with structural genes for arginine biosynthesis. The genetic interaction with genes regulating iron metabolism is interesting, because a previous study using a *crd1*Δ mutant has shown genetic interaction between CL and iron metabolism, especially with *ISU1* involved in the synthesis of Fe-S clusters, which are part of Fe-S proteins such as aconitase, succinate dehydrogenase, and sulfite reductase,

[150]. Briefly, that study showed that the loss of CL led to increased mitochondrial iron levels, upregulation of iron-uptake genes, growth sensitivity to $FeSO_4$, reduced activities of Fe-S proteins, loss of Fe-S cluster generation and maturation, and a negative genetic interaction with *ISU1* [150]. My SGA analysis with the *taz1*Δ mutant did not uncover genetic interactions with *ISU1*, but did show negative genetic interaction with *ISA2* and *GGC1,* which are required for the maturation of Fe-S proteins and for mitochondrial iron import across the IMS to the matrix. In addition, *TAZ1* also showed negative genetic interactions with *SIT1* and *FRE4,* which are involved in cellular iron uptake. The identification of these genes in my SGA screen further reinforces the role of CL in iron metabolism, but it warrants further investigations to better understand the mechanistic intricacies.

CHAPTER 6. SUMMARY

To summarize, in this thesis I generated a yeast model of BTHS by deleting *TAZ1*. I then showed that the *taz1*Δ yeast mutant, like BTHS patients, accumulated MLCL and showed a loss in CL mass. The *taz1*Δ yeast cells also showed defects in mitochondrial function when stressed, for they grew poorly at 37˚C in growth medium that required mitochondrial respiration. SGA analysis has been successfully used in the past to define so called query-gene function as it could identify genes that function in parallel compensatory pathways and pin-point genes that encode proteins that are in the same functional complex to that of the protein encoded by the query-gene [151]. Therefore, SGA analysis was performed with the *taz1*Δ mutant to better understand the functional role of *TAZ1* in yeast. This approach identified a negative genetic interaction between *TAZ1* and *YME1*, as loss of the latter gene hindered the growth of *taz1*Δ yeast cells. I then characterized the *taz1*Δ *yme1*Δ double mutant and found that it is defective in mitophagy. Loss of Yme1 in yeast caused a mild reduction in mitophagy but this defect was worsened in cells lacking both *YME1* and *TAZ1*. Further work is required to explain the mechanistic details of why there is a drastic loss of mitophagy in the double-mutant cells. However, with my data and the evidence from a recent study that the protease activity of Yme1 on Atg32 is crucial for the selective degradation of damaged mitochondria [140] I could hypothesize that *TAZ1* and *YME1* either act in concert to regulate Atg32 processing to ensure efficient mitophagy, or mature CL catalyzed by *TAZ1* regulates a parallel compensatory Atg32-independent mitophagy pathway. A recent study in yeast showed that unremodeled CL and mature CL are equally adept at supporting certain mitochondrial functions such as maintenance of electron transport capacity and

maintenance of mitochondrial morphology [83]. However, that study did not completely rule out the possibility of mitochondrial functions that specifically require mature CL or are inhibited by MLCL. I show here that mitophagy is inefficient in *yme1*Δ cells lacking *taz1*Δ (cannot make mature CL); therefore, I can speculate that with the help of SGA analysis I was able to identify a specific function of mature CL in mitophagy. I also found that the *yme1*Δ mutant is sensitive to H_2O_2, which drastically worsens when *TAZ1* is deleted from these cells. I suspect that this exacerbation is due to severe defects in the ROS scavenging capacity of the double mutant, but future studies are warranted to fully explain this. Detailed analysis (expression, activity, etc.) of ROS scavenging system, overexpression of *YAP1* (induces the expression of genes regulating glutathione peroxidases, dismutases, catalase and cytosolic thioredoxins in response to ROS [152]) and assessment of sensitivity to other ROS inducers such as menadione and paraquat might help to clarify this scenario.

CHAPTER 7. CONCLUSION

This thesis fills a major gap in knowledge by using a genome-wide screen to identify processes that participate along with Taz1 to regulate cell growth. Focusing in on the role of the i-AAA protease Yme1, I determined that (i) tafazzin and Yme1 together are required for efficient growth on a fermentable carbon source, and this growth defect is exacerbated when mitochondrial respiration is necessary, (ii) together these genes are necessary for the maintenance of normal mitochondrial morphology, (iii) cells lacking both genes are more sensitive to H_2O_2, and (iv) together both genes are required for efficient mitophagy. Future work should focus on further dissecting the mechanism(s) by which Taz1 and Yme1 regulate mitophagy, and characterizing the other processes identified by my SGA analysis that compromise cell growth in the absence of Taz1 function.

REFERENCES

1. Xu Y, Malhotra A, Ren M, Schlame M (2006) The enzymatic function of tafazzin. J Biol Chem 281: 39217–39224. doi:10.1074/jbc.M606100200.

2. Schlame M, Ren M (2006) Barth syndrome, a human disorder of cardiolipin metabolism. FEBS Lett 580: 5450–5455. doi:10.1016/j.febslet.2006.07.022.

3. Schlame M (2008) Cardiolipin synthesis for the assembly of bacterial and mitochondrial membranes. J Lipid Res 49: 1607–1620. doi:10.1194/jlr.R700018-JLR200.

4. Schneiter R (1999) Electrospray Ionization Tandem Mass Spectrometry (ESI-MS/MS) Analysis of the Lipid Molecular Species Composition of Yeast Subcellular Membranes Reveals Acyl Chain-based Sorting/Remodeling of Distinct Molecular Species En Route to the Plasma Membrane. J Cell Biol 146: 741–754. doi:10.1083/jcb.146.4.741.

5. Gebert N, Joshi AS, Kutik S, Becker T, Mckenzie M, et al. (2009) Mitochondrial cardiolipin involved in outer-membrane protein biogenesis: implications for Barth syndrome. Curr Biol 19: 2133–2139. doi:10.1016/j.cub.2009.10.074.

6. Horvath SE, Daum G (2013) Lipids of mitochondria. Prog Lipid Res 52: 590–614. doi:10.1016/j.plipres.2013.07.002.

7. Buckland AG, Kinkaid AR, Wilton DC (1998) Cardiolipin hydrolysis by human phospholipases A2. The multiple enzymatic activities of human cytosolic phospholipase A2. Biochim Biophys Acta 1390: 65–72.

8. Connerth M, Tatsuta T, Haag M, Klecker T, Westermann B, et al. (2012) Intramitochondrial transport of phosphatidic acid in yeast by a lipid transfer protein. Science 338: 815–818. doi:10.1126/science.1225625.

9. Tamura Y, Harada Y, Nishikawa S-I, Yamano K, Kamiya M, et al. (2013) Tam41 is a CDP-diacylglycerol synthase required for cardiolipin biosynthesis in mitochondria. Cell Metab 17: 709–718. doi:10.1016/j.cmet.2013.03.018.

10. Osman C, Haag M, Wieland FT, Brügger B, Langer T (2010) A mitochondrial phosphatase required for cardiolipin biosynthesis: the PGP phosphatase Gep4. EMBO J 29: 1976–1987. doi:10.1038/emboj.2010.98.

11. Beranek A, Rechberger G, Knauer H, Wolinski H, Kohlwein SD, et al. (2009) Identification of a cardiolipin-specific phospholipase encoded by the gene *CLD1* (*YGR110W*) in yeast. J Biol Chem 284: 11572–11578. doi:10.1074/jbc.M805511200.

12. Testet E, Laroche-Traineau J, Noubhani A, Coulon D, Bunoust O, et al. (2005) Ypr140wp, “the yeast tafazzin,” displays a mitochondrial lysophosphatidylcholine (lyso-PC) acyltransferase activity related to triacylglycerol and mitochondrial lipid synthesis. Biochem J 387: 617–626. doi:10.1042/BJ20041491.

13. Baile MG, Whited K, Claypool SM (2013) Deacylation on the matrix side of the mitochondrial inner membrane regulates cardiolipin remodeling. Mol Biol Cell 24: 2008–2020. doi:10.1091/mbc.E13-03-0121.

14. Potting C, Tatsuta T, König T, Haag M, Wai T, et al. (2013) TRIAP1/PRELI complexes prevent apoptosis by mediating intramitochondrial transport of phosphatidic acid. Cell Metab 18: 287–295. doi:10.1016/j.cmet.2013.07.008.

15. Zhang J, Guan Z, Murphy AN, Wiley SE, Perkins GA, et al. (2011) Mitochondrial phosphatase PTPMT1 is essential for cardiolipin biosynthesis. Cell Metab 13: 690–700. doi:10.1016/j.cmet.2011.04.007.

16. Claypool SM, Koehler CM (2012) The complexity of cardiolipin in health and disease. Trends Biochem Sci 37: 32–41. doi:10.1016/j.tibs.2011.09.003.

17. Lu B, Xu FY, Jiang YJ, Choy PC, Hatch GM, et al. (2006) Cloning and characterization of a cDNA encoding human cardiolipin synthase (hCLS1). J Lipid Res 47: 1140–1145. doi:10.1194/jlr.C600004-JLR200.

18. Houtkooper RH, Akbari H, van Lenthe H, Kulik W, Wanders RJA, et al. (2006) Identification and characterization of human cardiolipin synthase. FEBS Lett 580: 3059–3064. doi:10.1016/j.febslet.2006.04.054.

19. Neuwald AF (1997) Barth syndrome may be due to an acyltransferase deficiency. Curr Biol 7: R465–R466.

20. Xu Y, Zhang S, Malhotra A, Edelman-Novemsky I, Ma J, et al. (2009) Characterization of tafazzin splice variants from humans and fruit flies. J Biol Chem 284: 29230–29239. doi:10.1074/jbc.M109.016642.

21. Mancuso DJ, Sims HF, Han X, Jenkins CM, Guan SP, et al. (2007) Genetic ablation of calcium-independent phospholipase A2 gamma leads to alterations in mitochondrial lipid metabolism and function resulting in a deficient mitochondrial bioenergetic phenotype. J Biol Chem 282: 34611–34622. doi:10.1074/jbc.M707795200.

22. Taylor WA, Hatch GM (2009) Identification of the human mitochondrial linoleoyl-coenzyme A monolysocardiolipin acyltransferase (MLCL AT-1). J Biol Chem 284: 30360–30371. doi:10.1074/jbc.M109.048322.

23. Li J, Romestaing C, Han X, Li Y, Hao X, et al. (2010) Cardiolipin remodeling by ALCAT1 links oxidative stress and mitochondrial dysfunction to obesity. Cell Metab 12: 154–165. doi:10.1016/j.cmet.2010.07.003.

24. van den Brink-van der Laan E, Killian JA, de Kruijff B (2004) Nonbilayer lipids affect peripheral and integral membrane proteins via changes in the lateral pressure profile. Biochim Biophys Acta 1666: 275–288. doi:10.1016/j.bbamem.2004.06.010.

25. Osman C, Voelker DR, Langer T (2011) Making heads or tails of phospholipids in mitochondria. J Cell Biol 192: 7–16. doi:10.1083/jcb.201006159.

26. Tamura Y, Harada Y, Yamano K, Watanabe K, Ishikawa D, et al. (2006) Identification of Tam41 maintaining integrity of the TIM23 protein translocator complex in mitochondria. J Cell Biol 174: 631–637. doi:10.1083/jcb.200603087.

27. Schlame M, Rua D, Greenberg ML (2000) The biosynthesis and functional role of cardiolipin. Prog Lipid Res 39: 257–288. doi:10.1016/S0163-7827(00)00005-9.

28. Paradies G, Paradies V, Ruggiero FM, Petrosillo G (2014) Cardiolipin and Mitochondrial Function in Health and Disease. Antioxid Redox Signal 20: 1925–1953. doi:10.1089/ars.2013.5280.

29. Tatsuta T, Scharwey M, Langer T (2014) Mitochondrial lipid trafficking. Trends Cell Biol 24: 44–52. doi:10.1016/j.tcb.2013.07.011.

30. Scharwey M, Tatsuta T, Langer T (2013) Mitochondrial lipid transport at a glance. J Cell Sci 126: 5317–5323. doi:10.1242/jcs.134130.

31. Simbeni R, Pon L, Zinser E, Paltauf F, Daum G (1991) Mitochondrial membrane contact sites of yeast. Characterization of lipid components and possible involvement in intramitochondrial translocation of phospholipids. J Biol Chem 266: 10047–10049.

32. Epand RF, Tokarska-Schlattner M, Schlattner U, Wallimann T, Epand RM (2007) Cardiolipin clusters and membrane domain formation induced by mitochondrial proteins. J Mol Biol 365: 968–980. doi:10.1016/j.jmb.2006.10.028.

33. Malsburg von der K, Müller JM, Bohnert M, Oeljeklaus S, Kwiatkowska P, et al. (2011) Dual role of mitofilin in mitochondrial membrane organization and protein biogenesis. Dev Cell 21: 694–707. doi:10.1016/j.devcel.2011.08.026.

34. Harner M, Körner C, Walther D, Mokranjac D, Kaesmacher J, et al. (2011) The mitochondrial contact site complex, a determinant of mitochondrial architecture. EMBO J 30: 4356–4370. doi:10.1038/emboj.2011.379.

35. Hoppins S, Collins SR, Cassidy-Stone A, Hummel E, DeVay RM, et al. (2011) A mitochondrial-focused genetic interaction map reveals a scaffold-like complex required for inner membrane organization in mitochondria. J Cell Biol 195: 323–340. doi:10.1083/jcb.201107053.

36. Sesaki H, Dunn CD, Iijima M, Shepard KA, Yaffe MP, et al. (2006) Ups1p, a conserved intermembrane space protein, regulates mitochondrial shape and alternative topogenesis of Mgm1p. J Cell Biol 173: 651–658. doi:10.1083/jcb.200603092.

37. Song Z, Chen H, Fiket M, Alexander C, Chan DC (2007) OPA1 processing controls mitochondrial fusion and is regulated by mRNA splicing, membrane potential, and Yme1L. J Cell Biol 178: 749–755. doi:10.1083/jcb.200704110.

38. Osman C, Haag M, Potting C, Rodenfels J, Dip PV, et al. (2009) The genetic interactome of prohibitins: coordinated control of cardiolipin and phosphatidylethanolamine by conserved regulators in mitochondria. J Cell Biol 184: 583–596. doi:10.1083/jcb.200810189.

39. Choi S-Y, Huang P, Jenkins GM, Chan DC, Schiller J, et al. (2006) A common lipid links Mfn-mediated mitochondrial fusion and SNARE-regulated exocytosis. Nat Cell Biol 8: 1255–1262. doi:10.1038/ncb1487.

40. Joshi AS, Thompson MN, Fei N, Hüttemann M, Greenberg ML (2012) Cardiolipin and mitochondrial phosphatidylethanolamine have overlapping functions in mitochondrial fusion in *Saccharomyces cerevisiae*. J Biol Chem 287: 17589–17597. doi:10.1074/jbc.M111.330167.

41. Jiang F, Ryan MT, Schlame M, Zhao M, Gu Z, et al. (2000) Absence of cardiolipin in the crd1 null mutant results in decreased mitochondrial membrane potential and reduced mitochondrial function. J Biol Chem 275: 22387–22394. doi:10.1074/jbc.M909868199.

42. Beyer K, Klingenberg M (1985) ADP/ATP carrier protein from beef heart mitochondria has high amounts of tightly bound cardiolipin, as revealed by phosphorus-31 nuclear magnetic resonance. Biochemistry 24: 3821–3826.

43. Beyer K, Nuscher B (1996) Specific cardiolipin binding interferes with labeling of sulfhydryl residues in the adenosine diphosphate/adenosine triphosphate carrier protein from beef heart mitochondria. Biochemistry 35: 15784–15790. doi:10.1021/bi9610055.

44. Houtkooper RH, Vaz FM (2008) Cardiolipin, the heart of mitochondrial metabolism. Cell Mol Life Sci 65: 2493–2506. doi:10.1007/s00018-008-8030-5.

45. Claypool SM, Oktay Y, Boontheung P, Loo JA, Koehler CM (2008) Cardiolipin defines the interactome of the major ADP/ATP carrier protein of the mitochondrial inner membrane. J Cell Biol 182: 937–950. doi:10.1083/jcb.200801152.

46. Schägger H, Pfeiffer K (2000) Supercomplexes in the respiratory chains of yeast and mammalian mitochondria. EMBO J 19: 1777–1783. doi:10.1093/emboj/19.8.1777.

47. Paradies G, Paradies V, De Benedictis V, Ruggiero FM, Petrosillo G (2014) Functional role of cardiolipin in mitochondrial bioenergetics. Biochim Biophys Acta 1837: 408–417. doi:10.1016/j.bbabio.2013.10.006.

48. Zhang M, Mileykovskaya E, Dowhan W (2002) Gluing the respiratory chain together. Cardiolipin is required for supercomplex formation in the inner mitochondrial membrane. J Biol Chem 277: 43553–43556. doi:10.1074/jbc.C200551200.

49. Brandner K, Mick DU, Frazier AE, Taylor RD, Meisinger C, et al. (2005) Taz1, an outer mitochondrial membrane protein, affects stability and assembly of inner membrane protein complexes: implications for Barth Syndrome. Mol Biol Cell 16: 5202–5214. doi:10.1091/mbc.E05-03-0256.

50. Koshkin V, Greenberg ML (2002) Cardiolipin prevents rate-dependent uncoupling and provides osmotic stability in yeast mitochondria. Biochem J 364: 317–322.

51. Koshkin V, Greenberg ML (2000) Oxidative phosphorylation in cardiolipin-lacking yeast mitochondria. Biochem J 347 Pt 3: 687–691.

52. Acehan D, Khuchua Z, Houtkooper RH, Malhotra A, Kaufman J, et al. (2009) Distinct effects of tafazzin deletion in differentiated and undifferentiated mitochondria. Mitochondrion 9: 86–95. doi:10.1016/j.mito.2008.12.001.

53. Mckenzie M, Lazarou M, Thorburn DR, Ryan MT (2006) Mitochondrial respiratory chain supercomplexes are destabilized in Barth Syndrome patients. J Mol Biol 361: 462–469. doi:10.1016/j.jmb.2006.06.057.

54. Acehan D, Malhotra A, Xu Y, Ren M, Stokes DL, et al. (2011) Cardiolipin affects the supramolecular organization of ATP synthase in mitochondria. Biophys J 100: 2184–2192. doi:10.1016/j.bpj.2011.03.031.

55. Gonzalvez F, Gottlieb E (2007) Cardiolipin: setting the beat of apoptosis. Apoptosis 12: 877–885. doi:10.1007/s10495-007-0718-8.

56. Schlattner U, Tokarska-Schlattner M, Ramirez S, Tyurina YY, Amoscato AA, et al. (2013) Dual function of mitochondrial Nm23-H4 protein in phosphotransfer and intermembrane lipid transfer: a cardiolipin-dependent switch. J Biol Chem 288: 111–121. doi:10.1074/jbc.M112.408633.

57. Kagan VE, Chu CT, Tyurina YY, Cheikhi A, Bayir H (2014) Cardiolipin asymmetry, oxidation and signaling. Chem Phys Lipids 179: 64–69. doi:10.1016/j.chemphyslip.2013.11.010.

58. Garcia Fernandez M, Troiano L, Moretti L, Nasi M, Pinti M, et al. (2002) Early changes in intramitochondrial cardiolipin distribution during apoptosis. Cell Growth Differ 13: 449–455.

59. Lutter M, Fang M, Luo X, Nishijima M, Xie X, et al. (2000) Cardiolipin provides specificity for targeting of tBid to mitochondria. Nat Cell Biol 2: 754–761. doi:10.1038/35036395.

60. Gonzalvez F, Schug ZT, Houtkooper RH, MacKenzie ED, Brooks DG, et al. (2008) Cardiolipin provides an essential activating platform for caspase-8 on mitochondria. J Cell Biol 183: 681–696. doi:10.1083/jcb.200803129.

61. Lovell JF, Billen LP, Bindner S, Shamas-Din A, Fradin C, et al. (2008) Membrane binding by tBid initiates an ordered series of events culminating in membrane permeabilization by Bax. Cell 135: 1074–1084. doi:10.1016/j.cell.2008.11.010.

62. Kim T-H, Zhao Y, Ding W-X, Shin JN, He X, et al. (2004) Bid-cardiolipin interaction at mitochondrial contact site contributes to mitochondrial cristae reorganization and cytochrome C release. Mol Biol Cell 15: 3061–3072. doi:10.1091/mbc.E03-12-0864.

63. Gonzalvez F, Pariselli F, Dupaigne P, Budihardjo I, Lutter M, et al. (2005) tBid interaction with cardiolipin primarily orchestrates mitochondrial dysfunctions and subsequently activates Bax and Bak. Cell Death Differ 12: 614–626. doi:10.1038/sj.cdd.4401571.

64. Rytömaa M, Mustonen P, Kinnunen PK (1992) Reversible, nonionic, and pH-dependent association of cytochrome c with cardiolipin-phosphatidylcholine liposomes. J Biol Chem 267: 22243–22248.

65. Nicholls P (1974) Cytochrome c binding to enzymes and membranes. Biochim Biophys Acta 346: 261–310.

66. Kagan VE, Tyurin VA, Jiang J, Tyurina YY, Ritov VB, et al. (2005) Cytochrome c acts as a cardiolipin oxygenase required for release of proapoptotic factors. Nat Chem Biol 1: 223–232. doi:10.1038/nchembio727.

67. Choi S-Y, Gonzalvez F, Jenkins GM, Slomianny C, Chretien D, et al. (2007) Cardiolipin deficiency releases cytochrome c from the inner mitochondrial membrane and accelerates stimuli-elicited apoptosis. Cell Death Differ 14: 597–606. doi:10.1038/sj.cdd.4402020.

68. Ott M, Robertson JD, Gogvadze V, Zhivotovsky B, Orrenius S (2002) Cytochrome c release from mitochondria proceeds by a two-step process. Proc Natl Acad Sci USA 99: 1259–1263. doi:10.1073/pnas.241655498.

69. Clarke SLN, Bowron A, Gonzalez IL, Groves SJ, Newbury-Ecob R, et al. (2013) Barth syndrome. Orphanet J Rare Dis 8: 23. doi:10.1186/1750-1172-8-23.

70. Bolhuis PA, Hensels GW, Hulsebos TJ, Baas F, Barth PG (1991) Mapping of the locus for X-linked cardioskeletal myopathy with neutropenia and abnormal mitochondria (Barth syndrome) to Xq28. Am J Hum Genet 48: 481–485.

71. Ades LC, Gedeon AK, Wilson MJ, Latham M, Partington MW, et al. (1993) Barth syndrome: clinical features and confirmation of gene localisation to distal Xq28. Am J Med Genet 45: 327–334. doi:10.1002/ajmg.1320450309.

72. Jefferies JL (2013) Barth syndrome. Am J Med Genet C Semin Med Genet 163C: 198–205. doi:10.1002/ajmg.c.31372.

73. Schlame M, Ren M, Xu Y, Greenberg ML, Haller I (2005) Molecular symmetry in mitochondrial cardiolipins. Chem Phys Lipids 138: 38–49. doi:10.1016/j.chemphyslip.2005.08.002.

74. Cheng H, Mancuso DJ, Jiang X, Guan S, Yang J, et al. (2008) Shotgun lipidomics reveals the temporally dependent, highly diversified cardiolipin profile in the mammalian brain: temporally coordinated postnatal diversification of cardiolipin molecular species with neuronal remodeling. Biochemistry 47: 5869–5880. doi:10.1021/bi7023282.

75. Schlame M, Towbin JA, Heerdt PM, Jehle R, DiMauro S, et al. (2002) Deficiency of tetralinoleoyl-cardiolipin in Barth syndrome. Ann Neurol 51: 634–637. doi:10.1002/ana.10176.

76. Phoon CKL, Acehan D, Schlame M, Stokes DL, Edelman-Novemsky I, et al. (2012) Tafazzin knockdown in mice leads to a developmental cardiomyopathy with early diastolic dysfunction preceding myocardial noncompaction. J Am Heart Assoc 1: jah3–e000455–jah3–e000455. doi:10.1161/JAHA.111.000455.

77. Xu Y, Condell M, Plesken H, Edelman-Novemsky I, Ma J, et al. (2006) A Drosophila model of Barth syndrome. Proc Natl Acad Sci USA 103: 11584–11588. doi:10.1073/pnas.0603242103.

78. Gu Z, Valianpour F, Chen S, Vaz FM, Hakkaart GA, et al. (2004) Aberrant cardiolipin metabolism in the yeast taz1 mutant: a model for Barth syndrome. Mol Microbiol 51: 149–158.

79. Khuchua Z, Yue Z, Batts L, Strauss AW (2006) A zebrafish model of human Barth syndrome reveals the essential role of tafazzin in cardiac development and function. Circ Res 99: 201–208. doi:10.1161/01.RES.0000233378.95325.ce.

80. Vreken P, Valianpour F, Nijtmans LG, Grivell LA, Plecko B, et al. (2000) Defective remodeling of cardiolipin and phosphatidylglycerol in Barth syndrome. Biochem Biophys Res Commun 279: 378–382. doi:10.1006/bbrc.2000.3952.

81. Acehan D, Xu Y, Stokes DL, Schlame M (2007) Comparison of lymphoblast mitochondria from normal subjects and patients with Barth syndrome using electron microscopic tomography. Lab Invest 87: 40–48. doi:10.1038/labinvest.3700480.

82. Gonzalvez F, D'Aurelio M, Boutant M, Moustapha A, Puech J-P, et al. (2013) Barth syndrome: cellular compensation of mitochondrial dysfunction and apoptosis inhibition due to changes in cardiolipin remodeling linked to tafazzin (TAZ) gene mutation. Biochim Biophys Acta 1832: 1194–1206. doi:10.1016/j.bbadis.2013.03.005.

83. Baile MG, Sathappa M, Lu Y-W, Pryce E, Whited K, et al. (2014) Unremodeled and remodeled cardiolipin are functionally indistinguishable in yeast. J Biol Chem 289: 1768–1778. doi:10.1074/jbc.M113.525733.

84. Houtkooper RH, Turkenburg M, Poll-The BT, Karall D, Pérez-Cerdá C, et al. (2009) The enigmatic role of tafazzin in cardiolipin metabolism. Biochim Biophys Acta 1788: 2003–2014. doi:10.1016/j.bbamem.2009.07.009.

85. Malhotra A, Edelman-Novemsky I, Xu Y, Plesken H, Ma J, et al. (2009) Role of calcium-independent phospholipase A2 in the pathogenesis of Barth syndrome. Proc Natl Acad Sci USA 106: 2337–2341. doi:10.1073/pnas.0811224106.

86. Ye C, Lou W, Li Y, Chatzispyrou IA, Hüttemann M, et al. (2014) Deletion of the cardiolipin-specific phospholipase Cld1 rescues growth and life span defects in the tafazzin mutant: implications for Barth syndrome. J Biol Chem 289: 3114–3125. doi:10.1074/jbc.M113.529487.

87. Raja V, Greenberg ML (2014) The functions of cardiolipin in cellular metabolism-potential modifiers of the Barth syndrome phenotype. Chem Phys Lipids 179: 49–56. doi:10.1016/j.chemphyslip.2013.12.009.

88. Johnston J, Kelley RI, Feigenbaum A, Cox GF, Iyer GS, et al. (1997) Mutation characterization and genotype-phenotype correlation in Barth syndrome. Am J Hum Genet 61: 1053–1058. doi:10.1086/301604.

89. Ronvelia D, Greenwood J, Platt J, Hakim S, Zaragoza MV (2012) Intrafamilial variability for novel TAZ gene mutation: Barth syndrome with dilated cardiomyopathy and heart failure in an infant and left ventricular noncompaction in his great-uncle. Mol Genet Metab 107: 428–432. doi:10.1016/j.ymgme.2012.09.013.

90. Marziliano N, Mannarino S, Nespoli L, Diegoli M, Pasotti M, et al. (2007) Barth syndrome associated with compound hemizygosity and heterozygosity of the TAZ and LDB3 genes. Am J Med Genet A 143A: 907–915. doi:10.1002/ajmg.a.31653.

91. Lu B, Kelher MR, Lee DP, Lewin TM, Coleman RA, et al. (2004) Complex expression pattern of the Barth syndrome gene product tafazzin in human cell lines and murine tissues. Biochem Cell Biol 82: 569–576. doi:10.1139/o04-055.

92. Kirwin SM, Manolakos A, Barnett SS, Gonzalez IL (2014) Tafazzin splice variants and mutations in Barth syndrome. Mol Genet Metab 111: 26–32. doi:10.1016/j.ymgme.2013.11.006.

93. Vaz FM, Houtkooper RH, Valianpour F, Barth PG, Wanders RJA (2003) Only one splice variant of the human TAZ gene encodes a functional protein with a role in cardiolipin metabolism. J Biol Chem 278: 43089–43094. doi:10.1074/jbc.M305956200.

94. Ma L, Vaz FM, Gu Z, Wanders RJA, Greenberg ML (2004) The human TAZ gene complements mitochondrial dysfunction in the yeast taz1Delta mutant. Implications for Barth syndrome. J Biol Chem 279: 44394–44399. doi:10.1074/jbc.M405479200.

95. Xu Y, Kelley RI, Blanck TJJ, Schlame M (2003) Remodeling of cardiolipin by phospholipid transacylation. J Biol Chem 278: 51380–51385. doi:10.1074/jbc.M307382200.

96. Hsu Y-H, Dumlao DS, Cao J, Dennis EA (2013) Assessing Phospholipase A2 Activity toward Cardiolipin by Mass Spectrometry. PLoS ONE 8: e59267. doi:10.1371/journal.pone.0059267.

97. Schlame M, Acehan D, Berno B, Xu Y, Valvo S, et al. (2012) The physical state of lipid substrates provides transacylation specificity for tafazzin. Nat Chem Biol 8: 862–869. doi:10.1038/nchembio.1064.

98. Claypool SM, Boontheung P, McCaffery JM, Loo JA, Koehler CM (2008) The cardiolipin transacylase, tafazzin, associates with two distinct respiratory components providing insight into Barth syndrome. Mol Biol Cell 19: 5143–5155. doi:10.1091/mbc.E08-09-0896.

99. Chen S, He Q, Greenberg ML (2008) Loss of tafazzin in yeast leads to increased oxidative stress during respiratory growth. Mol Microbiol 68: 1061–1072. doi:10.1111/j.1365-2958.2008.06216.x.

100. Whited K, Baile MG, Currier P, Claypool SM (2013) Seven functional classes of Barth syndrome mutation. Hum Mol Genet 22: 483–492. doi:10.1093/hmg/dds447.

101. Malhotra A, Xu Y, Ren M, Schlame M (2009) Formation of molecular species of mitochondrial cardiolipin. 1. A novel transacylation mechanism to shuttle fatty acids between sn-1 and sn-2 positions of multiple phospholipid species. Biochim Biophys Acta 1791: 314–320. doi:10.1016/j.bbalip.2009.01.004.

102. Claypool SM, Whited K, Srijumnong S, Han X, Koehler CM (2011) Barth syndrome mutations that cause tafazzin complex lability. J Cell Biol 192: 447–462. doi:10.1083/jcb.201008177.

103. Claypool SM, McCaffery JM, Koehler CM (2006) Mitochondrial mislocalization and altered assembly of a cluster of Barth syndrome mutant tafazzins. J Cell Biol 174: 379–390. doi:10.1083/jcb.200605043.

104. Acehan D, Vaz F, Houtkooper RH, James J, Moore V, et al. (2011) Cardiac and skeletal muscle defects in a mouse model of human Barth syndrome. J Biol Chem 286: 899–908. doi:10.1074/jbc.M110.171439.

105. Soustek MS, Falk DJ, Mah CS, Toth MJ, Schlame M, et al. (2011) Characterization of a transgenic short hairpin RNA-induced murine model of Tafazzin deficiency. 22: 865–871. doi:10.1089/hum.2010.199.

106. Tong AH, Evangelista M, Parsons AB, Xu H, Bader GD, et al. (2001) Systematic genetic analysis with ordered arrays of yeast deletion mutants. Science 294: 2364–2368. doi:10.1126/science.1065810.

107. Kanki T, Kang D, Klionsky DJ (2009) Monitoring mitophagy in yeast: the Om45-GFP processing assay. Autophagy 5: 1186–1189. doi: 10.4161/auto.5.8.9854.

108. Gietz RD, Schiestl RH, Willems AR, Woods RA (1995) Studies on the transformation of intact yeast cells by the LiAc/SS-DNA/PEG procedure. Yeast 11: 355–360. doi:10.1002/yea.320110408.

109. Lorenz MC, Muir RS, Lim E, McElver J, Weber SC, et al. (1995) Gene disruption with PCR products in *Saccharomyces cerevisiae*. Gene 158: 113–117. doi:10.1016/0378-1119(95)00144-U.

110. Cherry JM, Adler C, Ball C, Chervitz SA, Dwight SS, et al. (1998) SGD: Saccharomyces Genome Database. Nucleic Acids Res 26: 73–79. doi:10.1093/nar/26.1.73.

111. Vaden DL, Gohil VM, Gu Z, Greenberg ML (2005) Separation of yeast phospholipids using one-dimensional thin-layer chromatography. Anal Biochem 338: 162–164. doi:10.1016/j.ab.2004.11.020.

112. Weisman LS, Bacallao R, Wickner W (1987) Multiple methods of visualizing the yeast vacuole permit evaluation of its morphology and inheritance during the cell cycle. J Cell Biol 105: 1539–1547.

113. Chen S, Tarsio M, Kane PM, Greenberg ML (2008) Cardiolipin mediates cross-talk between mitochondria and the vacuole. Mol Biol Cell 19: 5047–5058. doi:10.1091/mbc.E08-05-0486.

114. Reznick AZ, Packer L (1994) Oxidative damage to proteins: spectrophotometric method for carbonyl assay. Meth Enzymol 233: 357–363.

115. Diekert K, de Kroon AI, Kispal G, Lill R (2001) Isolation and subfractionation of mitochondria from the yeast *Saccharomyces cerevisiae.* Methods Cell Biol 65: 37–51.

116. Schägger H (2001) Blue-native gels to isolate protein complexes from mitochondria. Methods Cell Biol 65: 231–244.

117. Swamy M, Siegers GM, Minguet S, Wollscheid B, Schamel WWA (2006) Blue native polyacrylamide gel electrophoresis (BN-PAGE) for the identification and analysis of multiprotein complexes. Science's STKE 2006: pl4–pl4. doi:10.1126/stke.3452006pl4.

118. Langer T (2000) AAA proteases: cellular machines for degrading membrane proteins. Trends Biochem Sci 25: 247–251.

119. Campbell CL, Tanaka N, White KH, Thorsness PE (1994) Mitochondrial morphological and functional defects in yeast caused by yme1 are suppressed by mutation of a 26S protease subunit homologue. Mol Biol Cell 5: 899–905.

120. Stiburek L, Cesnekova J, Kostkova O, Fornuskova D, Vinsova K, et al. (2012) YME1L controls the accumulation of respiratory chain subunits and is required for apoptotic resistance, cristae morphogenesis, and cell proliferation. Mol Biol Cell 23: 1010–1023. doi:10.1091/mbc.E11-08-0674.

121. Thorsness PE, White KH, Fox TD (1993) Inactivation of YME1, a member of the ftsH-SEC18-PAS1-CDC48 family of putative ATPase-encoding genes, causes increased escape of DNA from mitochondria in *Saccharomyces cerevisiae*. Mol Cell Biol 13: 5418–5426.

122. Nebauer R, Schuiki I, Kulterer B, Trajanoski Z, Daum G (2007) The phosphatidylethanolamine level of yeast mitochondria is affected by the mitochondrial components Oxa1p and Yme1p. FEBS J 274: 6180–6190. doi:10.1111/j.1742-4658.2007.06138.x.

123. Campbell CL, Thorsness PE (1998) Escape of mitochondrial DNA to the nucleus in yme1 yeast is mediated by vacuolar-dependent turnover of abnormal mitochondrial compartments. J Cell Sci 111 (Pt 16): 2455–2464.

124. Youle RJ, Narendra DP (2011) Mechanisms of mitophagy. Nat Rev Mol Cell Biol 12: 9–14. doi:10.1038/nrm3028.

125. Kanki T, Klionsky DJ (2008) Mitophagy in yeast occurs through a selective mechanism. J Biol Chem 283: 32386–32393. doi:10.1074/jbc.M802403200.

126. Kurihara Y, Kanki T, Aoki Y, Hirota Y, Saigusa T, et al. (2012) Mitophagy plays an essential role in reducing mitochondrial production of reactive oxygen species and mutation of mitochondrial DNA by maintaining mitochondrial quantity and quality in yeast. J Biol Chem 287: 3265–3272. doi:10.1074/jbc.M111.280156.

127. Smith PK, Krohn RI, Hermanson GT, Mallia AK, Gartner FH, et al. (1985) Measurement of protein using bicinchoninic acid. Anal Biochem 150: 76–85.

128. Aung-Htut MT, Ayer A, Breitenbach M, Dawes IW (2012) Oxidative stresses and ageing. Subcell Biochem 57: 13–54. doi:10.1007/978-94-007-2561-4_2.

129. Ayer A, Gourlay CW, Dawes IW (2013) Cellular Redox Homeostasis, Reactive Oxygen Species and Replicative Ageing in *Saccharomyces cerevisiae*. FEMS Yeast Res. doi:10.1111/1567-1364.12114.

130. Nakamura N, Matsuura A, Wada Y, Ohsumi Y (1997) Acidification of vacuoles is required for autophagic degradation in the yeast, *Saccharomyces cerevisiae*. J Biochem 121: 338–344.

131. Allison AC, Young MR (1964) uptake of dyes and drugs by living cells in culture. Life Sci 3: 1407–1414.

132. Gebert N, Ryan MT, Pfanner N, Wiedemann N, Stojanovski D (2011) Mitochondrial protein import machineries and lipids: a functional connection. Biochim Biophys Acta 1808: 1002–1011. doi:10.1016/j.bbamem.2010.08.003.

133. Szappanos B, Kovács K, Szamecz B, Honti F, Costanzo M, et al. (2011) An integrated approach to characterize genetic interaction networks in yeast metabolism. Nat Genet 43: 656–662. doi:10.1038/ng.846.

134. Osman C, Merkwirth C, Langer T (2009) Prohibitins and the functional compartmentalization of mitochondrial membranes. J Cell Sci 122: 3823–3830. doi:10.1242/jcs.037655.

135. Tamura Y, Endo T, Iijima M, Sesaki H (2009) Ups1p and Ups2p antagonistically regulate cardiolipin metabolism in mitochondria. J Cell Biol 185: 1029–1045. doi:10.1083/jcb.200812018.

136. Potting C, Wilmes C, Engmann T, Osman C, Langer T (2010) Regulation of mitochondrial phospholipids by Ups1/PRELI-like proteins depends on proteolysis and Mdm35. EMBO J 29: 2888–2898. doi:10.1038/emboj.2010.169.

137. Schreiner B, Westerburg H, Forne I, Imhof A, Neupert W, et al. (2012) Role of the AAA protease Yme1 in folding of proteins in the intermembrane space of mitochondria. Mol Biol Cell 23: 4335–4346. doi:10.1091/mbc.E12-05-0420.

138. Kanki T, Wang K, Klionsky DJ (2010) A genomic screen for yeast mutants defective in mitophagy. Autophagy 6: 278–280.

139. Kanki T, Wang K, Cao Y, Baba M, Klionsky DJ (2009) Atg32 is a mitochondrial protein that confers selectivity during mitophagy. Dev Cell 17: 98–109. doi:10.1016/j.devcel.2009.06.014.

140. Wang K, Jin M, Liu X, Klionsky DJ (2013) Proteolytic processing of Atg32 by the mitochondrial i-AAA protease Yme1 regulates mitophagy. Autophagy 9: 1828–1836. doi:10.4161/auto.26281.

141. Okamoto K, Kondo-Okamoto N, Ohsumi Y (2009) Mitochondria-anchored receptor Atg32 mediates degradation of mitochondria via selective autophagy. Dev Cell 17: 87–97. doi:10.1016/j.devcel.2009.06.013.

142. Chu CT, Ji J, Dagda RK, Jiang JF, Tyurina YY, et al. (2013) Cardiolipin externalization to the outer mitochondrial membrane acts as an elimination signal for mitophagy in neuronal cells. Nat Cell Biol 15: 1197–1205. doi:10.1038/ncb2837.

143. Galbraith LCA (2014) The role of cardiolipin in mitophagy. University of Glasgow PhD thesis.

144. Pearce DA, Sherman F (1995) Degradation of cytochrome oxidase subunits in mutants of yeast lacking cytochrome c and suppression of the degradation by mutation of yme1. J Biol Chem 270: 20879–20882.

145. Fiumera HL, Dunham MJ, Saracco SA, Butler CA, Kelly JA, et al. (2009) Translocation and assembly of mitochondrially coded *Saccharomyces cerevisiae* cytochrome c oxidase subunit Cox2 by Oxa1 and Yme1 in the absence of Cox18. Genetics 182: 519–528. doi:10.1534/genetics.109.101196.

146. Palermo V, Falcone C, Mazzoni C (2007) Apoptosis and aging in mitochondrial morphology mutants ofS. cerevisiae. Folia Microbiol 52: 479–483. doi:10.1007/BF02932107.

147. Lee J, Giordano S, Zhang J (2012) Autophagy, mitochondria and oxidative stress: cross-talk and redox signalling. Biochem J 441: 523–540. doi:10.1042/BJ20111451.

148. Shouval RS, Shvets E, Fass E, Shorer H, Gil L, et al. (2007) Reactive oxygen species are essential for autophagy and specifically regulate the activity of Atg4. EMBO J 26: 1749–1760. doi:10.1038/sj.emboj.7601623.

149. Frank M, Duvezin-Caubet S, Koob S, Occhipinti A, Jagasia R, et al. (2012) Mitophagy is triggered by mild oxidative stress in a mitochondrial fission dependent manner. Biochim Biophys Acta 1823: 2297–2310. doi:10.1016/j.bbamcr.2012.08.007.

150. Patil VA, Fox JL, Gohil VM, Winge DR, Greenberg ML (2013) Loss of cardiolipin leads to perturbation of mitochondrial and cellular iron homeostasis. J Biol Chem 288: 1696–1705. doi:10.1074/jbc.M112.428938.

151. Boone C, Bussey H, Andrews BJ (2007) Exploring genetic interactions and networks with yeast. Nat Rev Genet 8: 437–449. doi:10.1038/nrg2085.

152. Jamieson DJ (1998) Oxidative stress responses of the yeast *Saccharomyces cerevisiae*. Yeast 14: 1511–1527. doi:10.1002/(SICI)1097-0061(199812)14:16<1511::AID-YEA356>3.0.CO;2-S.